ADVANCED ENERGY MATERIALS
www.advenergymat.de

Pure Tin Halide Perovskite Solar Cells: Focusing on Preparation and Strategies

Hairui Liu, Zuhong Zhang, Weiwei Zuo, Rajarshi Roy, Meng Li, Mahdi Malekshahi Byranvand,* and Michael Saliba**

Metal halide perovskite solar cells (PSCs) have emerged as an important direction for photovoltaic research. Although the power conversion efficiency (PCE) of lead-based PSCs has reached 25.7%, still the toxicity of Pb remains one main obstacle for commercial adoption. Thus, to address this issue, Pb-free perovskites have been proposed. Among them, tin-based perovskites have emerged as promising candidates. Unfortunately, the fast oxidation of Sn^{2+} to Sn^{4+} leads to low stability and efficiency. Many strategies have been implemented to address these challenges in Sn-based PSCs. This work introduces stability and efficiency improvement strategies for pure Sn-based PSCs by optimization of the crystal structure, processing and interfaces as well as, implementation of low-dimension structures. Finally, new perspectives for further developing Sn-based PSCs are provided.

1. Introduction

Solar energy is a promising renewable energy source. Especially perovskite solar cells (PSCs), as proposed by Kojima et al. in 2009,[1] have been skyrocketing in recent years, achieving a PCE world record of 25.7%.[2] Perovskite materials have a general ABX_3 formula where A is an organic or inorganic cation such as methylammonium ($CH_3NH_3^+$, MA^+), formamidinium ($NH_2CHNH_2^+$, FA^+), caesium (Cs^+) or rubidium (Rb^+) in the position (000) of the crystal lattice, B is the central metal cation such as lead (Pb^{2+}), tin (Sn^{2+}) or germanium (Ge^{2+}) in the position (1/2,1/2,1/2) of the crystal lattice and X is a halide or a pseudo halide such as chloride (Cl^-), bromide (Br^-), iodide (I^-) or thiocyanate (SCN^-) in the position of (1/2,0,1/2), (1/2,1/2,0) or (0,1/2,1/2) of the crystal lattice.[3] Perovskite materials present excellent optoelectronic properties such as tunable bandgap,[4] high absorption coefficient,[5] bidirectional charge transport,[6–8] defect tolerance,[9,10] and low exciton binding energy.[11,12] The best photovoltaic performance records have been achieved for Pb-based PSCs. However, the toxicity of Pb is a major challenge for further development on the industrial scale, which needs to be addressed carefully.[13–18] Therefore, finding an alternative for Pb with non-toxic or low-toxic elements is essential. For instance, germanium (Ge^{2+}) from group IVA (same group as Pb^{2+}) and bismuth (Bi^{3+}) or antimony (Sb^{3+}) from group VA have been introduced as nontoxic candidates. However, their photovoltaic properties are far inferior to Pb-based PSCs with 25.7% performance.[19] In addition, Sn-based perovskites have been widely studied as an alternative to achieve acceptable PCEs of 14.81% with lower toxicity compared to Pb-based counterparts. Sn and Pb from the same group of the periodic table, that is, IVA, with similar ionic electronic configurations of ns^2 np^2 in outer orbitals and very similar radius (Sn^{2+} 1.15 Å, Pb^{2+} 1.19 Å),[20–22] could be exchanged with only a slight crystal lattice distortion.[23] Although it is sometimes argued that Sn^{2+} may cause some harm to the environment,[24,25] it is also well accepted that SnO_2 is the primary degradation by-product of Sn-based perovskites is nontoxic and could be removed from the environment more readily compared to degradation by-products of Pb-based perovskites such as $Pb(CH_3COO)_2$, $Pb(NO_3)_2$.

Moreover, Sn-based perovskites have narrow bandgaps that can absorb a broader light spectrum, that is, infrared (NIR) region.[26–28] However, due to their energy band mismatch with the electron transport layer (ETL) or the hole transporting layer

H. Liu, Z. Zhang, M. Li
Key Lab for Special Functional Materials
Ministry of Education
National & Local Joint Engineering Research Center for High-efficiency Display and Lighting Technology
School of Materials Science and Engineering, and Collaborative Innovation Center of Nano Functional Materials and Applications
Henan University
Kaifeng 475004, China
E-mail: mengli@henu.deu.cn

H. Liu
School of Materials Science and Engineering
Henan Normal University
Xinxiang 453007, China

W. Zuo, R. Roy, M. M. Byranvand, M. Saliba
Institute for Photovoltaics
University of Stuttgart
faffenwaldring 47, 70569 Suttgart, Germany
E-mail: mahdi.malekshahi@ipv.uni-stuttgart.de; michael.saliba@ipv.uni-stuttgart.de

M. M. Byranvand, M. Saliba
Helmholtz Young Investigator Group FRONTRUNNER
IEK5-Photovoltaik
Forschungszentrum Jülich
52425 Jülich, Germany

The ORCID identification number(s) for the author(s) of this article can be found under https://doi.org/10.1002/aenm.202202209.

DOI: 10.1002/aenm.202202209

(HTL) in device structure, their best record PCE has reached 14.81%,[29] which is still lagging behind the Pb-based PSCs. Additionally, facile oxidation of Sn^{2+} to Sn^{4+} in the presence of oxygen is a major challenge in Sn-based perovskites, which leads to unfavorable optoelectronic properties as well as poor stabilities.[30–32] On the other hand, rapid crystallization of Sn-based perovskites is another major limitation, which leads to poor film morphology. So far, various strategies have been implemented to address these issues.[33–35] Historically, the first pure Sn-based perovskite was introduced as a light-absorbing layer in Schottky solar cells in 2012, which delivered only a PCE of 0.9%.[36] However, in 2014, Noel et al. reported an Sn-based PSC with a PCE of 6%.[30] Afterward, the device development was accelerated by introducing an inverted architecture with a PCE of 6.22% in 2016.[37] Interestingly, altering the perovskite crystal structure from a 3D feature to a lower dimension such as 2D, nanorods (NRs), and quantum dots (QDs) has been introduced as an efficient approach to push forward the PCE and stability of Sn-based PSCs in the recent years. First, in 2018, Ran et al. achieved 6.98% PCE by introducing a 2D/3D heterojunction perovskite film.[38] In 2019, the same research group synthesized 3D $FASnI_3$ perovskite and pushed the PCE to 9.6%.[39] Recently, He et al. reported the highest PCE of 14.81% for a 2D/3D structure.[29]

Other review articles about Sn-based PSCs have also been published. For example, Yan et al.[40] discussed the features of tin-based perovskites, including the fundamental properties, the device design and several promising recently developed approaches for improving the device performance. Loi et al.[41] discussed the general structure and optoelectronic properties of 3D Sn-based perovskites as well as the low-dimensional structures. Han et al.[42] review the recent efficiency progress and the possible approaches to improve the efficiency of Sn-based PSCs, such as optimizing the band gap, increasing the light-harvesting efficiency and carrier diffusion length, surface passivation and regulating the interface energy-level alignment. Finally, they pointed out the possibilities for reaching 20% PCE and considered the issues regarding the scaling-up of these types of PSCs in the future. Moreover, Huang et al.[43] reviewed recent developments and future perspectives regarding inverted Sn-based device structures.

In particular, this review focuses on Sn-based perovskite properties, device features and charge transport layers, and crystallization; it highlights the obstacles and opportunities for further progress. The current challenges and prospects

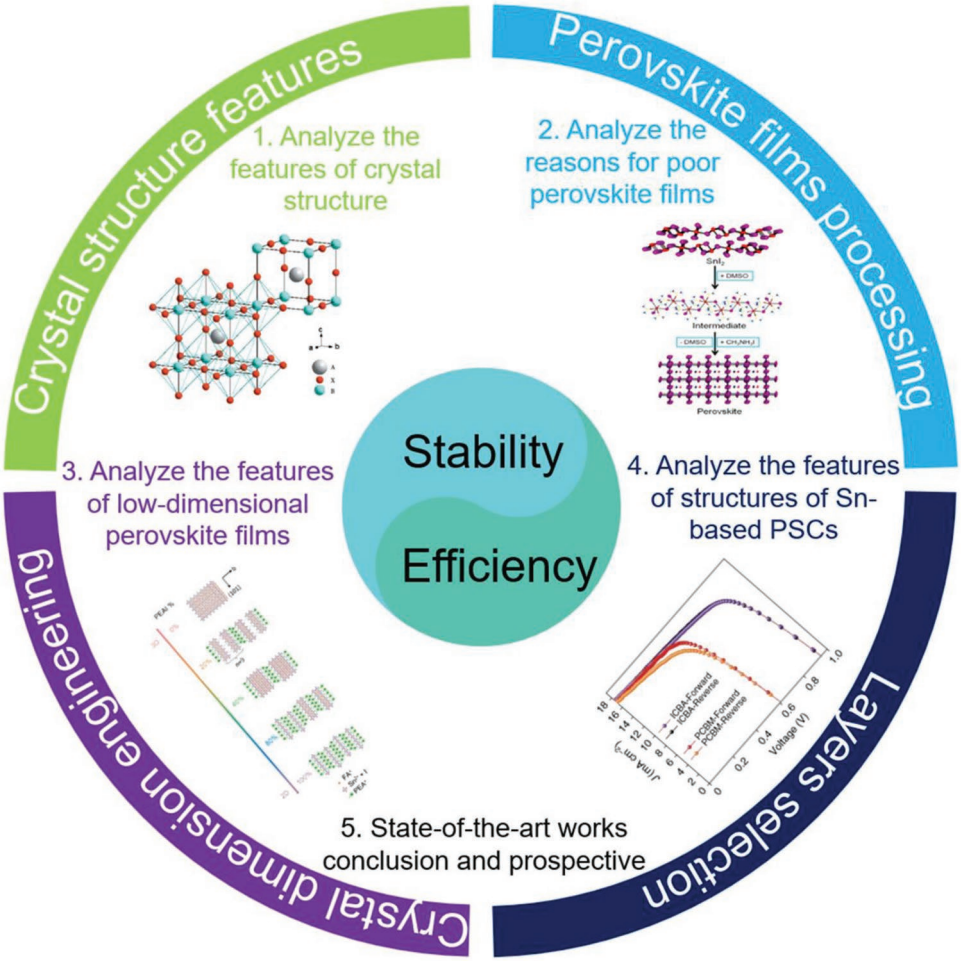

Figure 1. Schematic outline of the review. The copyright of insert pictures is all marked in the following article. Crystal structure features: Reproduced with permission.[45] Copyright 2007, International Union of Crystallography Printed in Singapore. Perovskite films processing: Reproduced with permission.[76] Copyright 2015, American Chemical Society. Crystal dimension engineering: Reproduced with permission.[160] Copyright 2017, American Chemical Society. Layers selection: Reproduced with permission.[180] Copyright 2020, Springer Nature Limited.

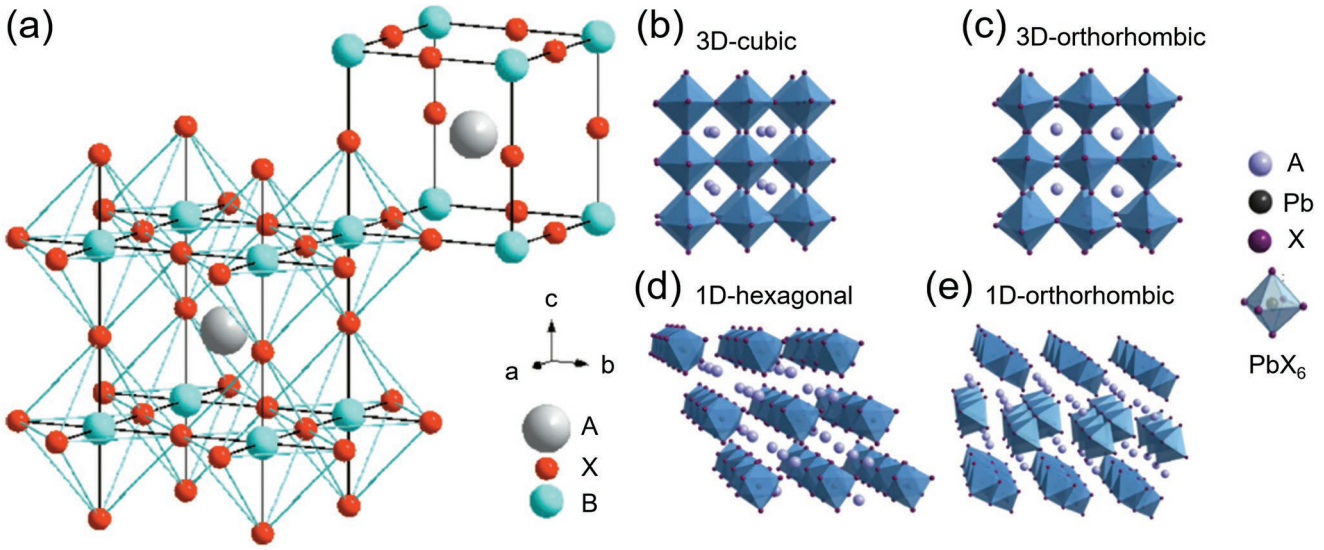

Figure 2. a) The cubic perovskite crystal structure. Reproduced with permission.[45] Copyright 2007, International Union of Crystallography. b) The cubic, c) 3D-orthorhombic, d) 1D-hexagonal, and e) 1D-orthorhombic perovskite crystal structure. Reproduced with permission.[46] Copyright 2017, American Association for the Advancement of Science.

are also discussed. Moreover, all film preparation and modification strategies for improving the properties of the Sn-based perovskite are categorized. As shown in **Figure 1**, we discuss the developments of Sn-based PSCs step by step by addressing four significant aspects: crystal structure features, perovskite film processing, low-dimensional structures, and layer selection. We systematically summarize the experimental steps, which provide a road map for future researchers. Moreover, the solvents and additives engineering are also discussed in detail. Besides, we summarize the device structures, optoelectronic parameters, and strategies used in previous work to provide a comprehensive state-of-the-art database for readers. Finally, we provide a perspective regarding the current research status and future possibilities in the pure Sn-based PSCs research field.

2. Crystal Structure Features

Numerous properties, such as high photoelectric coefficients, long carrier diffusion lengths and high defect tolerance, have been demonstrated for perovskite materials. Such properties are closely related to their crystal structure, leading to efficient solar cells.

Various crystal structures exist in perovskite materials. For example, the ideal crystal structure of ABX_3 perovskite consists of a cube system in space group $Pm\bar{3}m$.[44] As shown in **Figure 2**a, A cations with a larger radius occupy the body center of the cube where the 12-fold coordination site is, while the B cation with a smaller radius occupies the corner of the cube where the eightfold coordination site is, and X anions occupy the center of each edge of the cube.[45] The cubic system (Figure 2b) is the most common and favorable crystal system; being orthorhombic preserves the 3D connectivity (Figure 2c) possessing photoelectric and semiconducting properties, which may form due to octahedral tilting of the cubic perovskite structure.[44] However, perovskites can be crystallized in other crystal systems with inferior optoelectronic performance, such as 1D-orthorhombic and 1D-hexagonal structures (Figure 2d,e).[46] The crystal stability can also be evaluated by calculating the tolerance factor (t_{IR}). The t_{IR} is defined as:

$$t_{IR} = (R_A + R_X)/\left[\sqrt{2} \times (R_B + R_X)\right] \quad (1)$$

where R_A, R_B and R_X represent the ionic radii of A, B and X components. In the typical structure of the ABX_3 cube, the distance between B and X is equal to the side length of the crystal unit cell, and the distance between A and X is equal to the diagonal length of the crystal unit cell. Typically, the crystal structures with t_{IR} equals 1 are the most stable. However, according to the experimental data, the values of t_{IR} between 0.9–1 are a relatively stable state for ideal cubic structure, including FA^+ (radii of 2.53 Å), the MA^+ (radii of 2.17 Å) and Cs^+ (radii of 1.67 Å) cations.[47] Since the coordination number on the effective ionic radius and the required coordination number are not taken into account in some effective ionic radii[48,49] in 2007, Xue et al. calculated 376 ABX_3-type compounds based on the bond–valence model (BVM) and structure map technology, showing the t_{IR} is relatively stable between 0.822–1.139.[45] Only predicting the crystal structure by t_{IR} is not enough, and 74% of materials can be calculated as perovskite.[21] Subsequently, Bartel et al. accurately predicted 94% of perovskites by Equation (2):[50]

$$\tau = \frac{r_X}{r_B} - n_A \left\{ n_A - \frac{\frac{r_A}{r_B}}{lg\frac{r_A}{r_B}} \right\} \quad (2)$$

where nA is the oxidation state of A and r is the ionic radius. The radii of B site cations can also affect crystal structure. According to Palgrave et al.'s study, the radii of B-site cations must be greater than 0.41 times that of X-site anions.[21] There is an octahedral factor (μ) to judge whether B site cations are suitable for

the BX_6 octahedron structure; the 0.442 to 0.895 range is ideal for a stable perovskite structure. The μ is defined as:[51]

$$\mu = \frac{r_B}{r_A} \tag{3}$$

It is well agreed that the crystal phase stability can be determined by t_{IR}. However, besides this factor, other environmental factors, such as temperature and pressure, can also affect structural stability.[52] Besides the same properties between Pb-based and Sn-based perovskite films mentioned above, the lattice stability of Sn-based perovskites can be severely affected by exposure to environmental factors such as water and oxygen.[53,54] The stronger binding energy of Sn—O and H—I than Sn—I has also been accepted as the main reason for the instability of Sn-based perovskites by easily breaking the Sn—I bond and forming the Sn—O and H—I bonds instead.[55] Among the wide variety of Sn-based perovskites, cubic $MASnI_3$ composition is stable at more than 295 K[56] and converts into tetragonal at temperatures between 140 and 295 K.[57] However, it would crystallize in the orthogonal phase at temperatures lower than 110 K.[58] In contrast to $MASnI_3$, the $FASnI_3$ is an orientationally disordered cubic crystal structure because FA is not O_h site symmetry in the cubic perovskite structure. Besides, the FA has a more significant steric effect than MA because of the longer Sn—I bond (3.158 Å) in $FASnI_3$ than that in $MASnI_3$ (≈3.121 Å).[59] The $FASnI_3$ is a pseudo cubic *Amm2* crystal structure at 340 K and it has *Imm2* space group with an additional primitive monoclinic structure below 180 K.[8] However, Schueller et al. thought that the phase transition $FASnI_3$ happened from cubic $Pm\bar{3}m$ to tetragonal *P4/mbm* structures at a temperature between 225 and 250 K. Under 125 and 150 K, the $FASnI_3$ can be transferred to an orthorhombic *Pnma* structure.[60] While Kahmann et al. identified that the phase transition happened from a cubic phase to a tetragonal phase at around 255 K, and from the tetragonal phase to the orthorhombic phase at about 155 K.[61] Interestingly, the crystallographic phase of all-inorganic $CsSnI_3$ is also temperature-dependent and can be transferred from one phase to another by applying different temperatures (see **Figure 3**a). For example, the α converts to β phase at temperatures more than 440.5 K.[62] The migration of I^- can also affect the stability of the $CsSnI_3$ crystal structure, which could happen by inducing light and temperature to the perovskite film (see Figure 3b).[63] However, they emphasized that the β-$CsSnI_3$ possessed the best light stability.

3. Perovskite Films Processing

3.1. Raw Materials

The purity of the raw materials of the perovskite crystal greatly impacts the device's efficiency. For example, FAI, SnI_2, MAI, and CsI are the raw materials of Sn-based perovskite processing. However, the purity of SnI_2 in perovskite precursors could directly affect the perovskite films and PCE of resulting PSCs subsequently. As mentioned earlier, Sn^{2+} is the desired oxidation state of Sn perovskite precursors and films; however, the existence of even a small amount of Sn^{4+} in the perovskite precursors reduces the film's quality and device performance, significantly. Therefore, the purity of the perovskite precursors is crucial for efficient Sn-based perovskite processing. Since the production and packaging environments could be different for every company, it should be considered that SnX_2 must be produced and packed in a highly controllable oxygen-level environment; otherwise, the product oxidation, even partially, is undeniable. In this regard, Mathews et al.[64] pointed out that SnI_2 with a purity of 99% and even 99.999% is not sufficient to achieve a high-quality film due to inducing high content of unfavorable SnI_4, that is, Sn^{4+}, into the perovskite precursor. Based on this, analyzing the purity of SnI_2 precursor became an important topic in the Sn-based perovskite research, avoiding any undesirable chemical reaction in the perovskite precursor and the resulting films. For example, Kanatzidis et al.[65] confirmed that self-synthesized SnI_2 with vacuum purification leads to better Sn-based perovskite quality. However, it has been confirmed that higher purity could be achieved for self-synthesized SnI_2. However, most researchers still have to process the Sn-based perovskites by using the commercial SnI_2 due to the synthesis limitation in some laboratories. For this reason, researchers tried to improve the quality of the commercial SnI_2 precursor. For instance, Huang et al.[66] demonstrated that adding a small amount of metallic Sn powder to a perovskite precursor solution containing low-purity SnI_2 could convert all the Sn^{4+} content to Sn^{2+} by catalyzing the redox reaction, leading to high-quality Sn-based perovskite films that are even better than the perovskite precursor solution containing high purity SnI_2 (99.999%). To reduce the cost of the raw materials and suppress the Sn^{2+} oxidation, Ning et al.[67] proposed an in situ reaction between metallic Sn and I_2 in dimethyl sulfoxide (DMSO), and *N*,*N*-dimethylformamide (DMF) to prepare high-quality Sn-based perovskite films with an electron diffusion length of 290 ± 20 nm. The fabricated devices delivered a PCE of 14.6%. The in situ reaction and the preparation process of perovskite film are shown in **Figure 4**. Besides, the Sn-based perovskite film can also vertically grow by using an in situ reaction of SnI_2.

3.2. Ideal Solvent

In the Pb-based PSCs, DMSO, and DMF have been frequently used as the primary solvents for perovskite solution preparation.[68–73] According to the Lewis acid–base theory, Sn^{2+} has a stronger Lewis acidity than Pb^{2+}.[74,75] Hence SnI_2 can react with the organic ammonium cations rapidly, leading to an uncontrollable perovskite crystallization and discontinuous film fabrication with many pinholes. As a result, this low-quality film showed low resistance against water or oxygen with a large leakage current in the resulting devices. So, it can be concluded that only using DMF as the solvent for Sn-based perovskites precursor solution might not be suitable. Therefore, numerous solvents have been explored to prepare an ideal Sn-based perovskite solution. For example, in 2015, Kanatzidis et al. analyzed four kinds of solvents such as DMF, DMSO, γ-butyrolactone (GBL), and *N*-methyl-2-pyrrolidone (NMP). They confirmed that the perovskite crystallization rate with DMSO was much slower than others, which led to a better intermediate phase of SnI_2-DMSO and a pinhole-free $MASnI_3$ film, subsequently.[76] **Figure 5**a shows the

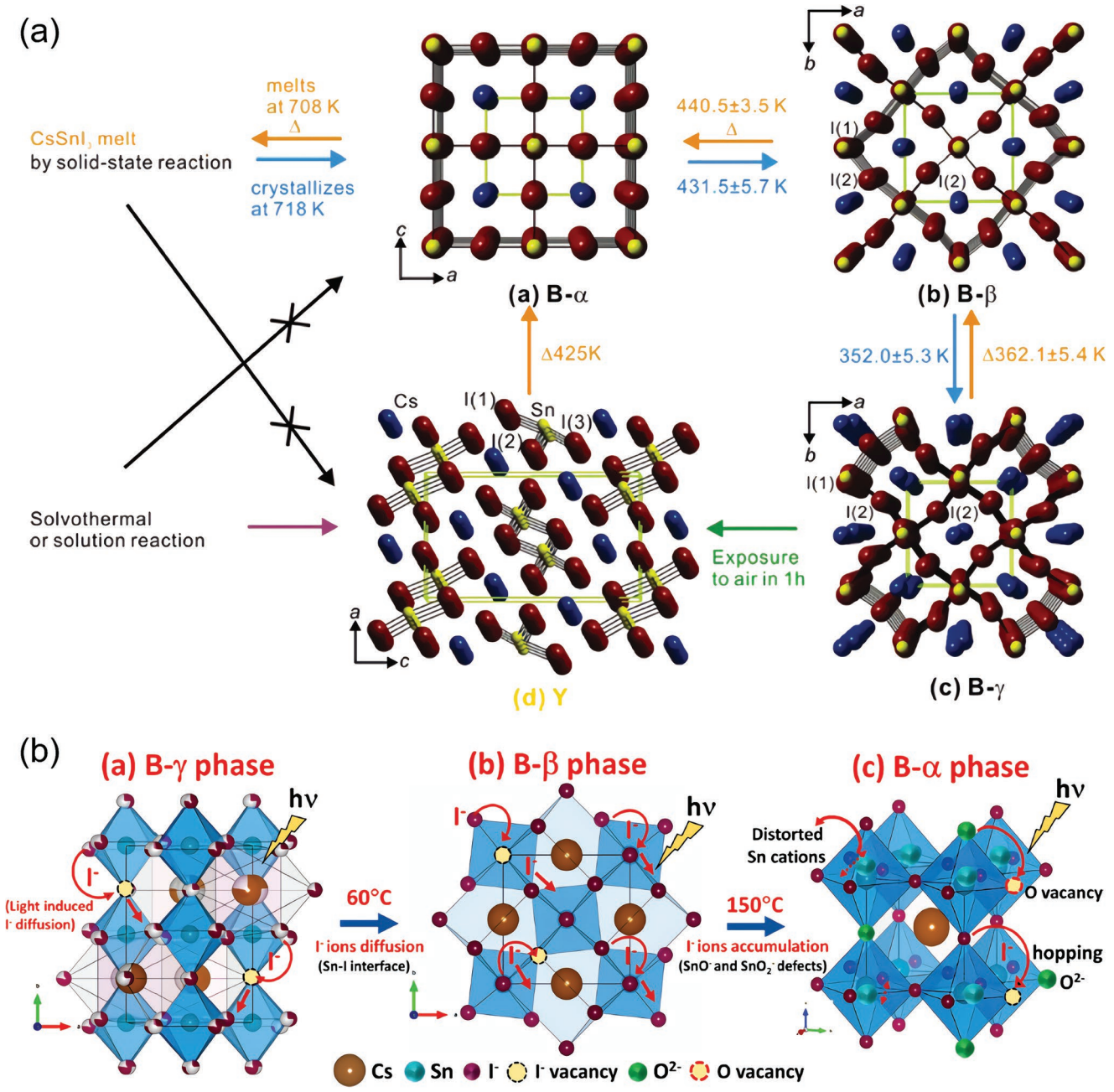

Figure 3. a) The different $CsSnI_3$ crystal structures and their conversion conditions. Reproduced with permission.[62] Copyright 2012, American Chemical Society. b) The mechanism of I^- migration is due to the light and temperature. Reproduced with permission.[63] American Chemical Society.

process of preparing perovskite film using DMSO solvent. Although DMSO is beneficial to the preparation of 3D Sn-based perovskite films,[76] it is not suitable for the processing of low-dimensional Sn-based perovskites. In low-dimensional films, the long-chain organic molecules can further retard the crystallization of perovskite, resulting in poor film coverage.[77–79] However, the ion liquid solvent methylammonium acetate (MAAc) was introduced as an ideal solvent, yielding a dense and high-roughness low-dimensional perovskite film through an ion exchange mechanism.[80] In this regard, Huang et al.[33] utilized a mixed solvent of DMSO and MAAc to fabricate high-quality low-dimensional Ruddlesden–Popper (LDRP) Sn-based perovskite films with large grains of up to 9 µm (Figure 5b). Finally, the fabricated devices have shown excellent stability upon storage in the glove box for 94 days. Interestingly, Abate et al.[81] pointed out another challenge of using DMSO as a solvent for Sn-based perovskite precursor solutions. They demonstrated that DMSO could accelerate the Sn^{2+} oxidation during dissolving the precursor powders at 100 °C in 30 min, turning the solution color from orange to dark red (Figure 5c). The Abate group[82] reported 12 possible solvents from a database of over 2000 solvents, which could be

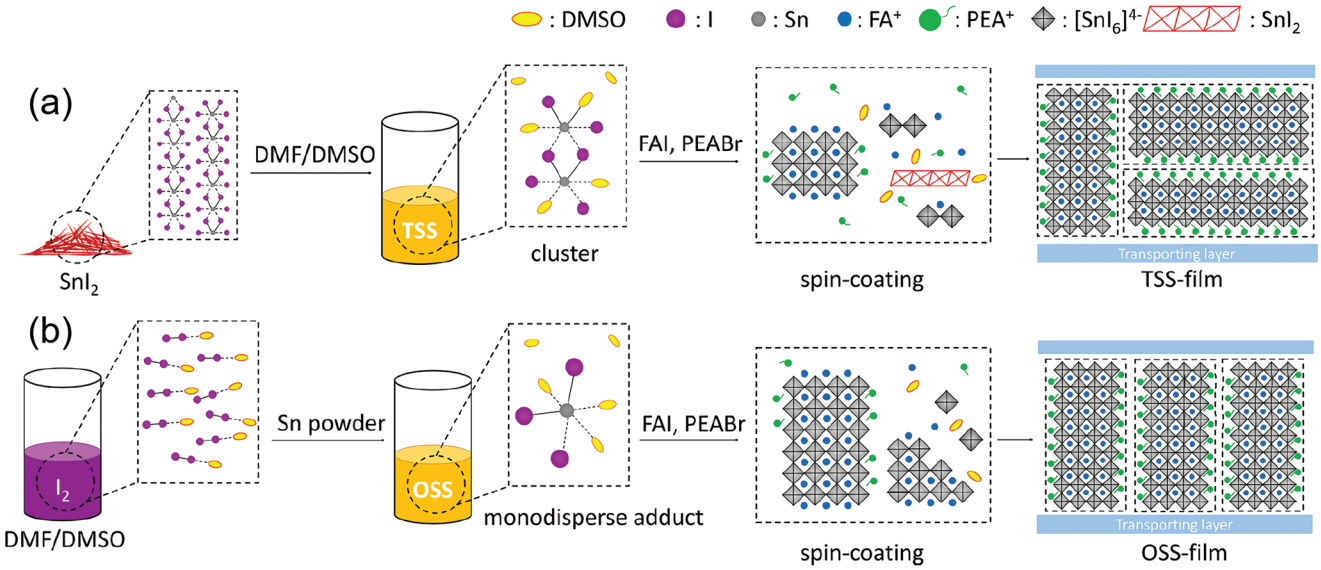

Figure 4. The schematic diagram of the preparation of Sn-based perovskite film with a) SnI_2 powder b) in situ reaction between metallic Sn and I_2. Reproduced with permission.[67] Copyright 2021, American Chemical Society.

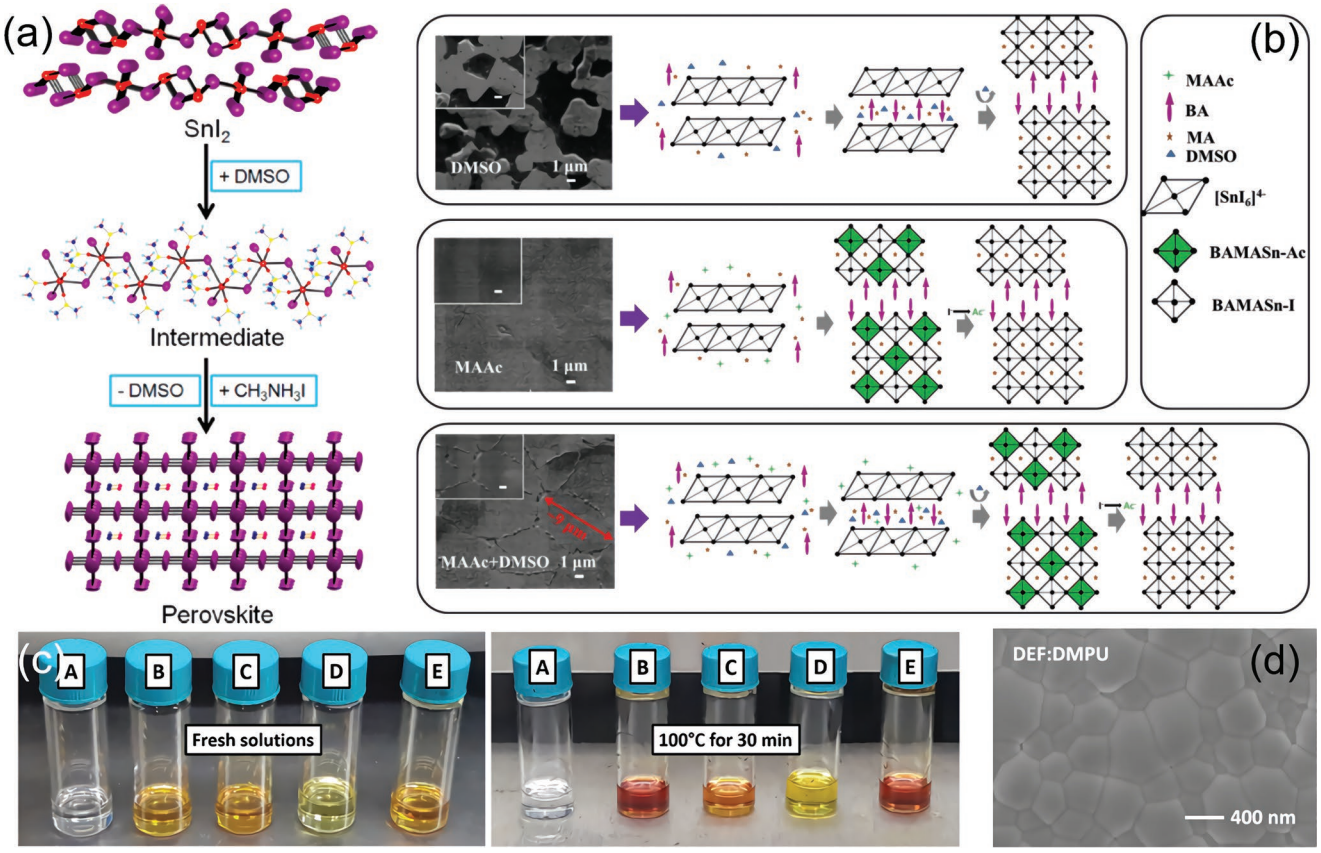

Figure 5. a) A process of the film's formation of the $CH_3NH_3SnI_3$ perovskite films when DMSO is the precursor solvent. Reproduced with permission.[76] Copyright 2015, American Chemical Society. b) SEM images and schematic diagram of prepared perovskite films using DMSO, MAAc, and mixture solvent with MAAc and DMSO. Reproduced according to the terms of the CC-BY license.[33] Copyright 2018, The Authors. Published by WILEY-VCH. c) (A–E) were FAI, SnI_2, and $FASnI_3$ with 10% SnF_2 and $CsSnI_3$ in DMSO, and $FASnI_3$ in DMF, respectively. The left picture was a fresh solution; The right picture was a solution under 100 °C annealing for 30 min. Reproduced with permission.[81] Copyright 2020, The Royal Society of Chemistry. d) SEM images of processed $FASnI_3$ films using a mixing solvent with DEF and DMPU. Reproduced with permission.[82] Copyright 2021, American Chemical Society.

used as suitable candidates for $FASnI_3$ solution preparation. As shown in Figure 5d, using a mixture of *N,N*-dimethylformamide (DEF) and dimethylacrylic urea (DMPU) solvents are beneficial to fabricating high-quality Sn-based films due to better solubility, stability, and crystallization.

The mixed DMF and DMSO solvent can also prepare high-quality perovskite films. Kanatzidis et al.[83] and Seok et al.[84] separately demonstrated that dissolving the perovskite precursor material in a mixed solvent of DMF:DMSO with volume ratios of 9:1 and 4:1 leads to better controlling the crystallization process and achieving higher quality films. Therefore, we think both DMSO and DMF:DMSO mixed solvents are suitable for perovskite film processing. However, the mixed DMF:DMSO is more ideal for preparing Sn-based perovskite films and high efficiencies PSCs.[29,67]

3.3. Ideal Antisolvent

Using the antisolvents is necessary to extract the solvents from perovskite precursors more efficiently during the spin-coating process, assisting in more uniform nucleation.[85–90] So far, chlorobenzene (CB) and toluene (TL) have been frequently used as antisolvent for different perovskite films.[91–97] However, Yan et al.[37] proposed diethyl ether (DE) as a better alternative for Sn-based perovskite crystallization. They demonstrated that DE could better retard the $FASnI_3$ perovskite crystallization compared to CB or toluene, which leads to better film quality. Additionally, Huang et al.[34] compared the effects of DE, toluene, and CB antisolvents on $FA_{0.75}MA_{0.25}SnI_3$ perovskite films crystallization. **Figure 6**a–d shows the scanning electron microscopy (SEM) images of the formed films without antisolvent and

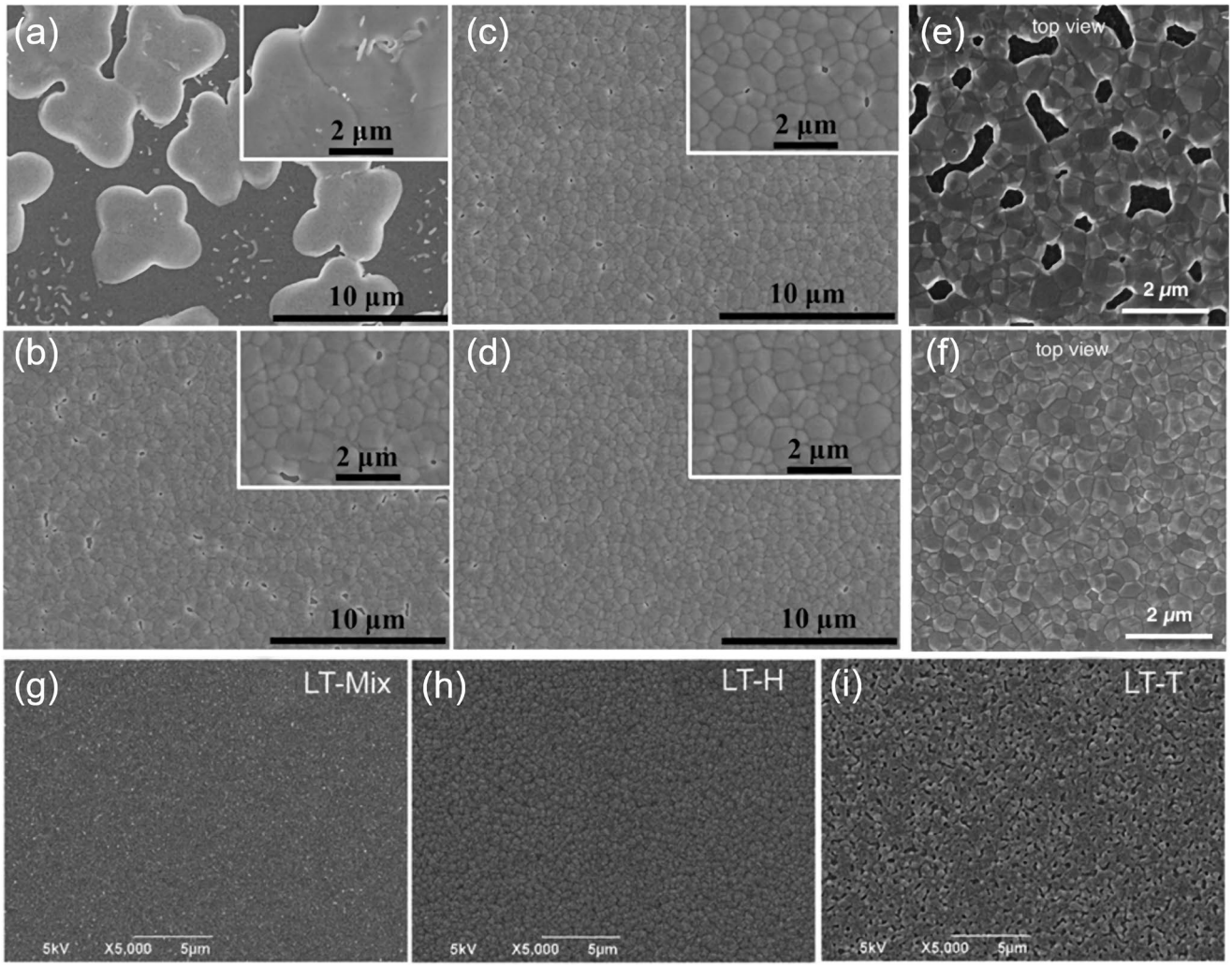

Figure 6. SEM images of $FA_{0.75}MA_{0.25}SnI_3$ films at different antisolvent conditions a) without antisolvent, b) with DE, c) with TL, and d) with CB. Reproduced with permission.[34] Copyright 2018, American Chemical Society. SEM images of $FA_{0.75}MA_{0.25}SnI_3$ films adopting different temperatures CB as antisolvent e) at room temperature and f) at 65 °C. Reproduced with permission.[35] Copyright 2018, WILEY-VCH. SEM images of $MASnI_3$ using antisolvent bathing with different antisolvent g) with 1:1 mixed toluene and hexane, h) with toluene, and i) with hexane. Reproduced with permission.[98] Copyright 2017, The Royal Society of Chemistry.

using antisolvents, demonstrating that CB provides the dense films without pinholes, which is in contrast to the observation by Yan et al.[37] The fabricated $FA_{0.75}MA_{0.25}SnI_3$ PSCs with CB showed significant stability (maintained up to 75% of the original PCE over 30 days under glove box conditions). This could be due to the achieving uniform and fully packed perovskite films. Therefore, it can be concluded that the performing of antisolvents might also be related to the perovskite composition. Additionally, the functionality of CB during Sn-based perovskite crystallization could be affected by its temperature. For example, Wakamiya et al.[35] explored the effect of CB temperature on Sn-based perovskite film formation. They demonstrated that uniform and pinhole-free films could be achieved with 65 °C preheated CB, leading to significant device stability over 70 h under glovebox conditions (Figure 6e,f). Besides dropping antisolvents during the spin coating, antisolvent bathing (ASB) has been introduced to facilitate Sn-based perovskite crystallization. In this regard, Adachi et al. explored the effect of mixed toluene and hexane ASB on the perovskite films crystallization. The resulting films showed a low thickness of 123 nm compared to pure toluene and hexane ASB, but with higher density and pinhole-free morphology (see the SEM images in Figure 6g–i).[98] By comparison, CB is a commonly used and most effective antisolvent. Therefore, we recommend CB as the preferred antisolvent because it has been the most frequently used antisolvent to achieve a more controllable deposition process.

3.4. Processing Methods

3.4.1. One-Step Method

The preparation methods of perovskite films can be divided into the one-step method, two-step method, vacuum deposition, etc. In the one-step method, all the perovskite components should be dissolved into a solvent to form a homogeneous precursor solution; then perovskite film will be spin-coated onto the substrates in one step followed by annealing the films. This method is currently the most mature process for achieving highly efficient and stable Sn-based PSCs. However, the fast crystallization of Sn-based perovskite is the most important challenge to using this method for film fabrication. Therefore, the proper selection of solvents, antisolvents additives and annealing temperatures are critical to achieving a high-quality perovskite film, as outlined in the other parts of this work.

3.4.2. Two-Step Method

The two-step method was mainly used for preparing Pb-based perovskite films but was less frequent for Sn-based perovskites. In this method, first, PbI_2 or SnI_2 should be deposited on the substrates by spin coating. Subsequently, FAI, MAI or other types of cations should be spin-coated on the prepared PbI_2 or SnI_2 films, followed by an annealing process. In this method, the solvent selection for PbI_2 or SnI_2 and organic cations is very challenging. Because the solvent in the second step should not dissolve the metal halide film excessively. For example, the solubility of SnI_2 in isopropanol, IPA, (solvent of organic cation) is higher than that of PbI_2, therefore, using a two-step method for depositing Sn-based perovskites is a bit tricky. First, in 2017, Jen et al.[99] prepared $FASnI_3$ perovskite film by two-step method. Trimethylaluminum (TMA) and a small amount of SnF_2 (10 mol%) were added to the SnI_2 precursor solution to form a SnI_2–TMA complexes and retard the $FASnI_3$ film crystallization based on Lewis's theory.

Afterward, Diau et al.[100] developed a novel two-step deposition method for achieving high-quality $FASnI_3$ film. First, the SnI_2 solution in DMSO was deposited on the substrate to form SnI_2 film. Then the FAI solution in a mixed solvent of hexafluoro-2-propanol (HFP):IPA:CB with 5:5:2 ratio was deposited on the SnI_2 film (see **Figure 7**a). They emphasized that HFP is necessary to slow down the $FASnI_3$ film crystallization by forming hydrogen bonding with IPA and FAI. The stability of devices with the modified film was more than 4000 h in the glove box. So, selecting the solvent of the second step solution is indispensable to preserve favorable solubility and guarantee not destroying the SnI_2 film.

3.4.3. Thermal Evaporation

In contrast to the one-step method, the prepared films by thermal evaporation deposition have shown more uniform and controllable thickness. However, the performance of such a prepared device is lower than the solution-based methods. This method has been used for the deposition of Sn-based perovskites as well. In this regard, Qi et al.[101] deposited $MASnBr_3$ perovskite films with relatively high quality and stability by a continuous thermal evaporation method. Afterward, Yan et al.[102] also deposited $MASnI_3$ film utilizing this method with a relatively high open-circuit voltage (V_{OC}) of 494 mV with ITO/PEDOT:PSS/Poly[*N*,*N*′bis(4-butylphenyl)-*N*,*N*′-bis(phenyl)benzidine] (poly-TPD)/$MASnI_3$/fullerene (C_{60})/2,9-dimethyl-4,7-diphenyl-1,10-phenanthroline (BCP)/Ag device structure. Subsequently, Song et al.[103] proposed a novel ion-exchange/insertion reaction to obtain $MASnI_3$ film. The reaction process is shown in Equations (4)–(6). As shown in Figure 7b, $MASnI_3$ perovskite was formed on SnF_2/PEDOT:PSS substrate in the presence of MAI vapor. In this method, after forming $MASnI_3$ still most of the SnF_2 remains in the film, which can promote the formation of high-quality perovskite film with 7.78% device efficiency.

$$SnF_2 + 2CH_3NH_3I \rightarrow SnI_2 + 2CH_3NH_3F \quad (4)$$

$$CH_3NH_3F \rightarrow CH_3NH_2 \uparrow + HF \uparrow \quad (5)$$

$$SnI_2 + CH_3NH_3I \rightarrow CH_3NH_3SnI_3 \quad (6)$$

Besides the organic–inorganic Sn-based perovskite, all-inorganic Sn-based perovskites such as $CsSnI_3$, $CsSnCl_3$, and $CsSnBr_3$ also can be deposited by this method. For example, Lunt et al.[104] deposited $CsSnBr_3$ doped with a small amount of SnF_2 perovskite film by a thermal evaporation method. They demonstrated that a ratio of 1:1 of $SnBr_2$ and CsBr along with 2.5% SnF_2 could provide the best PCE with significant device stability in ambient conditions for 50 min. However, after 3 h, the PCE dropped to 50% of the initial value due to severe degradation. Besides, it should be mentioned that $CsSnI_3$ and

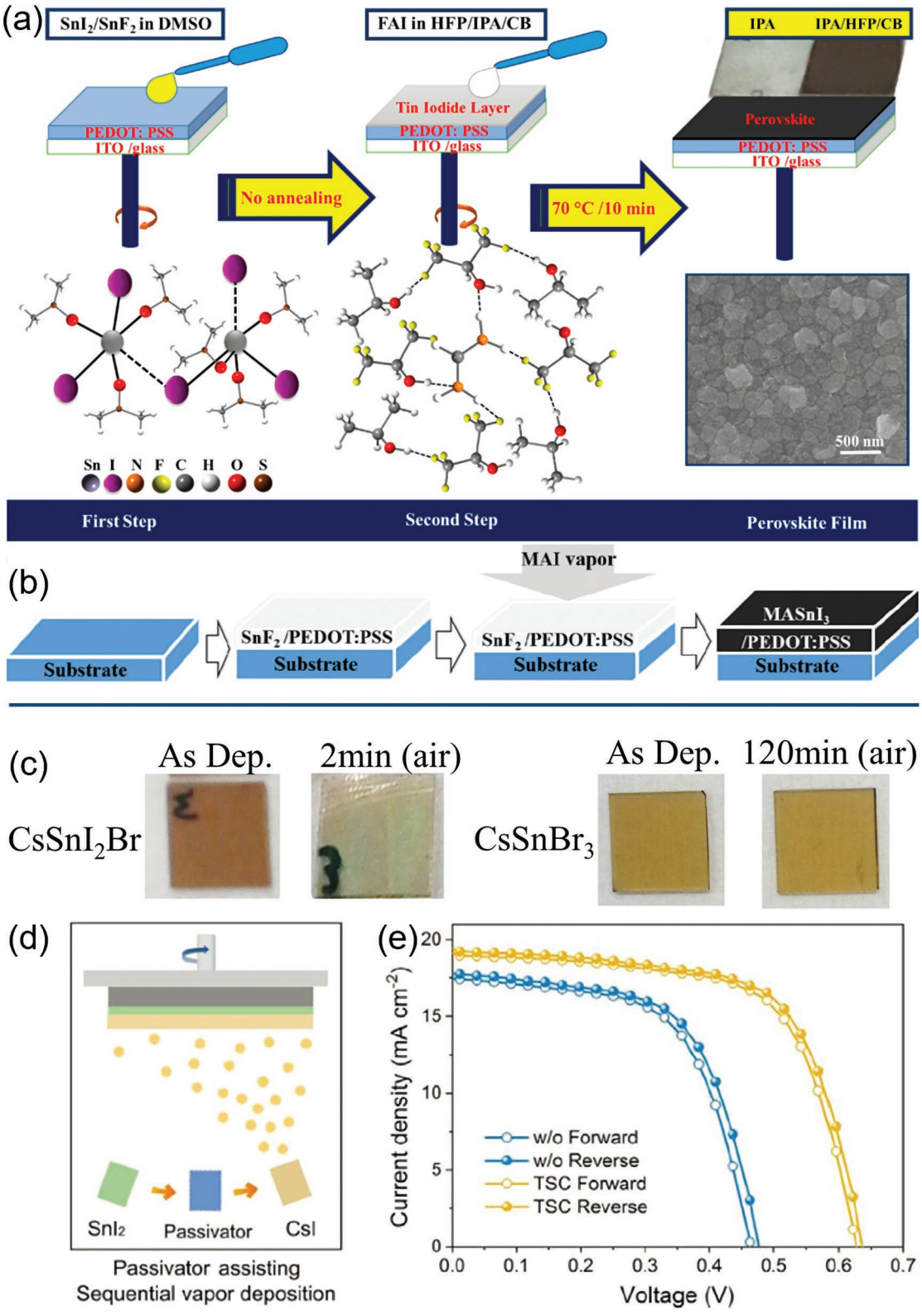

Figure 7. a) Schematic diagram of preparing $FASnI_3$ perovskite film using the two-step method. Reproduced with permission.[100] Copyright 2020, American Chemical Society. b) Using ion-exchange/insertion reaction process prepares perovskite films of $MASnI_3$. Reproduced according to the terms of the CC-BY license.[103] Copyright 2020, The Authors. Published by WILEY-VCH. c) Comparison of $CsSnI_2Br$ and $CsSnBr_3$ perovskite degradation in air. Reproduced with permission.[104] Copyright 2016, Elsevier Ltd. d) The steps of sequential vapor deposition. e) The *J*–*V* cures of devices. Reproduced with permission.[105] Copyright 2021, WILEY-VCH.

$CsSnCl_3$ are super sensitive to ambient condition and could be degraded in a few seconds. While $CsSnBr_3$ is relatively stable for several hours in ambient conditions. For example, as shown in Figure 7c, $CsSnI_2Br$ with mixed halides I^- and Br^- degrades completely after 2 min in the ambient condition, while the pure $CsSnBr_3$ shows no noticeable degradation over 2 h. Yin et al.[105] proposed the novel continuous thermal evaporation deposition to prepare high-quality $CsSnI_3$ film. They introduced thiosemicarbazide (TSC) as an additive to passivate uncoordinated Sn^{2+} by S=C−N functional groups. Figure 7d presents the deposition process. As shown in Figure 7e, a PCE of 8.2% was attained. Besides, 90% of the initial PCE was maintained after 500 h under continuous illumination. As the passivator of continuous thermal evaporation deposition, there are two criterions: i) easy to evaporate under high vacuum; and ii) specific reactions with perovskites. Compared with the prepared perovskite film using one-step and two-step methods, prepared films by thermal evaporation are more environmentally friendly and less toxic during preparation due to the absences of organic solvents. Therefore, Sn-based PSCs prepared by thermal evaporation may have good commercial application prospects.

3.4.4. Mixed Evaporation-Solution-Assisted Methods

The Sn-based perovskite films grown by the low-temperature mixed evaporation-solution-assisted methods have shown acceptable stability in ambient conditions compared to the traditional pure solution-based methods. However, the achieved PCEs are not as high as a conventional one-step method. But, the one-step method is not suitable for depositing all types of Sn-based perovskites. As proof of concept, Kanatzidis et al.[106] compared the characteristics of prepared $MASnI_3$ perovskite films by one-step method and low-temperature mixed evaporation-solution assisted method. According to the X-ray photoelectric energy spectrometer data, at the evaporation temperature of MAI (150 °C), I^- ions of MAI could not diffuse into the SnX_2 film (X = Br, I); as a result, Sn^{2+} ions could convert to SnO and $Sn(OH)_2$ secondary phases, leading to reduced hole carriers concentration and adjusting the Sn vacancies to improve the air stability of Sn-based perovskite. As shown in **Figure 8**a, the fabricated devices by the one-step method present a faster degradation in ambient conditions. Due to the extreme instability of $CsSnI_3$ perovskite, it is challenging to obtain uniform and pinhole-free films utilizing the traditional one-step thermal evaporation methods. Based on this, Zhu et al.[107] proposed a solution-assisted thermal evaporation method to grow the $CsSnI_3$ films successfully. The SnI_2 solution, including a small amount of SnF_2, was spin-coated onto the substrates, followed by the deposition of CsI by thermal evaporation. They demonstrated that the CsI thickness could affect the final coverage and compactness film. For example, the perovskite film with a CsI thickness of over 80 nm or below 60 nm led to poor surface morphology with many pinholes. Although the one-step preparation of Sn-based perovskite films has been relatively matured, however, developing new preparation methods is also worth promoting. Currently, the PCE of fabricated lead-based devices by thermal evaporation technology reached around 24%.[108] Therefore, by optimizing the thermal evaporation process, the efficiency of the Sn-based device could also exceed 14.81%.

As mentioned, overcoming oxidation is a major challenge in improving the stability of Sn-based perovskites.[109] Such Sn^{2+}oxidation lowers the current density (J_{SC}). To address this challenge, researchers have conducted various experiments. To summarize such experiments, the preparation of Sn-based perovskite films is assisted by reducing gases and reducing the Sn^{4+} cations during the preparation process. Hydrazine is well known as a reducing agent to suppress Sn^{2+}oxidation to a certain extent. For instant, Kanatzidis et al.[110] proposed hydrazine vapor to assist crystallization and grow stable Sn-based perovskite films. Hydrazine was directly dropped on the hot perovskite film to quickly volatilize the solvent, leading to a reduction reaction in the hydrazine atmosphere and reducing the ratio of Sn^{4+}/Sn^{2+}, improving J_{SC} from 5 to 19.9 mA cm^{-2}. Figure 8b shows the mechanism of the hydrazine vapor effect on Sn-based perovskites and the reaction process as Equation (7):

$$2SnI_6^{2-} + N_2H_4 \rightarrow 2SnI_4^{2-} + N_2 + 4HI \quad (7)$$

Some researchers have improved the quality of Sn-based perovskite films. The Sn^{4+} cation contents were reduced by ion exchange or polar gas-assisted film formation. According to Jiang et al.'s report, the high carrier concentration limited the overall PCEs of Sn-based PSCs due to the facile oxidation of Sn^{2+} to Sn^{4+}.[111] To improve the PCE, they designed a cation exchange method to synthesize high-quality $MASnI_3$ films. As schematically illustrated in Figure 8c, after deposition of hydrazinium Sn iodide ($HASnI_3$) perovskite on the substrates, they were exposed to methylamine vapor to exchange the HA^+ cations with MA^+ cations, obtaining a high-quality $MASnI_3$ perovskite film with a PCE of 7.13% and good reproducibility. It is well accepted that fast nucleation and slow crystal growth are preferred to achieve high-quality perovskite films with a low trap state density and smooth morphology. However, Sn-based perovskites usually suffer from uncontrolled random crystal orientation.[112,113] Based on this, Chen et al.[114] proposed an ethyl acetate (EA) vapor incubation nucleation strategy. As shown in Figure 8d, the EA solvent was dropped onto a glass substrate before film deposition to form a high-quality $FASnI_3$ perovskite with an excellent device performance of over 10%. Stability tests demonstrated that after 600 h light soaking, the modified devices remained at 83% of the initial PCE. Besides, the modified devices could maintain 80% of the initial PCE under N_2 atmosphere for 100 h.

Usually, the Sn^{2+} tends to oxidize and form its more stable Sn^{4+} analogue by breaking down the perovskite structure and decomposing the oxides/hydroxides of Sn. Recently, Zhou et al.[115] introduced chemo-thermal removal of the Sn(IV) *p*-type dopant from the Sn-based perovskite film.[116] Besides, they found the Sn^{4+} mainly accumulated in the surface regions of Sn-based perovskite films ($FA_{0.75}MA_{0.25}SnI_3$), resulting in an inferior perovskite film. As shown in Figure 8e, the FACl was vapored onto the neat $FA_XMA_{1-X}SnI_3$ surface to generate a volatile $SnI_4 \cdot x$FACl compound at 60 °C. By contrast, the

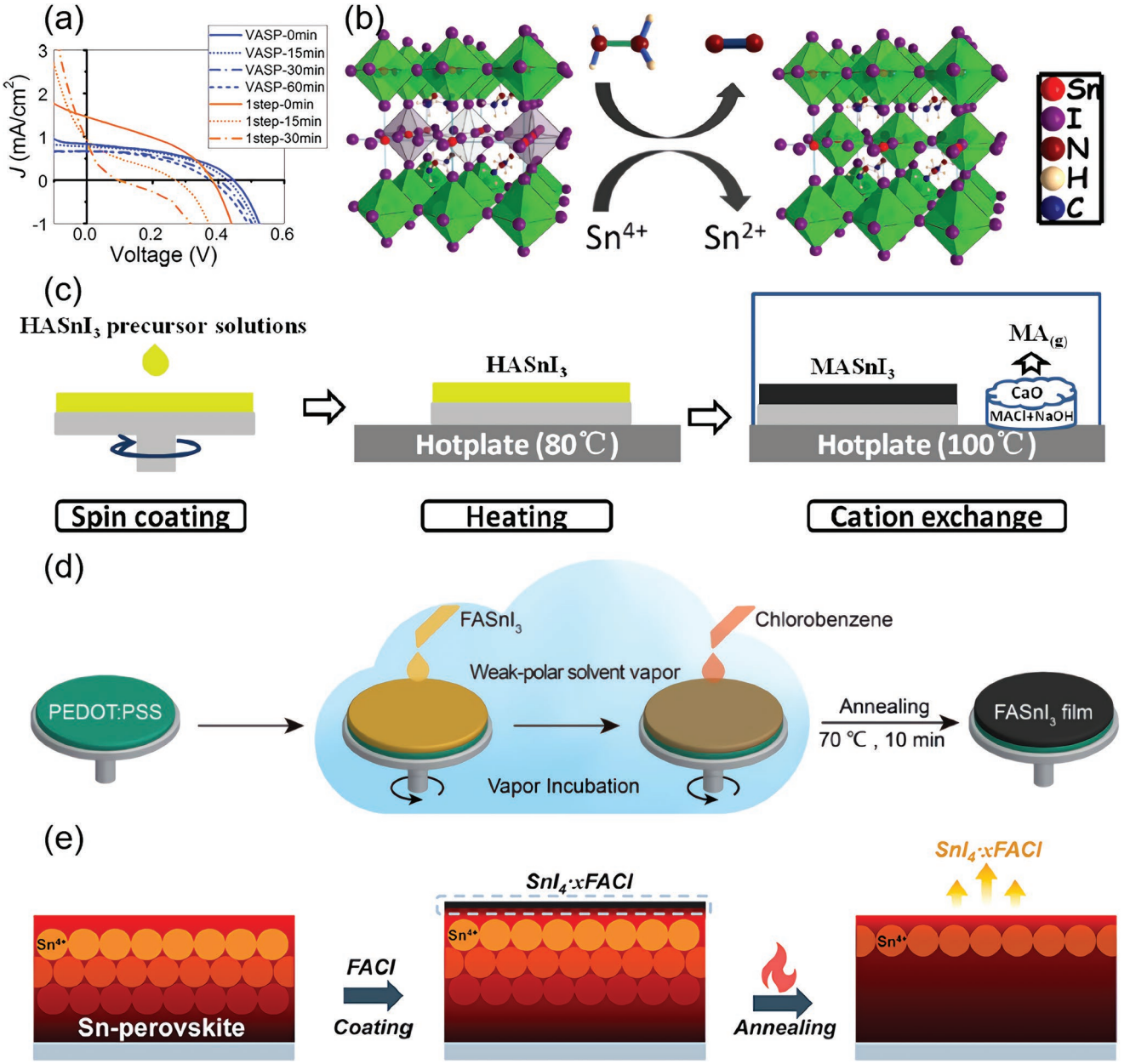

Figure 8. a) Comparison of the stability of devices prepared by the one-step method and low-temperature vapor-assisted methods. Reproduced with permission.[106] Copyright 2016, American Chemical Society. b) Mechanism of hydrazine vapor effect on Sn-based perovskite materials. Reproduced with permission.[110] Copyright 2016, American Chemical Society. c) Schematic of a cation exchange between HA^+ and MA^+. Reproduced with permission.[111] Copyright 2019, WILEY-VCH. d) Schematic of EA vapor incubation nucleation. Reproduced with permission.[114] Copyright 2021, The Royal Society of Chemistry. e) Schematic of chemo-thermal removal of the Sn(IV) *p*-type doping. Reproduced with permission.[115] Copyright 2021, Elsevier Inc.

carrier lifetime of the modified perovskite film was enhanced threefold than the control film, and the trap density was reduced twofold. The devices with modified perovskite film attained a PCE of 14.7% and maintained 95% of the initial PCE under glovebox conditions after 1000 h. Ion exchange is also an excellent approach to preparing high-quality perovskite films. It uses chemical reactions to reduce defects in thin film preparation.

3.5. Additives

3.5.1. Inorganic Additives

Adding different materials to perovskite precursor solution or into the films during the formation process has been introduced as an efficient approach to improve the quality of perovskite films.[117,118] Additives can passivate the defect states,

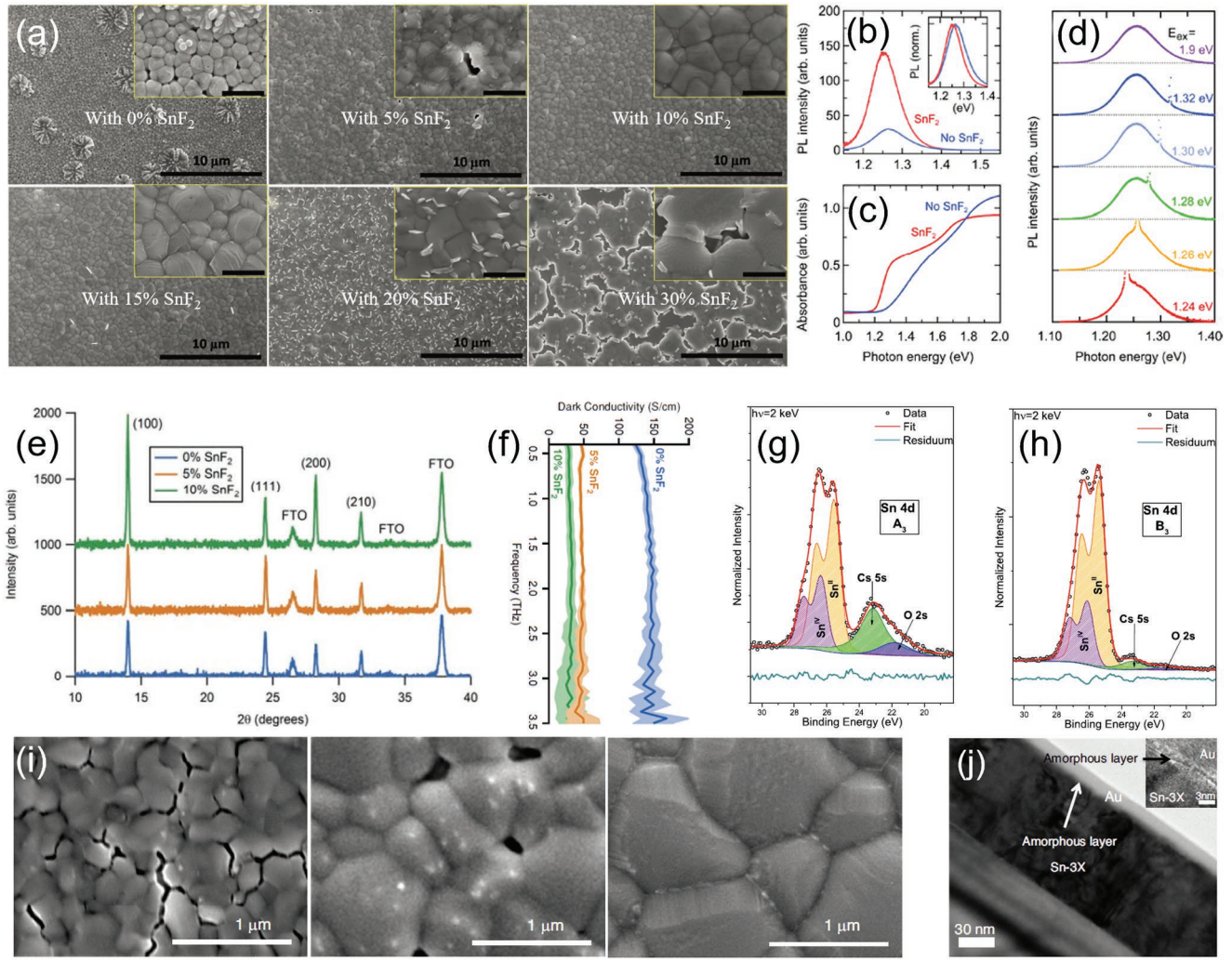

Figure 9. a) SEM images of $FASnI_3$ perovskite films with different concentrations of SnF_2. Reproduced with permission.[37] Copyright 2016, WILEY-VCH. b) PL spectra of, c) absorption spectra of different perovskite films, and d) PL spectra of perovskite films with SnF_2 under excitation wavelength. Reproduced with permission.[119] Copyright 2017, American Chemical Society. e) X-ray diffraction (XRD) images and f) dark conductivity spectra for $FASnI_3$ perovskite films with different concentrations of SnF_2. Reproduced according to the terms of the CC-BY license.[123] Copyright 2018, The Authors. Published by WILEY-VCH. The near-surface bulk-sensitive synchrotron-based hard X-ray photoelectron spectroscope (HAXPES) spectra of g) $CsSnBr_3$ perovskite films and h) $CsSnBr_3$ perovskite films with SnF_2. Reproduced with permission.[124] Copyright 2020, American Chemical Society. i) SEM images of Sn-1X, Sn-2X, and Sn-3X and j) TEM and HRTEM (inset) images for Sn-3X films. Reproduced according to the terms of the CC-BY license.[125] Copyright 2020, The Authors. Published by Springer Nature Limited.

improve the antioxidant properties of Sn-based perovskites, as well as controlling the nucleation rate. Tin halides are common inorganic additives that could be added to precursor solutions alone or mixed with other substances to improve the film quality. For Sn-based perovskite, SnF_2 is an indispensable additive because SnF_2 has excellent oxidation resistance to prevent further oxidation of Sn-based perovskite films, and F^- also has a certain hydrophobicity, standing as an excellent additive. In 2014, Mathews et al.[64] found that a modest amount of SnF_2 decreased the Sn vacancies in $CsSnI_3$ crystals. Although SnF_2 could not effectively control the yellow phase formation of $CsSnI_3$, but it could reduce the influence of the yellow phase on the perovskite properties to some extent. Another benefit of SnF_2 could be providing full contact with the $CsSnI_3$ without negatively affecting its crystal lattice. Finally, the J_{SC} of modified devices was extremely improved from 0.19 to 23.5 mA cm^{-2}, resulting in the PCE from 3×10^{-4}% to 2.02%. Yan et al.[37] studied the effect of adding a mixed-solution of SnF_2 and DEE to the $FASnI_3$ precursor solution. **Figure 9**a shows the effect of SnF_2 content on the film's morphology at six different concentrations of 0%, 5%, 10%, 15%, 20%, and 30%. The fabricated inverted PSCs with 15% SnF_2 achieved the highest PCE of 6.2%. Kanemitsu et al.[119] demonstrated that adding SnF_2 to $MASnI_3$ solution leads to a shift in the absorption edges of perovskite to low photon energy (see Figure 9b,c), promising higher luminescence efficiency. Besides, the width of the photoluminescence peaks does not change at different exciting energies (see Figure 9d), meaning the stronger electron–photon coupling.[58,120–122] Moreover, Kanatzidis et al.[65] revealed the antioxidant ability of SnF_2, which as an additive, could suppress the Sn^{4+} formation and reduce the defects formation, and improve the carrier diffusion length. Herz et al.[123] also found

that SnF_2 could eliminate pinholes in the perovskite films by improving the crystallization processes (see Figure 9e). Besides, SnF_2 also reduces the conductivity of the perovskite films by changing the doping concentration (see Figure 9f). Although SnF_2 as an additive has many advantages, using a nonproper amount of this additive could form plate-like aggregates in the perovskite films. To address this challenge, Seok et al.[84] suggested use of pyrazine along with SnF_2 as co-additive in the perovskite precursor, which leads to a dense perovskite film without any aggregation. Additionally, Bar et al.[124] explored the effect of SnF_2 on the chemical and electronic structures of $CsSnBr_3$ perovskite. By adding 20% SnF_2 to the precursor solution, a uniform film with good coverage on the TiO_2 layer was formed. As shown in Figure 9g,h, the O2s signal of TiO_2 (left) vanished after adding SnF_2 (right). This demonstrates the full coverage perovskite films and reduced the Sn^{2+} to the Sn^{4+} conversion ratio. Han et al.[125] introduced a stable amorphous-polycrystalline structure of triple-halide $CsFASnX_3$ ($X = I^-$, F^-, Cl^-) perovskite films. They explored the morphology of different Sn-based perovskites with the Sn-X ($CsFASnI_3$ with I^- only), Sn-2X ($CsFASnI_3$-10 mol% SnF_2; $F^-$and I^-), and Sn-3X ($CsFASnI_3$-10 mol% SnF_2-20 mol% $SnCl_2$; F^-, Cl^-, and I^-) (see SEM images in Figure 9i). The Sn-3X showed the pinhole-free and high-quality perovskite films. The transmission electron microscopy (TEM) and magnified high-resolution TEM (HRTEM) (inset) images for amorphous-polycrystalline structure are shown in Figure 9j, revealing an amorphous layer with the thickness of 3–4 nm on polycrystalline perovskite. Finally, the fabricated PSCs with Sn-3X perovskite films showed over 10% PCE and maintained 95% of their initial PCE under maximum power point (MPP) tracking for 1000 h. We believe that SnF_2 is essential for preparing high-quality tin-based perovskite films, and according to experiments, the optimal amount of SnF_2 additive should be between 10% and 20%.

3.5.2. Organic Additives

Organic additives can be divided into two categories. The first category is amine-based additives, and the second category is other additives. Amine-based molecules have been introduced as effective additives, including PEABr,[126] F-PEABr,[29] phenyl ethylammonium chloride (PEACl),[127] etc. These additives have been confirmed to enter the perovskite lattice and divide the perovskite into low-dimensional perovskites; however, some of them have only been used as auxiliary additives. These additives generally act on perovskites through hydrogen bonding or based on Lewis acid–base theory. Different additives from this category have been used for solving different problems in Sn-based perovskites such as the tin halides aggregation, the fast crystallization, the instability challenges.

To solve the aggregation problem of tin halides, He and co-workers[128] found that using the SnF_2 additive alone could cause segregation on the surface of Sn-based perovskite films. Therefore, they introduced 2,2,2-trifluoroethylamine hydrochloride (TFEACl) as a co-additive to eliminate surface segregation and improve the quality of the films. Similarly, Yan et al.[129] improved the film quality by adding gallic acid (GA) to $SnCl_2$ in Sn-based perovskite solution as a co-additive ($SnCl_2$-GA). Although $SnCl_2$ is essential to inhabit Sn^{2+}, however, the superfluous $SnCl_2$ harms charge transport in final films. While GA not only eliminates the adverse impact of superfluous $SnCl_2$ but also protects the perovskite grains. As schematically shown in **Figure 10**a, the presence of GA suppresses the $SnCl_2$ aggregation during the perovskite crystallization, leading to PCE of 9.03% and remaining ≈80% of the initial PCE after 1000 h storage in 20% relative humidity.

To solve the problem of Sn^{2+} oxidation, Islam and his collaborators[130] added SnF_2-N_2H_5Cl to the Sn-based perovskite precursor to form a co-additive system. In this system, hydrazine ion provides electrons to inhibit Sn^{2+} oxidation, thereby creating a pinhole-less perovskite film, reaching 5.4% PCE with the remaining 65% of original PCE after 1000 h in the N_2 glovebox. The influence of ammonium hypophosphite (AHP, $NH_4H_2PO_2$) as an additive on Sn-based perovskite was studied by Yan and co-workers.[131] They related the improved film morphology in the presence of AHP to the antioxidation role of H_2PO^{2-} and inhibiting the Sn^{2+} oxidation. They used CuSCN as the HTL to achieve better energy alignment matching with perovskite, leading to a PCE of 7.34%. Hydroxybenzene sulfonic acid or salt could also be used for Sn-based perovskite films because their functional groups could prevent Sn^{2+} oxidation. Yan and co-workers[132] also studied the effects of the following three molecules, phenolsulfonic acid (PSA), 2-aminophenol-4-sulfonic acid (APSA), and the potassium salt of hydroquinone sulfonic acid (KHQSA) as co-additives on Sn-based perovskites. The results demonstrated that they could form complexes by reacting sulfonic acid in their structures with Sn^{2+} ions, which is beneficial for creating smooth pinhole-free films by suppressing aggregation and phase separation. Different anions and cations with coordination could also play an important role in inhibiting Sn^{2+} oxidation. In this regard, Oh et al.[133] found that coordination of SCN^- ions (FASCN additive) to Sn^{2+}could improve the reproducibility and stability of Sn-based PSCs. The fabricated PSC with perovskite precursor containing FASCN and SnF_2 obtained a PCE of over 8%. Bidentate ligand 8-hydroxyquinoline (8-HQ) is an antioxidant, and N and O in its structure could coordinate with Sn^{2+} ions to improve the antioxidant properties of Sn-based perovskite.[134] Generally, the addition of antioxidants mainly selects additives with reducing groups, such as sulfonic acid groups, phosphoric acid groups, etc.

The migration of I^- ions is an important factor affecting the stability of the device. To stabilize the tin-based perovskite phase, it is necessary to suppress the migration of these ions. To solve the I^- migrating problem, recently, Mora-Seró et al.[135] added dipropylammonium iodide (DipI) and sodium borohydride ($NaBH_4$) into the $FASnI_3$ precursor solution to reduce iodine loss. As shown in Figure 10b, the Sn^{4+} reacted with I^- to form I_2 gas, while the DipI and $NaBH_4$ can inhibit the I^- migrating to the surface. The fabricated PSCs with modified perovskite films showed almost no decay in the initial PCE after 5 h under 60% relative humidity. Besides, the devices maintained 95% of the initial PCE after 1300 h under inert glovebox conditions.

Sn-based perovskites often suffer from poor film quality due to the fast crystallization rate, so it is crucial to control the crystallization. That is why researchers have conducted studies on crystal formation dynamics. To address this challenge, Jen et al.[99] formed Lewis acid–base complexes by adding trimethylamine (TMA) and SnF_2 to SnI_2. As shown in Figure 10c, a dense and excellent $FASnI_3$ perovskite film was

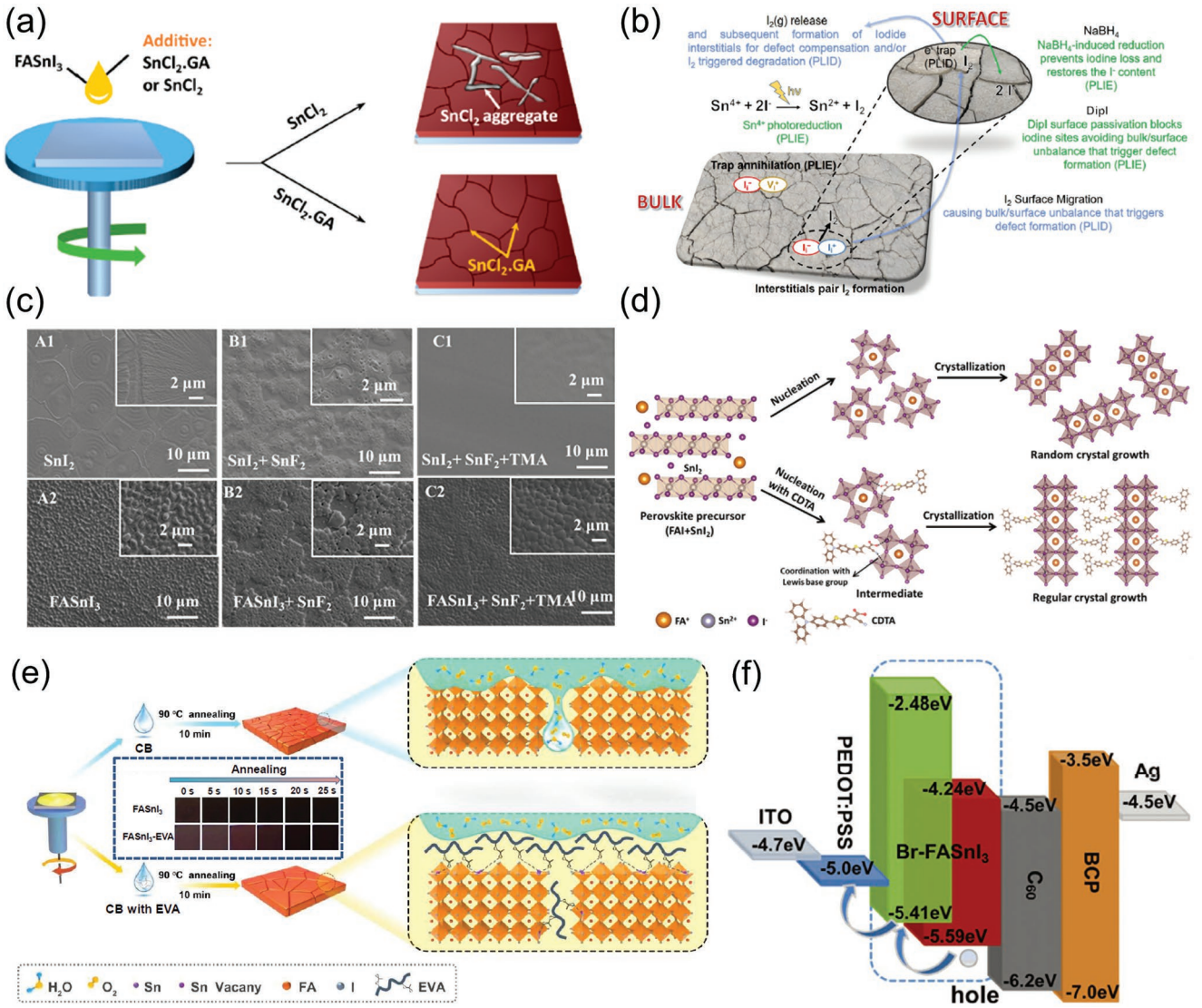

Figure 10. a) Schematic of preparation $FASnI_3$ films with different additions. Reproduced with permission.[129] Copyright 2020, American Chemical Society. b) Schematic of $NaBH_4$ and DipI effect on $FASnI_3$ perovskite films. Reproduced according to the terms of the CC-BY license.[135] Copyright 2022, The Authors. Published by Elsevier Inc. c) SEM images of different films. Reproduced with permission.[99] Copyright 2017, WILEY-VCH. d) Normal perovskite film formation process and CDTA-treated perovskite film formation process. Reproduced with permission.[136] Copyright 2019, Science China Press and Springer-Verlag GmbH Germany, part of Springer Nature. e) Schematic of EVA effect on $FASnI_3$ perovskite films. Reproduced with permission.[137] Copyright 2020, American Chemical Society. f) Energy band alignment. Reproduced with permission.[139] Copyright 2019, WILEY-VCH.

achieved by reacting this complex with FAI, controlling the speed of SnI_2 and FAI reaction during the film formation. They demonstrated that the formed intermediate adducts of TMA and SnY_2 ($Y = I^-$, F^-) could slow down the reaction rate. The fabricated PSCs with the resulting films presented PCEs of 4.34% and 7.09% for *n-i-p* and *p-i-n* PSCs, respectively. In 2019, Han and co-workers[136] also used the Lewis acid–base theory to form intermediate products, slowing down the crystallization rate. They synthesized three Π-conjugated Lewis bases, including 2-cyano-3-[5-(2,4-difluorophenyl)-2-thienyl]-propenoic acid (CTA-F), 2-cyano-3-[5-(2,4-dimethoxyphenyl)-2-thienyl]-propenoic acid (CTA-OMe), and 2-cyano-3-[5-[4(diphenylamino) phenyl]-2-thienyl]-propenoic acid (CDTA). They all contain carboxyl group (C=O) and cyano group (C≡N), which provide a high density of electronic states on these molecules and prevent the Sn^{2+} oxidation subsequently. Although these three molecules improved the device stability by forming high-quality Sn-based perovskites, however, CDTA showed the best improvement effect. The strong electron delocalization at the triphenylamine unit in CDTA molecule facilitates electron donation from the conjugated group, improving the Sn-based perovskite's antioxidant properties. Figure 10d shows the schematic diagram of controlling the perovskite crystallization using CDTA, leading to a PCE of 9%. Moreover, CDTA improved the hydrophobicity of the film significantly, leading to maintaining more than 90% of its initial PCE value after 1000 h

under light soaking (AM 1.5 G, 100 mW cm^{-2}) in an ambient atmosphere. Poly (ethylene-co-vinyl acetate) (EVA) polymer with C=O functional groups can react with free Sn^{2+} atoms and form an intermediate adduct, which slows down the perovskite crystal growth and improves the quality of the films with excellent hydrophobicity (see Figure 10e).[137] Wang et al.[138] introduced 1-(4-carboxyphenyl)-2-thiourea (CPT) molecule to passivate the defect states and control the crystallization of the $CsSnI_3$ film. In the CPT molecule, C=S and C=O can coordinate with uncoordinated surface Sn^{2+} to decrease the defect density. And the two-step annealing method (40 and 70 °C) can make a strong crystal of $CsSnI_3$ perovskite film. Finally, the devices showed a PCE of over 8% and only decreased 10% of the initial PCE after 3000 h in the N_2 atmosphere. Additionally, Chen and co-workers in 2019 proposed that the Π-conjugated group in poly[tetraphenylethene3,3′-(((2,2-diphenylethene-1,1-diyl) bis (4,1-phenylene)) bis (oxy)) bis (*N*,*N*-dimethylpropan-1-amine) tetraphenylethene] (PTN-Br) polymer structure could facilitate forming an intermediate adduct with free Sn^{2+} ions, thereby improving the quality of the films.[139] The biggest feature of this polymer was the ability of attachment to the grain boundaries, which could well block moisture, oxygen and ultraviolet light degradation of the Sn-based perovskite films. Moreover, this polymer-$FASnI_3$ possesses the highest occupied molecular orbital energy level (−5.41 eV) between poly(3,4-ethylenedioxythiophene):poly (styrenesulfonate) (PEDOT:PSS) (−5.0 eV) and $FASnI_3$ (−5.59 eV), leading to improved V_{CO} from 0.44 to 0.57 V due to smooth energy band alignment (See Figure 10f).

From the crystal regulation of Sn-based perovskites point of view, additives with amine groups can be selected to slow down crystallization and improve film quality through hydrogen bonds between amine groups and halide ions. Based on this, many researchers have studied the passivation of Sn-based perovskite films by amine-based additives. Islam et al.[140] observed that 5-ammonium valeric acid iodide (5-AVAI) additive controls crystallization through hydrogen bonds with I^- from SnI_6^{4-} units. As a result, the films showed a pinhole-free homogeneous morphology. As a result, the modified PSCs showed a PCE of over 7%, while the control device showed only 3.4% PCE. Interestingly, the modified devices showed record stability at that time. They maintained their initial PCE after 100 h under 1-sun continuous illumination at MPP condition. Wu et al.[39] introduced conjugated organic cation,3-phenyl-2-propen-1-amine (PPA), into $FASnI_3$ perovskite precursor to modulate crystallization, leading to improved charge extraction and device stability. As shown in **Figure 11**a–c, PPA-modified $FASnI_3$ perovskite presented a preferential orientation compared to control perovskite, which reduced the hysteresis (PCE for the forward scan was 9.44%, and PCE for the reverse scan was 9.61%) and obtained a PCE of 7.08% with a larger active area of 1 cm^2. The mechanism of PPA action on $FASnI_3$ film is shown in Figure 11d. Moreover, the PPA-modified device maintains 90% of the initial PCE after 1440 h storage in the glove box. Subsequently, Han et al.[141] proposed template-assisted growth of $FASnI_3$ crystals (see Figure 11e) by spin-coating n-propylammonium iodide (PAI) onto the intermediate phase of perovskite films before the annealing step, eliminating the disadvantages of rapid crystallization of Sn-based perovskites and leading to accredited PCE of 11.2% with the remaining 95% of the initial PCE after 1000 h under operation condition at MPP. Priya et al.[142] introduced phthalimide (PTM) into B-γ $CsSnI_3$ perovskite film to reduce defect density and improve grain-ordered perovskite film by Sn^{2+} coordination with NH and two CO units. As a result, the devices showed PCEs of 10.1% and 9.6% for rigid and flexible substrates. Besides, these encapsulated devices retained 94.3%, 83.4% and 81.3% of the initial PCE after 60 days under an N_2 atmosphere, 45 days under air and 2000 min under 1 Sun continuous illumination at ≈70 °C conditions. Recently, Mi et al. proposed that trimethylthiourea (3T) can effectively passivate $FASnI_3$ perovskite films by forming S−Sn and N−H...I chemical bonds.[143] The 3T-$FASnI_3$ solution showed slower crystallization than control films, leading to smooth and compact films with carriers lifetime of 123 ns (see Figure 11f). As a result, the V_{OC} of fabricated solar cell with this perovskite film enhanced from 0.65 (control device) to 0.92 V with a PCE of 14.3% (certified 14.0%). Finally, the modified device could retain 85% of its initial PCE under 75% humidity condition.

Hydrogen bonding is one of the primary mechanisms for most of additives in the passivation of Sn-based perovskite films. Especially, amine and hydroxyl functional groups in additive chemical structures can form hydrogen bonds with halide ions. Han et al.[144] found that hydrogen bonding has a significant effect on film quality. The slowing down of the crystal growth rate is the most important aspect of this effect. The formed hydrogen bonds could also affect the position of the crystal nucleus and determine the crystal growth direction. Moreover, it could also inhibit the I^- ions migration and stabilize the perovskite phase. For example, the hydroxyl groups in PVA structure could form hydrogen bonds (O−H...I) with I^- ions in the perovskite precursors.[145,146] The encapsulated Sn-based PSCs with PVA additive showed a high PCE of 8.9% without any degradation within 400 h under continuous light illumination.

Large organic cations as additives reduce the dimension of 3D perovskite, improving the film stability. However, various long-chain cations with different overall chain lengths, planarity, and molecular structure can play different roles in perovskite films. Han et al.[147] proposed a noteworthy crystal growth strategy by adding ortho-fluorine (2-F-PEA) ligand into the perovskite precursor, improving the crystal growth and oxidation resistance. Diau et al.[148] also used ethylenediammonium diiodide ($EDAI_2$) and butylammonium iodide (BAI) as additive and surface modifiers of Sn-based perovskite, respectively. They demonstrated that using both BAI and $EDAI_2$ is essential to passivate the defects more efficiently. As shown in Figure 11g, the primary role of BAI was to determine the dimension of the crystal. A small amount of BAI could guide the crystallization direction and improve the crystallinity. While, the key role of $EDAI_2$ was to passivate the defects, balance nucleation and crystallization, optimize the crystal structure, and improve charge separation. They demonstrated that the best device performance and stability could be achieved by adding 1% EDAI and 15% BAI into the perovskite precursor. The modified devices showed a PCE of 8.9% with negligible degradation after 2000 h under an N_2 atmosphere.

The chemical instability of Sn-based perovskite and the inferior energy band level alignment with charge transport layers is

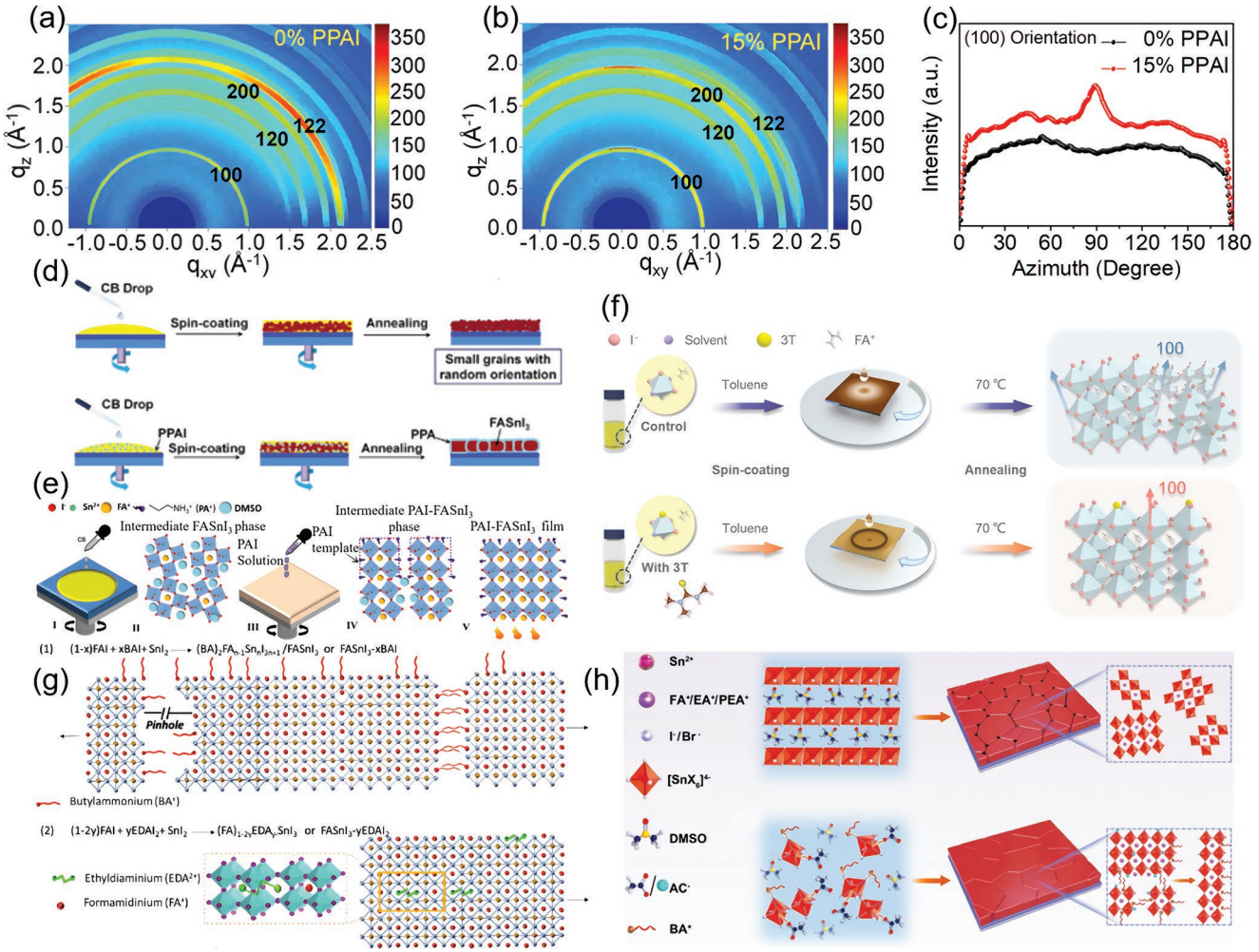

Figure 11. Grazing incidence X-ray diffraction (GIXRD) images of $FASnI_3$ perovskite films a) with 0% PPAI and b) with 15% PPA. c) Radially integrated intensity plots of the GIXRD profiles along the (100) ring. d) The mechanism of action of PPA. Reproduced with permission.[39] Copyright 2019, Elsevier Inc. e) A schematic of templated growth. Reproduced with permission.[141] Copyright 2020, The Royal Society of Chemistry. f) Schematic illustration of the crystallization process without and with 3T. Reproduced with permission.[143] Copyright 2022, American Chemical Society. g) A schematic of BAI and EDAI action on $FASnI_3$ perovskite films. Reproduced with permission.[148] Copyright 2018, The Royal Society of Chemistry. h) A schematic of BAAc IL action on Sn-based perovskite films. Reproduced according to the terms of the CC-BY license.[126] Copyright 2021, The Authors. Published by WILEY-VCH.

the main obstacles to achieving highly efficient Sn-based PSCs. To address these challenges, Hayase et al.[149] introduced ethylammonium (EA) into the $FASnI_3$ crystal lattice to modulate the band alignment and improve charge extraction between the perovskite and charge transport layers, resulting in a promising PCE of 13.24% for Ge_2I doped $(FA_{0.9}EA_{0.1})_{0.98}EDA_{0.01}SnI_3$-based device.

The self-healing properties of additives can improve the damaged parts of Sn-based perovskite films in a water–oxygen environment. The water–oxygen instability of Sn-based perovskites makes their commercial application prospects much weaker than Pb-based perovskites, therefore, improving the damaged tin-based perovskites in the air could be an important research direction. Based on this, Huang et al.[150] found that the Sn-based PSCs could undergo a self-repairing process by inducing the phenylhydrazine hydrochloride (PHCl) molecules to the perovskite films. Notably, the modified devices recovered to their initial status after exposure to air.

Using materials with hydrophobic groups as additives is also a strategy to improve the stability of perovskite films. From the perspective of the protective layer, Han et al.[112] reported that the Sn-based perovskite films' morphology and fabricated PSCs' stability could be improved utilizing pentafluorophen-oxyethylammonium iodide (FOEI) additive. The FOEI devices demonstrated high operational stability after 500 h under light soaking with negligible degradation.

Flexible devices also have become a new direction for developing next-generation photovoltaics. In this regard, Chen et al. introduced graphite phase-C_3N_4 (g-C_3N_4) into $FASnI_3$ films and fabricated flexible Sn-based PSCs. The devices retained 91% of the initial PCE after 1000 h under 1-sun illumination and N_2 atmosphere. Moreover, the PCE only decreased to 92% of its initial amount after 300 bending cycles with a 3 mm curvature radius.[151]

Ionic liquids (ILs) have been widely used for Pb-based perovskites,[152–154] but there are few reports about their application

for Sn-based counterparts. For example, Chen et al.[155] reported 1-butyl-3-methylimidazolium bromide (BMIBr) IL could trigger the Ostwald ripening effect in Sn-based perovskite, meaning increased grain sizes and decreased defects at the grain boundaries. The unencapsulated devices remain 85% of the original PCEs after 1200 h stored in N_2 atmosphere. However, the original PCEs decreased to 40% after 48 h under ambient conditions. Abate et al.[126] introduced n-butylammonium acetate (BAAc) IL into $FASnI_3$ precursor to modulate the perovskite crystallization. The Ac^- ($CHCOO^-$) groups in the BAAc structure react with SnI_2 and form O...Sn bonds.[156] On the other side, BA^+ reacts with I^- and Br^- through N—H...X hydrogen bonds.[157] Figure 11h shows the performing mechanism of BAAc IL on Sn-based perovskite film formation. Finally, the BAAc-modified Sn-based PSCs obtained over 10% PCE and showed 1000 h stability under N_2-filled glovebox conditions.

4. Structure Selection

4.1. "Hollow" Structure

The most common 3D crystal structure of Sn-based perovskites has the disadvantage of poor stability, therefore, researchers have done a lot of research on improving this structure. The "hollow" structure is a novel conceptual design for Sn-based perovskite, meaning ethylenediammonium (en) replaces part of FA^+ or MA^+, which has relatively higher stability than common 3D perovskite. Based on this, in 2017, Kanatzidis et al.[158] proposed a "hollow" 3D structure to improve the stability of perovskite materials by replacing some fragments in the $FASnI_3$ lattice without changing the 3D structure, that is, en-$FASnI_3$. The surface morphology is shown in **Figure 12**a. Figure 12b shows the cross-sectional SEM image for en-$FASnI_3$ PSCs. The degradation tests demonstrated the better of the standard devices, and the devices with en-added perovskite films in the air demonstrated that en could improve the $FASnI_3$ perovskite films stability. Besides, even after the device was exposed to air for 1000 h, it showed a PCE of 6.37%. In the same year, Kanatzidis et al.[159] proposed "hollow" en-$MASnI_3$ PSCs as well. This structure was also beneficial in improving film stability. The original $MASnI_3$ films could be completely degraded in the air in two minutes. However, the PSCs with "hollow" en-$MASnI_3$ structure films could maintain 60% performance for 10 min under air conditions.

4.2. Low-Dimensional Perovskites

The low-dimensional perovskites have attracted enormous attention due to their excellent stability.[160,161] Similarly, these structures are also very common for the preparation of Sn-based perovskites to achieve high efficiency and stability PSCs. Therefore, researchers have focused in this direction, as well. For example, in 2017, Ning et al.[160] synthesized a low-dimensional $(PEA)_2(FA)_{n-1}Sn_nI_{3n+1}$ perovskite, where n changes with the proportion of the additives. As shown in Figure 12c, the pure 2D structure formed after PEA^+ occupied 100% of the A site of crystal structure, while the low-dimensional structure could be achieved with the PEA^+ percentages between 0% and 100%. The located PEA^+ at the grain boundaries of these low-dimensional structures, prevents oxygen from entering the crystal, thereby improving the perovskite oxidation resistance. To prove the stability improvement, they tested the device stability with 20% PEA in the glove box. After 100 h, the PCE of the control device decreased by 77%, while the PCE of the 20% PEA-device decreased only by 4%. In the same year, Kanatzidis et al.[161] synthesized a 2D perovskite with $(CH_3(CH_2)_3NH_3)_2(CH_3NH_3)_{n-1}Sn_nI_{3n+1}$ formulation, which made a significant contribution to improving the perovskite stability. In the stability test, the original device degraded in 3 min completely, while the device with 2D perovskite degraded after 30 min. Besides, the PCEs of encapsulated 2D- and 3D-based PSCs dropped by 10% and 100% of the initial value after one month under the air atmosphere. Abate et al.[127] added PEACl into the $FASnI_3$ precursor. The PEACl not only acted as a protective layer to prevent Sn^{2+} oxidation but also allowed for forming a 2D vertical crystal structure. As shown in Figure 12d, there were intermittent and unconnected spots in unannealed films, meaning randomly distributed crystal orientations. However, the film shows a perfect 2D structure with the (111) plane after annealing at 100 °C for 10 min. The resulting device showed a 9% PCE with excellent stability over 1680 h under N_2 condition. Organic alkyl chain length could affect the photovoltaic and stability of the 2D perovskite devices. Liu et al.[162] explored the alkyl chains containing 4, 8, and 12 carbons effect on the $A_2(FA)_{n-1}Sn_nI_{3n+1}$ perovskite films, respectively. The crystal showed vertical growth with a moderate length of the alkyl chain additive. The perpendicular crystal was beneficial for charge carrier transportation and preventing Sn^{2+} oxidation.

4.3. Quasi-2D perovskites

Quasi-2D perovskites have also shown better stability and photoelectric properties than their 3D counterparts. In 2018, Oh et al.[133] reported the quasi-2D Sn-based perovskites and studied the effect of FASCN on the film properties (**Figure 13**a). Their results demonstrated that SCN^- could form a coordination bond with Sn^{2+} and suppress the oxidation process. The quasi-2D Sn-based perovskites showed excellent device stability by decreasing only 10% PCE after 1000 h under N_2 atmosphere. In 2019, Chen et al.[163] introduced 5-ammoniumvaleric acid ($5\text{-}AVA^+$) into the Sn-based perovskite precursor to form a quasi-2D Sn-based $AVA_2FA_{n-1}Sn_nI_{3n+1}$ perovskite (see Figure 13b). Although the quasi-2D perovskite showed good stability, the photoelectric performance was somehow poor.[99,161,164] They used NH_4Cl to modify the synthesized quasi-2D Sn-based perovskite to address this challenge, improving the stability, and photoelectric performance. The fabricated devices with NH_4Cl-modified quasi-2D retained 90% of the initial PCE after 400 h under N_2 condition.

4.4. Hybrid 2D/3D Perovskites

It is also a research direction to transform some parts of 3D structures into 2D structures to improve the efficiency and

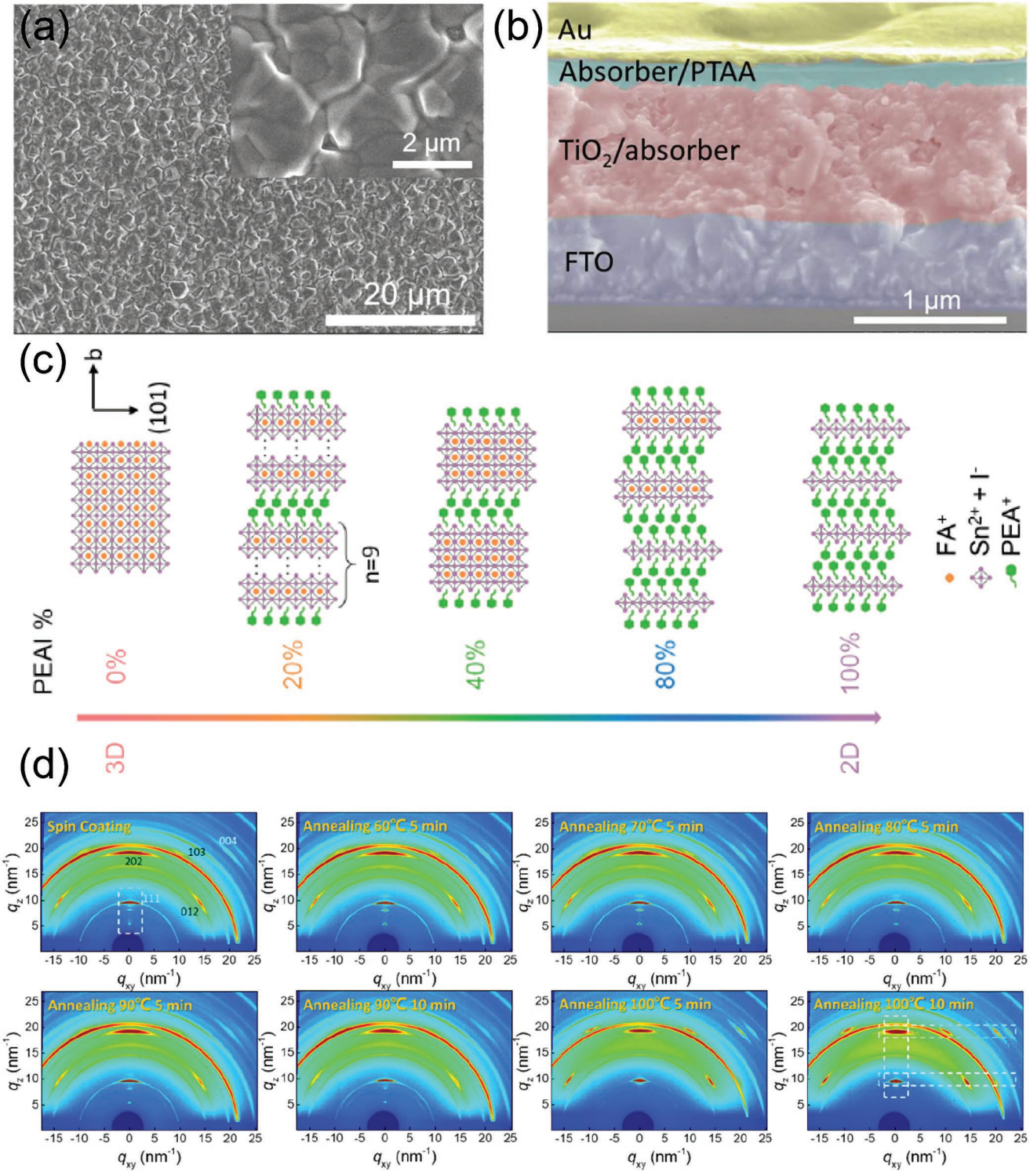

Figure 12. a) SEM image of en-$FASnI_3$ perovskite crystal and b) cross-sectional SEM image for en-$FASnI_3$ PSCs. Reproduced with permission.[158] Copyright 2017, American Association for the Advancement of Science. c) Schematic structures of $FASnI_3$ with different concentrations of PEAI. Reproduced with permission.[160] Copyright 2017, American Chemical Society. d) GIXRD images of $FASnI_3$:PEACl under different annealing conditions. Reproduced with permission.[127] Copyright 2020, American Chemical Society.

stability of the Sn-based perovskites. Besides, 2D/3D perovskite is the most promising structure for breakthrough efficiency and stability of Sn-based perovskites because this structure combines the optoelectronic properties of 3D perovskites with the stability advantages of 2D perovskites. Based on this, in 2017, Loi et al.[165] studied the 2D/3D mixed structure of

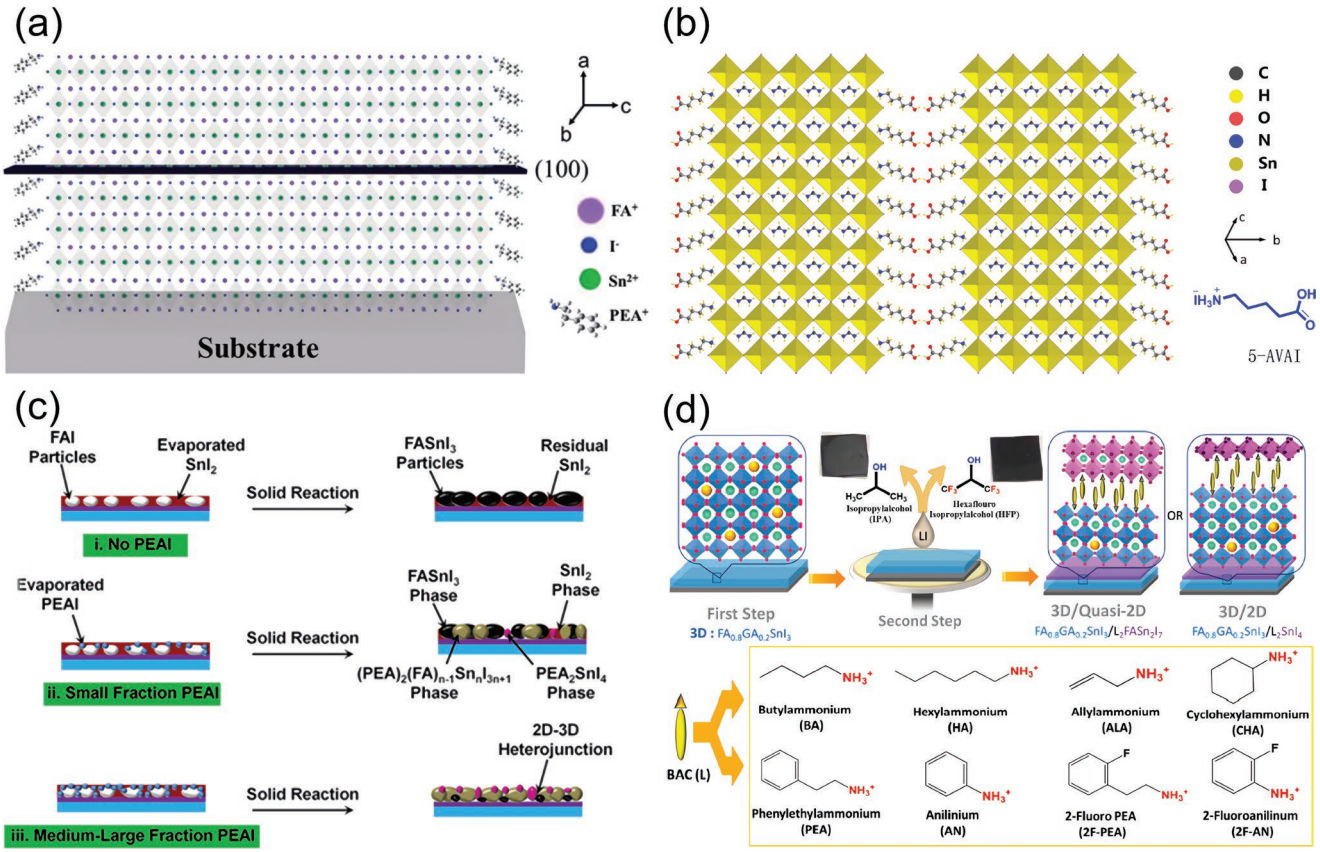

Figure 13. a) Crystal structure diagram of quasi-2D Sn-based perovskite (adding 10% PEAI) after modification by FASCN. Reproduced with permission.[133] Copyright 2018, American Chemical Society. b) Structure of quasi-2D Sn-based perovskite ($AVA_2FA_{n-1}Sn_nI_{3n+1}$ ($<n> = 5$)). Reproduced with permission.[163] Copyright 2019, WILEY-VCH. c) Schematic of preparation of different perovskite films. Reproduced with permission.[38] Copyright 2018, American Chemical Society. d) Schematic of preparation hybrid perovskite films and eight bulky ammonium cation structures. Reproduced with permission.[167] Copyright 2021, American Chemical Society.

Sn-based perovskites. The PCE of the fabricated 2D/3D device reached 9.0%, which was higher than that of pure 2D and 3D perovskites.[158,160,161] In contrast to the control device, the 2D/3D perovskite structure improves the device stability under continuous illumination in N_2 environment for 2 h. Moreover, the 2D/3D devices maintained up to 59% of the initial PCE under ambient conditions, while the 3D devices were utterly degraded within 76 h. Through a double-boundary engineering strategy, Wu et al.[38] fabricated 2D/3D Sn-based heterojunction perovskite films. First, FAI was deposited on the substrates to form a large gap between the particles (Figure 13c). Unencapsulated standard device ($FASnI_3$) and hybrid device (PEA, FA) SnI_3 maintained 45% and 85% of the original PCE under N_2 glove boxes after five days. In 2018, Wang et al.[164] constructed a 2D-quasi-2D-3D hierarchy structure. NH_4SCN played an important role in the manufacturing process of this structure. It could separate the crystal nuclei and control the crystal growth. The films showed good stability due to the formed 2D perovskite at the surface. The PCE of fabricated devices with 2D-quasi-2D-3D hierarchy structure was declined by only 10% after 300 h storage in N_2-filled glove box. Hayase et al.[166] also added PEA^+ to the perovskite precursor to form a 2D/3D perovskite structure. Although this structure could improve the stability of perovskite, it could not passivate the defects inside the crystal. For this reason, they added a small amount of Ge^+ metal ion to the 2D/3D hybrid structure, improving the device stability up to 192 h. He et al.[29] prepared a 2D/3D Sn-based perovskite by adding 4-fluoro-phenethylammonium bromide (FPEABr), leading to obtain a PCE of 14.81% (certified 14.03%). They found that pure 2D perovskite can modulate the 3D perovskite orientation. Also, they revealed that the 2D phase was mainly located at 3D grain boundaries, suppressing the Sn^{2+} oxidation at the top and bottom surfaces of the films. Diau et al.[167] compared eight bulky ammonium cations acting on $FASnI_3$ to form 2D/quasi-2D perovskite films on 3D perovskites (see Figure 13d). However, only adding anilinium (AN) to the perovskite precursor formed an ultrathin 2D ($n = 1$). Finally, the Sn-based PSCs with AN additive attained a PCE of 10.06%. The PCE of unencapsulated devices was maintained over 150 h at 40% relative humidity. The 3D Sn-based PSCs suffer low V_{OC} of 0.2 to 0.7 V due to their fast nonradiative carrier recombination.[40,42] To answer this challenge, Yan et al.[168] prepared tin-based PSCs with a 2D/3D vertical heterojunction by vacuum-assisting annealing and guanidinium thiocyanate (GuaSCN) treatment. The V_{OC} was enhanced from 0.83 to 1.01 V, and 95% of the initial PCE was maintained after 1200 h storage in N_2-filled glovebox. In this case, GuaSCN improved the film crystallinity and passivated the traps in the perovskite films, resulting in

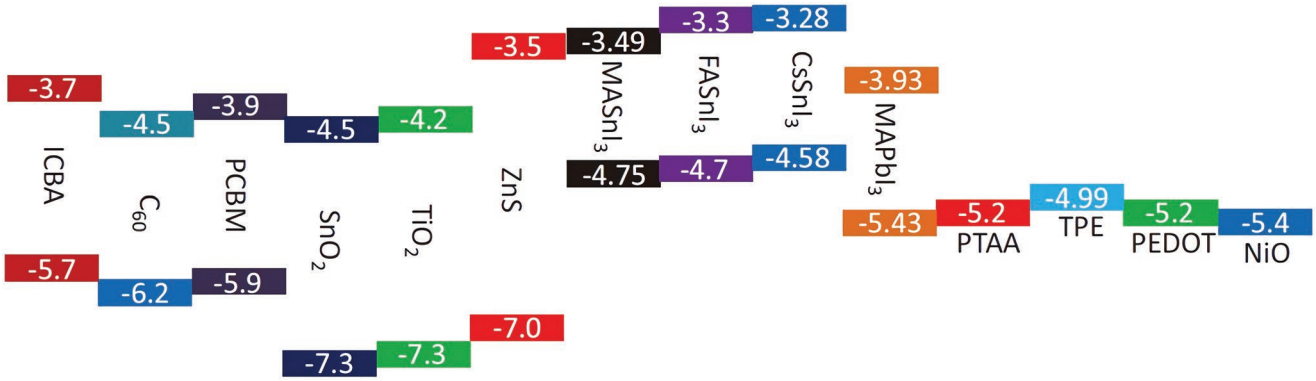

Figure 14. Energy band alignment of Sn- and Pb-based perovskite, ETLs, and HTLs. Reproduced with permission.[173] Copyright 2018, WILEY-VCH.

a prolonged carrier lifetime of over 140 ns and improved V_{oc} as a result. Besides, GuaSCN-modified 2D/3D heterojunction was beneficial to better charge transport due to the energy band alignment of ideal type II.

5. Layers Selection

In contrast to n-i-p Sn-based PSCs, the p-i-n structure has the advantages of low-temperature fabrication, negligible hysteresis behavior, and cost-effectiveness.[169] However, the p-i-n structure has some disadvantages as follows: 1) energy band alignment mismatch; 2) easy oxidation; and 3) fast crystallization. As shown in **Figure 14**, the energy band of Sn-based is preferred to match with [6,6]-phenyl-C_{61}-butyric acid methyl ester (PCBM) and indene-C_{60} bisadduct (ICBA) in p-i-n structure in contrast to TiO_2 and SnO_2 for n-i-p structure, resulting in fast charge exaction and reducing charge recombination in the interfaces. In addition, charge carrier recombination was intensified due to Ti—O—Sn bonds at the interface between TiO_2 and tin-based perovskites.[170] Nevertheless, the dopants of the 2,2′,7,7′-Tetrakis[*N*,*N*-di(4-methoxyphenylamino]-9,9′-spirobifluorene (spiro-OMeTAD) HTL in n-i-p structure PSCs can damage Sn-based perovskite due to post-oxidation.[171,172] As mentioned, the Sn-based perovskites often suffer fast crystallization; therefore, they need a smooth substrate for better crystallization. To sum up, we think the p-i-n structure is more suitable for Sn-based PSCs.

5.1. Electron Transport Layers (ETLs)

The charge-transporting layers play an important role in PSCs. In the early days of the emergence of PSCs, there was no such concept as a charge transport layer. In 2009, the Kojima group[1] invented photovoltaic cells using $MAPbBr_3$ and $MAPbI_3$ as light-absorbing materials. At the time, TiO_2 was used as the ETL material of the first generation of n-i-p PSCs. In 2014, the emergence of the Sn-based PSCs took place with mainly TiO_2 as ETL.[30,31,174] Although TiO_2 has a strong electron transport capability, however, it reduces the V_{OC} of the Sn-based PSCs due to its high back-hole carriers density, which leads to recombination of the electrons from TiO_2 with the holes from perovskite, easily. This affects the carrier transport stability of the devices.[83] Based on this, Kanatzidis et al.[83] added a layer of ZnS on top of the TiO_2 layer to form a smooth stepped band structure (**Figure 15**a). The ZnS layer not only made the electron transport smoother but also prevented electron and hole recombination. Finally, under the bias voltage of 0.261 V, the device with TiO_2-ZnS ETL achieved a stable current density of 18.94 mA cm^{-2}. On the other hand, in 2016, Cao et al.[175] used the pulsed laser deposition (PLD) to grow ZnO nanorods as ETL for Sn-based PSCs, which could solve the problem of pore filling in spin-coated ZnO films, leading to improved charge transportability and holes blocking properties. Figure 15b shows the influence of the ZnO layers morphology and growth method on the solar cell performance. The introduction of ZnO reduced electron and hole recombination.

The fullerene-based ETL played an important role in PSCs. For example, Huang et al.[176] demonstrated that the fabricated Pb-based PSCs with C_{60} deliver a better performance than PCBM and ICBA. In the same year, Wang et al.[177] used C_{60} and its derivative PCBM as ETL for $FASnI_2Br$-based PSCs, confirming that C_{60} facilitated the photoelectric performance of the devices. But PCBM improved the device stability more efficiently. The unencapsulated devices maintained 66% of PCE (1.43% to 0.95%), 73% of J_{SC} (7.27 to 5.34 mA cm^{-2}), 95% of V_{OC} (0.362 to 0.345 V), and 94% of FF (0.543 to 0.513) under a nitrogen environment after 30 h.

The ETL formed by fullerene derivatives and SnO_2 could be well combined with Sn-based perovskite. SnO_2 as the ETL could not match the energy level of other layers of the device very well; however, adding C_{60} Pyrrolidine tris-acid (CPTA) could modify the energy levels mismatch, allowing better carrier transport and reducing the chance of recombination. It is worth noting that the V_{OC} was increased by 50% (0.48 to 0.72 V) by such modification. The PCE of the devices reached 7.4%. Figure 15c shows the normalized PCE, V_{OC}, J_{SC}, and FF changes over time for unencapsulated devices in the air (60% humidity, $T = 25$ °C). After 200 min, the PCE of the device could still maintain 80% of the initial value.[178] Hatton et al.[179] compared PCBM, ICBA, and C_{60} materials as ETL for Sn-based $CsSnI_3$ devices. They proved that ICBA is the best ETL among them, delivering a device PCE of 2.76%. Ning et al.[180] introduced ICBA as a new ETL. The device attained a voltage of 0.94 V and a PCE of 12.4% (see Figure 15d). Besides, the device could retain the 90% of initial PCE after 3800 h being stored in N_2.

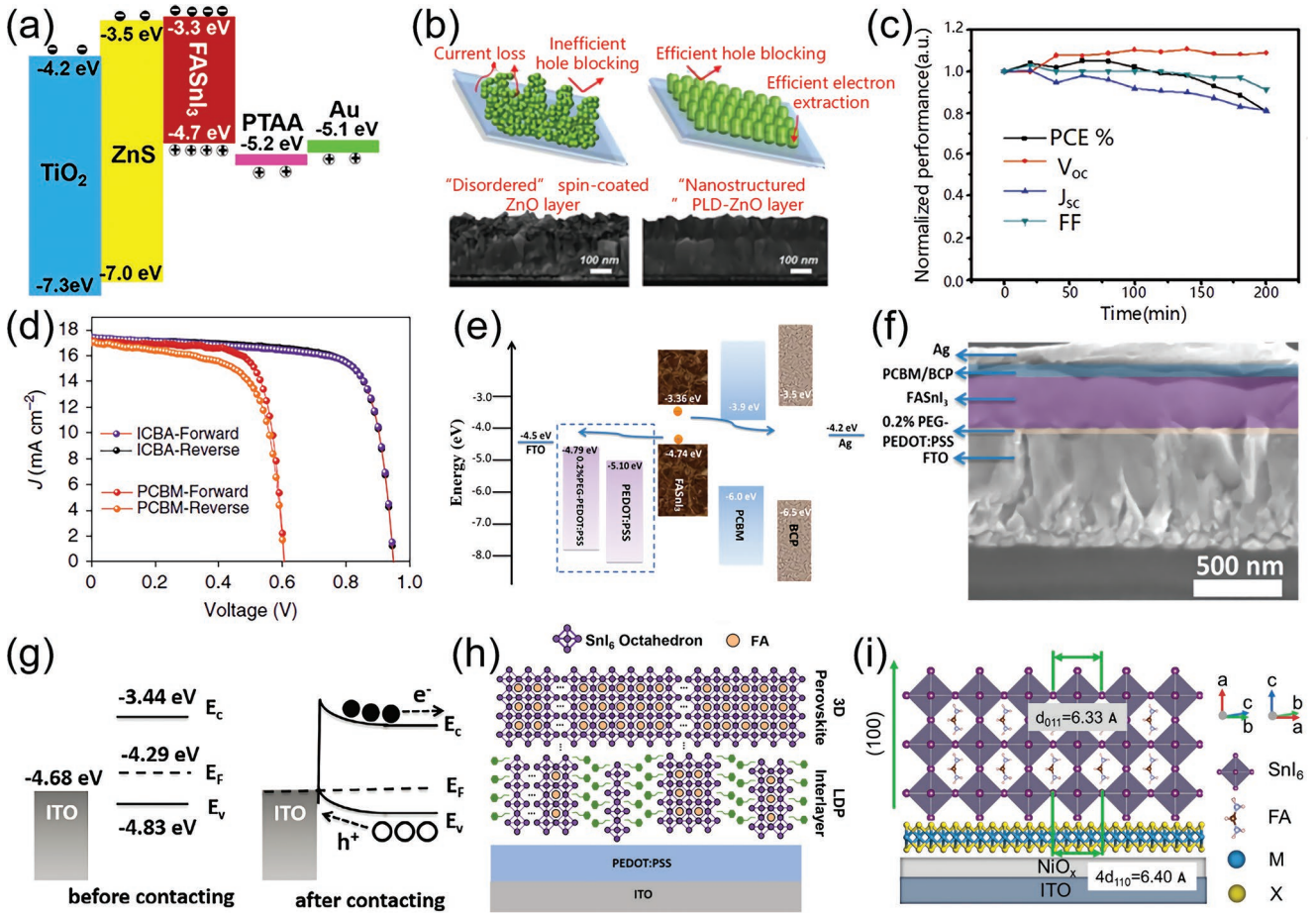

Figure 15. a) The energy level diagram of layers in Sn-based PSCs. Reproduced with permission.[83] Copyright 2016, American Chemical Society. b) The influence on morphology by ZnO layer through different growth methods. Reproduced with permission.[175] Copyright 2016, WILEY-VCH. c) The attenuation of parameters when the encapsulation PSCs were exposed to air for 200 min (60% humidity, $T = 25$ °C). Reproduced with permission.[178] Copyright 2019, WILEY-VCH. d) J–V curve of $FASnI_3$ PSCs using PCBM and ICBA as ETL. Reproduced according to the terms of the CC-BY license.[180] Copyright 2020, The Authors. Published by Springer Nature Limited. e) The energy level diagram of layers in Sn-based PSCs and f) SEM cross-section images of Sn-based PSCs. Reproduced with permission.[54] Copyright 2018, American Chemical Society. g) Schematic of energy band bending in $FASnI_3$. Reproduced with permission.[182] Copyright 2021, WILEY-VCH. h) The LDP layer lies in the middle of the perovskite layer and PEDOT:PSS layer. Reproduced with permission.[183] Copyright 2018, Elsevier Ltd. i) $FASnI_3$ crystal structure along with (100) crystal orientation. Reproduced according to the terms of the CC-BY license.[187] Copyright 2021, The Authors. Published by WILEY-VCH.

5.2. Hole Transporting Layers (HTLs)

In PSCs, the HTL transports holes from the perovskite to metal back contact. Additionally, HTL can prevent electrons from being transferred to the positive electrode, reducing the recombination probability of electrons and holes, enabling rapid separation of photogenerated excitons, and improving the device's performance. In p-i-n PSCs, PEDOT:PSS is the most common HTL due to its simple solution processability and ability to combine well with the conductive glass (ITO and FTO).[174] By changing the PEDOT:PSS composition, its work function could be modified. For example, Han et al.[54] introduced polyethylene glycol (PEG) into PEDOT:PSS. The energy level diagram of layers in Sn-based PSCs is shown in Figure 15e. The valence band maximum of $FASnI_3$ is around –4.7 eV, but the work function of PEDOT:PSS is around –5.1 eV. This high energy level difference will cause severe J–V hysteresis. The work function of the PEG/PEDOT:PSS composition raised to –4.79 eV, which significantly reduced the energy level mismatch between $FASnI_3$ and PEDOT:PSS (see Figure 15f). The PCE of the devices with 0.2% PEG modified PEDOT:PSS as the HTL remained at 95% and 90% of the initial PCE after being stored the air for 4 h and 30 days, respectively. Commonly spiro-OMeTAD HTL needs to be doped to improve the adaptability for photovoltaic devices. However, this doping process induces some water and oxygen into devices, leading to the rapid degradation of the Sn-based perovskites. To solve the instability and low PCE problems, Kanatzidis et al.[171] introduced tetrakis-triphenylamine (TPE) small molecules as HTL for the Sn-based PSCs, obtaining a PCE of 7.23%. The experimental results showed that the TPE improves the device's performance and strengthens stability. The modified devices can maintain a PCE of 6.85% and the J_{SC} is of 19.13 mA cm^{-2} for 100 s under MPP at the applied voltage of 0.385 V. Subsequently, Kanatzidis et al.[181] also synthesized benzodithiophene (BDT)-based small organic molecules for HTL application. As a result, the PCE of modified

devices reached 7.59%. Han et al.[182] prepared the HTL-free Sn-based PSCs with compact and dense perovskite films, which obtained a PCE of over 10.6%. Adding heterogeneous ammonium cations to $FASnI_3$ perovskite as the nucleation sites led to energy band bending, which facilitates hole transport to ITO directly (see Figure 15g). Besides, the devices remained at 95% of the initial PCE under light soaking for 40 days and 90% of the initial PCE under 80 °C annealing for 100 h.

5.3. Interface Layers

Different interfaces could also affect internal and external stability significantly. The internal stability is mainly caused by some defect states that affect the transmission of photogenerated carriers and interface connections. External stability means the resistance of PSCs against external factors such as water, oxygen, and ultraviolet light. To improve the stability of Sn-based PSCs, Gong et al.[183] proposed low-dimensional perovskites as novel interface materials. They deposited phenylethylammonium bromide (PEABr) on PEDOT:PSS. Figure 15h shows PEABr could convert some part of 3D phase of Sn-based perovskite into low-dimension perovskite (LDP), that is, 2D, based on the steric effect.[184] This LDP makes the perovskite layer and the lower layer more closely combined, reducing defect formation and improving the carrier transmission stability. During the stability test, the LDP device showed a stable current output of ≈19.60 mA cm^{-2} with a PCE of ≈6.30%. He et al.[185] also proved that the LDP formed by PEABr on the perovskite surface could improve the Sn-based perovskite stability significantly. They coated PEABr on the perovskite and then annealed it to form an ultra-thin 2D Sn-based perovskite interlayer. It is worth noting that the device stability improved significantly. The PCE of PEABr-treated PSC maintains 80% of the initial value under continuous light illumination in the air for 350 h, while the untreated device degraded after 140 h, completely. Han et al.[186] covered the surface of Sn-based perovskite with 4-fluorobenzohydrazide (FBH) as an antioxidant interlayer. Due to the low surface energy of the FBH layer, it could cover the surface of Sn-based perovskite films perfectly. FBH reacts with Sn^{2+} through carbonyl groups to promote the crystal growth in the same direction, thereby increasing the diameter of particles, reducing grain boundaries, passivating defects, increasing the carrier's lifetime and preventing film degradation by external conditions. The devices with FBH interlayer could remain 93% of the initial PCE (initial PCE of 9.03%) under the air and light soaking conditions after 600 h, while the device without FBH interlayer only maintained 43% of the original PCE (initial PCE of 4.14%). Therefore, the stability of PSCs with FBH interlayer was increased by two orders. 2D interface material can also promote the formation of high-quality and stable films. Yan et al.[187] reported $FASnI_3$ films along the (100) growth orientation on a series of 2D interface materials (MoS_2, WS_2, and WSe_2). The schematic is shown in Figure 15i. Finally, the WSe_2 showed a better energy band match with $FASnI_3$ and NiO_X, which was a benefit for hole extraction. The PCE of 10.47% was obtained in WSe_2-modified devices. Recently, Padture et al. researched the flexible Sn-based PSCs based on PET/ITO/NiO_X/$FAGe_{0.1}Sn_{0.9}I_3$/PCBM/BCP/Ag device structure.[188] Based on this, the GeO_2 passivation layer can form by situ formation between Ge^{4+} in perovskite and O^{2-} in NiO_X HTL, blocking ionic diffusion and enhancing the mechanical bonding. Interestingly, the f-PSCs can attain PCE of 10.43% and retain 80% of the initial PCE after bending 2500 cycles at radius $R = 5$ mm under N_2 atmosphere.

6. Conclusion

This review expounds on the relationship of Sn-based perovskite with crystal structure features, perovskite film processing, low-dimension structure, and layer selection. The important previous works were concluded as in **Table 1**, including device structure, photoelectric parameters, stability and strategies. As shown in **Figure 16**, we illustrate the critical development of PCE for Sn-based PSCs from 2014 to 2021. And the PCE has increased from 6.4% to 14.81%. Although the PCE of Sn-based PSCs is far below that of Pb-based PSCs, the slightly toxic Sn-based perovskite makes it a good application prospect.

In the crystal structure, the cubic crystal in perovskite absorbing materials is beneficial for high-efficiency Sn-based PSCs, achieving excellent photoelectric and semiconducting properties.

Therefore, obtaining a high-quality crystal structure has become a hot research direction in the Sn-based PSCs. Although the 3D-orthorhombic provides the photoelectric and semiconducting properties of perovskite materials, it may turn into 1D-orthorhombic or 1D-hexagonal structures by tilting octahedral units of the cubic perovskite structure during the crystallization process, leading to inferior optoelectronic properties. We can calculate t_{IR} to evaluate the structural stability when we want to dope or replace the perovskite component.

In processing, as mentioned earlier, Sn^{2+} is the desired oxidation state of Sn for preparation of perovskite precursors and films; however, the existence of even a tiny amount of Sn^{4+}, that is, undesirable oxidation state, in SnX_2 as the Sn source could reduce the films quality and device performance, significantly. Therefore, the purity of the perovskite precursors is crucial for Sn-based perovskite processing. Since the production and packaging environments could be different for every company, it should be considered that SnX_2 must be produced and packed in a highly controllable oxygen-level environment; otherwise, the product oxidation, even partially, is undeniable. So, we can add a small amount of metallic Sn powder, redox additions to a perovskite precursor solution or redox gas-assisted preparation to convert the Sn^{4+} content to Sn^{2+}.

The precursor solvents and antisolvent are important in preparing low trap density and full coverage Sn-based perovskite films. According to the Lewis acid–base theory, Sn^{2+} has a stronger Lewis acidity than Pb^{2+};[74,75] hence SnI_2 reacts with the organic ammonium cations very rapidly, leading to an uncontrollable perovskite crystallization and discontinuous films with many pinholes, consequently. As a result, this low-quality film forms a large leakage current and decreases the film's resistance against water or oxygen. So, DMSO usually has been used as a suitable precursor solvent. However, DMSO could accelerate the Sn^{2+} oxidation.[81] Therefore, finding a suitable solvent for excellent performance Sn-based perovskite films is of the

Table 1. Strategy to improve stability and summary of stability (a is additions, s is solvent, as is anti-solvent, m is interlayer).

Device structure	Cell parameters				Stability	Strategy	Ref.
	V_{OC} [V]	J_{SC} [mA cm^{-2}]	FF [%]	PCE [%]			
ITO/PEDOT:PSS/$BA_2MA_3Sn_4I_{13}$/PCBM/LiF/Ag	0.38	21.87	48.3	4.03	94 d in N_2, no decrease	BAI+SnF_2+HAC (a), DMSO+MAAc (s)	[33]
ITO/PEDOT:PSS/$FASnI_3$/C_{60}/BCP/Ag	0.48	21.92	57.23	6.03	2700 s stable output	DE (as), SnF_2 (a), DMF+DMSO (s)	[37]
ITO/PEDOT:PSS/$FA_{0.75}MA_{0.25}SnI_3$/C_{60}/BCP/Ag	0.55	24.3	67.3	9.06	30 d in N_2, 25% decrease	CB (as), DMSO+DMF (s), SnF_2 (a)	[34]
ITO/PEDOT:PSS/$FA_{0.75}MA_{0.25}SnI_3$/C_{60}/BCP/Ag	0.55	19.4	67	7.2	70 h in N_2, no decrease	CB (as, 65 °C), DMSO assisted annealing, DMSO (s), SnF_2 (a)	[35]
FTO/c-TiO_2/m-TiO_2/$MASn(I_{0.33}Br_{0.67})_3$/Ag	0.58	11.09	49.5	3.2	48 h in N_2	DMSO+DMF (s), mixed halogen	[189]
ITO/PEDOT:PSS/$MASnI_3$/C_{60}/BCP/Ag	0.45	11.82	40	2.14	200 h at AM 1.5	Toluene, hexane (as), SnF_2 (a)	[98]
FTO/c-TiO_2/m-TiO_2/$MASnI_3$/PTAA/Au	0.49	22.91	64	7.13	30 min in air, 50% decrease	Cations exchange, ethanol (s)	[111]
ITO/PEDOT:PSS/$FASnI_3$/C_{60}/BCP/Ag	0.53	17.37	73.47	6.8	4000 h in darkness, no decrease	Two steps, DMSO (s); HFP, IPA, CB (s), $EDAP_2$ +SnF_2 (a)	[100]
FTO/c-TiO_2/$CsSnI_3$/m-TDATA/Au	0.21	22.7	34	2.02	11 d in N_2	SnF_2 (a), different HTL, DMSO (s)	[64]
FTO/c-TiO_2/$CsSnI_3$/spiro-OMeTAD/Au	0.24	25.8	30	1.87	/	SnF_2 (a), different HTL, DMSO (s)	[64]
FTO/c-TiO_2/$CsSnI_3$/no-HTL/Au	0.15	21.6	27	0.87	/	SnF_2 (a), different HTL, DMSO (s)	[64]
FTO/PEDOT:PSS/$CsFASnX_3$/PCBM/BCP/Ag	0.65	21.78	76.2	10.79	1000 h in N_2, 5% decay	SnF_2+$SnCl_2$+$EDAI_2$ (a), CB (as)	[125]
ITO/PEDOT:PSS/$FASnI_3$/C_{60}/BCP/Ag	0.56	17.7	62.5	6.19	860 h in N_2, 10% decrease	Sn source purification, DMSO (s), CB (as)	[66]
FTO/c-TiO_2/m-TiO_2/$FASnI_3$/spiro-OMeTAD/Au	0.265	15.25	46.05	1.86	120 s stable output	Evaporation-assisted, DMSO+DMF (s), SnF_2 (a), CB (as)	[107]
ITO/PEDOT:PSS/poly-TPD/$MASnI_3$/C_{60}/BCP/Ag	0.377	12.1	36.6	1.7	/	Evaporation deposition	[102]
ITO/PEDOT:PSS/$MASnI_3$/PCBM/BCP/Ag	0.57	20.68	0.66	7.78	200 h in N_2 at light soak, 30% decay	Evaporation deposition	[103]
ITO/MoO_3/$CsSnBr_3$/C_{60}/BCP/Ag	0.4	1.25	45	/	350 min in air, 50% decrease	Evaporation deposition	[104]
FTO/c-TiO_2/m-TiO_2/$MASnI_3$/PTAA/Au	0.273	17.36	39.1	1.86	60 min in air, 31% decrease	Evaporation-assisted, DMF+DMSO (s), DE (as)	[106]
FTO/m-TiO_2/$CsSnI_3$/PTAA/Ag	0.38	25.71	49.05	4.81%	500 min in air, 2% decrease	Hydrazine atmosphere, more SnI_2, DMSO+DMF (s)	[116]
FTO/c-TiO_2/m-TiO_2/$CsSnBr_3$/PTAA/Au	0.378	19.92	51.73	3.89	5 min in air, no decrease	Evaporation-assisted, DMSO (s), CB (as)	[110]
ITO/PEDOT:PSS/$MA_{0.25}FA_{0.75}SnI_3$/PCBM/C60/BCP/Ag	0.76	22	0.69	11.5	50 days in N_2, no decay	Sn nanoparticles, EDA (m), DMSO (s), CB (as)	[190]
FTO/c-TiO_2/m-TiO_2/$MASnI_3$/PTAA/Au	0.25	26.1	30	1.94	500 min in air, 30% decrease	SnF_2 (a), DMSO (s), CB (as)	[119]
FTO/c-TiO_2/m-TiO_2/$MASnI_3$/PTAA/Au	0.3775	19.92	51.73	3.89	/	Evaporation-assisted, DMF+DMSO (s)	[110]
FTO/c-TiO_2/m-TiO_2/$CsSnI_3$/PTAA/Au	0.17	30.75	34.88	1.83	/	Evaporation-assisted, DMF+DMSO (s)	[110]
FTO/c-TiO_2/m-TiO_2/$CsSnBr_3$/PTAA/Au	0.367	13.96	59.36	3.04	/	Evaporation-assisted, DMF+DMSO (s)	[110]
ITO/PEDOT:PSS/$FASnI_3$/C60/BCP/Ag	0.62	24.2	72	10.8	600 h at MPP, 18% decay	Evaporation-assisted, DMF+DMSO (s), CB (as)	[114]
ITO/PEDOT:PSS/$FASnI_3$/PCBM/BCP/Ag	0.455	17.63	67.3	5.4	1000 h in N_2, 35% decrease	SnF_2-N_2H_5Cl+SnF_2 (a), DMSO (s), CB (as)	[130]
ITO/PEDOT:PSS/$MA_{0.25}FA_{0.75}SnI_{2.75}Br_{0.25}$/PCBM/BCP/Ag	0.6	22.48	0.69	9.31	300 h in N_2 at light soak, 20% decay	SnF_2+PEABr+MABr (a), DMF+DMSO (s), CB (as)	[191]
FTO/c-TiO_2/m-TiO_2/$FASnI_3$/Spiro-OMeTAD/Au	0.275	24	60	4.1	50 s stable output	SnF_2-pyrazine (a), DMF+DMSO (s), toluene (as)	[84]
PDMS/PEDOT:PSS-$Zn(TFSI)_2$/$FASnI_3$/PCBM/BCP/Ag	0.608	19.75	65.73	7.95	300 h in air, 10% decay	SnF_2+g-C_3N_4+PEAI+$DEAI_2$ (a), DMF+DMSO (s), CB (as)	[151]
ITO/PEDOT:PSS/$FASnI_{2.95}Cl_{0.05}$/PCBM/BCP/Al/Ag	0.38	21.89	62	5.17	350 h in N_2, 40% decay	TFEACl+SnF_2 (a), DMF+DMSO (s), CB (as)	[128]
ITO/CuSCN/$FASnI_3$/PCBM/Ag	0.5	19.55	63.71	6.25	10 h in air, 40% decrease	$NH_4H_2PO_2$+SnCl (a), CuSCN (HTL), DMSO+DMF (s)	[131]

Table 1. Continued.

Device structure	Cell parameters				Stability	Strategy	Ref.
	V_{OC} [V]	J_{SC} [mA cm^{-2}]	FF [%]	PCE [%]			
ITO/PEDOT:PSS/$FASnI_3$/PCBM/Al	0.48	18.5	57.2	7.66	1000 h in N_2, less 10% decrease	FASCN+SnF_2+PEAI (a), quasi-2D, DMSO+DMF (s), CB (as)	[133]
ITO/PEDOT:PSS/$FASnI_3$/C_{60}/BCP/Ag	0.538	19.99	67.66	7.28	5 h in UV, 44% decrease	PTNBr+SnF_2 (a), DMOS+DMF (s), CB (as)	[139]
ITO/PEDOT:PSS/$FASnI_3$/PCBM/BCP/Ag	0.481	21.08	62.77	6.37	24 h in air, 60% decrease	8-hydroxyquinoline+SnF_2, DMSO+DMF (s), CB (as)	[192]
ITO/NiO_x/$FASnI_3$/PCBM/Ag	0.552	17.64	69.4	6.76	500 h in air (en), 20% decrease	KHQSA-$SnCl_2$ (a), DMSO+DMF (s), CB (as)	[132]
ITO/NiO_x/$FASnI_3$/PCBM/Ag	0.518	14.07	70.8	5.16	/	APSA-$SnCl_2$(a), DMSO+DMF (s), CB (as)	[132]
ITO/NiO_x/$FASnI_3$/PCBM/Ag	0.491	16.18	70.2	5.58	/	PSA-$SnCl_2$ (a), DMSO+DMF (s), CB (as)	[132]
ITO/PEDOT:PSS/$FASnI_3$/PCBM/BCP/Ag	0.59	18.89	62.3	7	100 h in N_2, no decrease	5-AVA+SnF_2 (a), DMSO (s), CB (as)	[140]
ITO/PEDOT:PSS/$FASnI_3$/C_{60}/BCP/Ag	0.67	21.59	0.75	10.81	/	POEI+SnF_2 (a), DMSO (s), CB (as)	[112]
ITO/PEDOT:PSS/$FASnI_3$/C_{60}/BCP/Ag	0.583	21.3	71.8	8.9	2000 h in N_2, slight decrease	BAI+$EDAI_2$+SnF_2 (a), DMSO (s), CB (as)	[148]
ITO/PEDOT:PSS/$FASnI_3$/PCBM/BCP/Ag	0.517	21.27	66.91	7.36	800 h in N_2, 9.9% decrease	EVA+SnF_2 (a), DMSO+DMF (s), CB (as)	[137]
ITO/c-SnO_2/C_{60}/$FASnI_3$/spiro-OMeTAD/Ag	0.31	21.65	64.7	4.34	20 d in N_2, 20% decrease	Two steps, TMA+SnF_2 (a), DMSO+DMF (s), CB (as)	[99]
ITO/PEDOT:PSS/$FASnI_3$/C_{60}/BCP/Ag	0.47	22.45	67.8	7.09	20 d in N_2, 8% decrease	Two steps, TMA+SnF_2 (a), DMSO+DMF (s), CB (as)	[99]
ITO/PEDOT:PSS/$FASnI_3$/C_{60}/BCP/Ag	0.614	20.159	68.6	8.71	400 h in N_2, no decrease	PVA+SnF_2 (a), DMSO (s), CB (as)	[144]
ITO/PEDOT:PSS/$FASnI_3$/C_{60}/BCP/Ag	0.63	21.6	74.7	10.17	1000 h in air (en), 10% decrease	CDTA+SnF_2 (a), DMSO (s), CB (as)	[136]
ITO/PEDOT:PSS/$FASnI_3$/C_{60}/BCP/Ag	0.57	20.45	69.1	8.05	/	CTA-F+SnF_2 (a), DMSO (s), CB (as)	[136]
ITO/PEDOT:PSS/$FASnI_3$/C_{60}/BCP/Ag	0.59	21.05	72.1	8.96	/	CTA-OMe+SnF_2 (a), DMSO (s), CB (as)	[136]
ITO/PEDOT:PSS/$FASnI_3$/C_{60}/BCP/Ag	0.73	22.37	72	11.78	1000 h in N_2, 5% decay	PAI+SnF_2 (a), DMSO (s), CB (as)	[141]
ITO/PEDOT:PSS/$FASnI_3$/C_{60}/BCP/Ag	0.69	21.53	68.46	10.17	1600 h in N_2, less 15% decay	2-F-PEAI+SnF_2 (a), DMF+DMSO (s), CB (as)	[147]
ITO/PEDOT:PSS/$FASnI_3$/C_{60}/BCP/Ag	0.68	20.24	68.5	9.4	/	3-F-PEAI+SnF_2 (a), DMF+DMSO (s), CB (as)	[147]
ITO/PEDOT:PSS/$FASnI_3$/C_{60}/BCP/Ag	0.67	18.91	65.27	8.27	/	4-F-PEAI+SnF_2 (a), DMF+DMSO (s), CB (as)	[147]
ITO/NiO_x/$FASnI_3$/PCBM/BCP/Ag	0.64	19.75	71.4	9.03	1000 h in air (en), 20% decay	GA+$SnCl_2$ (a), DMF+DMSO (s), CB (as)	[129]
ITO/PEDOT:PSS/$FASnI_3$/C_{60}/BCP/Ag	0.76	23.5	64	11.4	120 d in N_2, no decay	PHCl+SnF_2 (a), DMSO (s), CB (as)	[150]
FTO/NiO_x/$FASnI_3$/PCBM/BCP/Ag	0.69	21.15	0.74	10.86	500 h under 1-sun illumination in N_2 at 40 °C, 23% decay	4AMPI_2 (a), DMF+DMSO (s), CB (as)	[193]
FTO/PEDOT:PSS/$FASnI_3$/C_{60}/BCP/Ag	0.65	22.2	71.6	10.4	1000 h in N_2, 4% decay	BAAc+SnF_2+PEABr+EABr (a), DMSO (s), CB (as)	[126]
ITO/PEDOT:PSS/$FASnI_3$/BCP/ICBA/Ag	0.92	20.4	76.6	14.3	500 min unencapsulated in air at 75% RH, 15% decay	PEAI+3T+N-methylthiourea (a), DMF+DMSO, toluene (as)	[143]
ITO/TiO_2/$CsSnX_3$/spiro-OMeTAD/Au	0.86	23.2	65	12.96	12 d in N_2, 43% decay	Perovskite quantum rods	[194]
ITO/PEDOT:PSS/$CsSnI_3$/PCBM/Ag	0.42	23.792	/	4.13	30 d in N_2, 28% decay	Perovskite quantum rods	[195]
ITO/PEDOT:PSS/$FASnI_3$/C_{60}/BCP/Ag	0.525	24.1	71	9	76 h in air, 41% decay	2D, 3D hybrid, PEAI+SnF_2 (a), DE (as)	[165]
FTO/PEDOT:PSS/$FA_{0.92}PEA_{0.08}Sn_{0.925}Ge_{0.075}I_3$/$C_{60}$/BCP/Ag/Au	0.46	21.92	76	7.45	250 min in air, 30% decay	Quasi-2D, 3D hybrid, GeI_2+SnF_2 (a), DMSO+DMF (s), CB (as)	[166]
ITO/LiF/PEDOT:PSS/$PEA_2FA_nSn_{n-1}I_{3n+1}$/C60/BCP/Ag	0.47	20.07	74	6.98	5 d in N_2, 10% decay	2D, 3D hybrid, PEAI (a), evaporation deposition	[38]
ITO/NiO_x/$PEA_2FASn_2I_7$-$FASnI_3$/PCBM/BCP/Ag	0.61	22	70.1	9.41	600 h in N_2, 25% decay	2D, 3D hybrid, PEAI+SnF_2+NH_4SCN (a), DMF+DMSO (s), toluene (as)	[164]
ITO/NiO_x/$(PEA)_2(FA)_8Sn_9I_{28}$-$FASnI_3$/PCBM/Ag	0.59	14.44	69	5.95	100 h in N_2, no decay	2D, 3D hybrid, PEAI+SnF_2 (a), DMF+DMSO (s),	[160]

Table 1. Continued.

Device structure	Cell parameters				Stability	Strategy	Ref.
	V_{OC} [V]	J_{SC} [mA cm^{-2}]	FF [%]	PCE [%]			
ITO/PEDOT:PSS/$FASnI_3$/PCBM/Ag	0.53	21.8	66.5	7.66	1000 h in N_2, less 10% decay	Quasi-2D, PEAI+FASCN+SnF_2 (a), DMSO+DMF (s), CB (as)	[133]
ITO/c-TiO_2/m-TiO_2/(n-$CH_3(CH_2)_3NH_3)_2(CH_3NH_3)_2$ Sn_3I_{10}/PTAA/Au	0.229	24.1	45.7	2.53	30 d in N_2, 6.8% decay	2D, TEP+SnF_2 (a), DMF+DMSO (s),	[161]
FTO/NiO_x/$FASnI_3$/C60/BCP/Ag	0.59	22.06	69	9.1	1680 h in N_2, no decay	2D, PEACl+SnF_2, DMSO (s), CB (as)	[127]
ITO/PEDOT:PSS/$FASnI_3$/PCBM/BCP/Ag	0.61	21	68	8.71	400 h in N_2, no decay	Quasi-2D,5-AVAI+SnF_2+NH_4Cl, DMSO+DMF (s),	[163]
FTO/c-TiO_2/m-TiO_2/$FASnI_3$/PTAA/Au	0.48	22.54	65.96	7.14	1000 h in N_2, no decay	3D, en+SnF_2 (a), DMSO+DMF (s)	[158]
FTO/c-TiO_2/m-TiO_2/$MASnI_3$/PTAA/Au	0.43	24.28	63.72	6.63	10 min in air, 30% decay	3D, en+SnF_2 (a), DMSO+DMF (s)	[159]
ITO/PEDOT:PSS/$FASnI_3$/C_{60}/BCP/Ag	0.56	23.34	73.5	9.61	1440 h in N_2, less 10% decay	3D, PPAI+SnF_2 (a), DMSO (s)	[39]
ITO/PEDOT:PSS/$FASnI_3$/ICBA/BCP/Al	0.84	24.91	70.76	14.81	/	2D, 3D hybrid, SnF_2+FPEABr (a), DMF+DMSO (s), CB (as)	[29]
ITO/CuI/$CsSnI_3$/C_{60}/BCP/Al	0.282	11.6	43.4	1.72	/	More SnI_2, DMF (s)	[179]
ITO/PEDOT:PSS/$FASnI_3$/C_{60}/BCP/Ag	0.65	21.10	76.30	10.40	150 h unencapsulated in air at 40% RH, no decay	2D, 3D hybrid, GAI+SnF_2+AN (a), DMSO (s)	[167]
ITO/PEDOT:PSS/$FASnI_3$/ICBA/BCP/Al	0.84	24.91	70.76	14.81	/	2D, 3D hybrid, FPEABr+SnF_2 (a), DMSO+DMF (s), CB (as)	[29]
ITO/NiOX/$FASnI_3$/ICBA/BCP/Ag	1.01	20.32	67.2	13.79	1200 h in N_2, 10% decay	2D, 3D hybrid, PEAI+SnF_2+GuaSCN (a), DMF+DMSO (s), CB (as)	[168]
ITO/CuI/$CsSnI_3$/PCBM/BCP/Al	0.355	8.94	53.8	2.07	/	More SnI_2, DMF (s)	[179]
ITO/CuI/$CsSnI_3$/ICBA/BCP/Al	0.491	7.1	50	2.6	10 d in N_2, 37.5% decay	More SnI_2, DMF (s)	[179]
ITO/NiOx/WSe_2/$FASnI_3$/PCBM/BCP/Ag	0.63	22.71	73.2	10.47	1000 h in air at 20% RH, 17% decay	$SnCl_2$+ gallic acid (a), WSe_2 (m), DMSO+DMF (s), CB (as)	[187]
FTO/c-TiO_2/ZnS/$FASnI_3$/PTAA/Au	0.38	23.09	60.01	5.27	/	SnF_2 (a), ZnS (m), DMSO+DMF (s), DE (as)	[83]
FTO/c-TiO_2/CdS/$FASnI_3$/PTAA/Au	0.328	22.02	52.11	3.76	/	SnF_2 (a), CdS (m), DMSO+DMF (s), DE (as)	[83]
ITO/PEDOT:PSS/$FASnI_3$/ICBA/Ag	0.94	17.4	75	12.4	3800 h in N_2, 10% decay	PEAI+SnF_2+NH_4SCN (a), DMF+DMSO (s), toluene (as)	[180]
ITO/PEDOT:PSS/$FASnI_3$/ICBA/Ag	0.78	17.8	72	10.1	/	PEAI+SnF_2 (a), DMF+DMSO (s), toluene (as)	[180]
ITO/PEDOT:PSS/$FASnI_3$/PCBM/Ag	0.6	17.1	74	7.7	/	PEAI+SnF_2+NH_4SCN (a), DMF+DMSO (s), toluene (as)	[180]
FTO/SnO_2/CPTA/$FASnI_3$/PTAA/Au	0.687	16.45	65	7.4	200 min in air, 20% decay	CPTA (m), SnF_2+enI_2 (a), DMF+DMSO (s), CB (as)	[178]
FTO/PEG-PEDOT:PSS/$FASnI_3$/PCBM/BCP/Ag	0.37	22.06	62.7	5.12	30 d in N_2, 5% decay	SnF_2 (a), DMF+DMSO (s), CB (as)	[54]
FTO/TiO_2/$FASnI_3$/TPE/Au	0.465	21.96	68.52	7	60 min in air, 35% decrease	TPE (HTL), SnF_2+en (a), DMF+DMSO (s)	[171]
FTO/TiO_2/$FASnI_3$/BDT-4D/Au	0.497	22.41	68.21	7.59	/	BDT-4D+SnF_2+en (a), DMF+DMSO (s)	[181]
ITO/PEG-PEDOT:PSS/$FASnI_3$/C_{60}/BCP/Ag	0.593	20.94	72.7	9.03	600 h light soaking in N_2, 7% decay	FBH (m), SnF_2 (a), DMSO (s), CB (as)	[186]
ITO/PEDOT:PSS/$FASnI_3$/C_{60}/BCP/Ag	0.45	24.87	63	7.05	/	SnF_2 (a), PEABr (m), DMF+DMSO (s), DE (as)	[183]
FTO/PEDOT:PSS/$Ge_{0.01}(FA_{1-x}EA_x)_{0.98}EDA_{0.01}SnI_3$/ C_{60}/BCP/Ag	0.84	20.38	74	13.24	/	GeI+$EDAI_2$+SnF_2 (a), DMF+DMSO (s), CB (as)	[149]
ITO/$FASnI_3$/PCBM/BCP/Ag	0.67	22.03	68.5	10.58	40 d light soaking in N_2, 5% decay	SnF_2+$EDAI_2$+MAI (a), DMSO (s), CB (as)	[182]
ITO/MeO-2PACz/$FASnI_3$/C_{60}/BCP/Ag	0.475	20.3	67.3	6.49	1900 h in N_2, 20% decay	Two steps, $EDAI_2$+SnF_2 (a), SAM (m), DMSO (s), IPA+HFB+CB (s), CB (as)	[196]
PET-ITO/NiO_X/GeO_2/$FASn_{0.9}Ge_{0.1}I_3$/4AMPI_2/PCBM/ BCP/Ag	0.69	21.3	71	10.43	700 h light soaking in N_2, 20% decay	SnF_2+GeI_2 (a), GeO_2+4AMPI_2 (m), DMF+DMSO+NMP (s), CB (as)	[188]

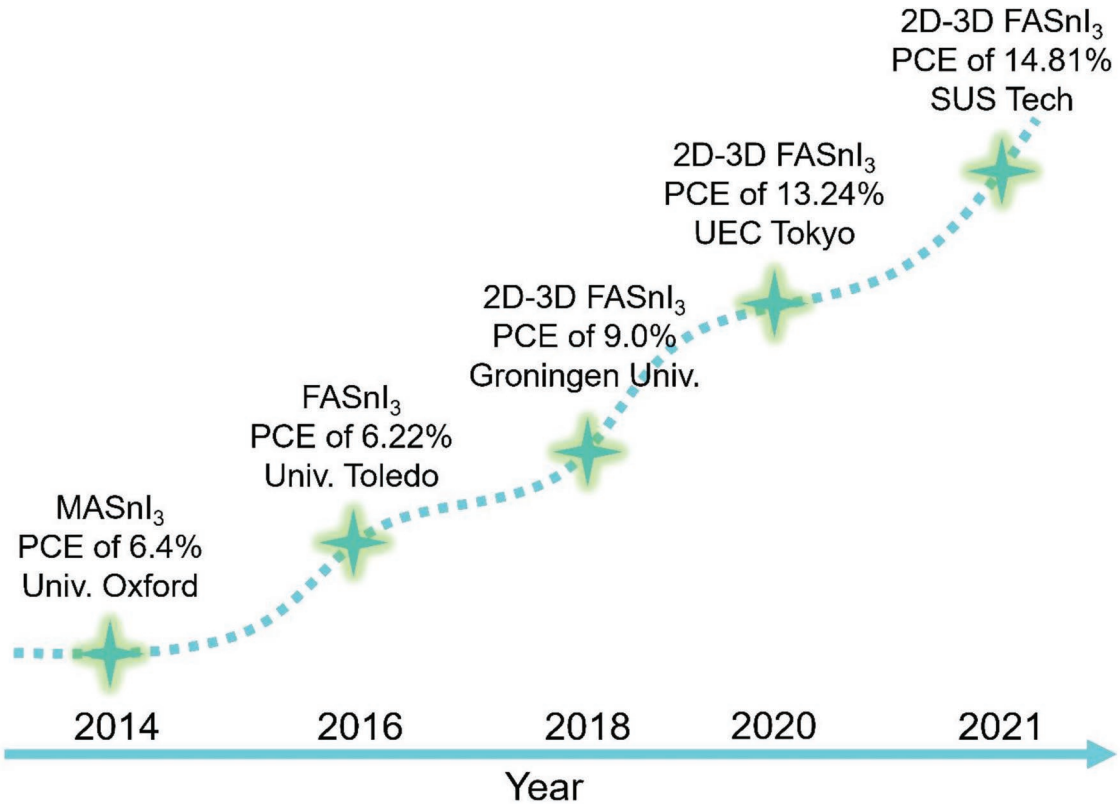

Figure 16. The efficiency roadmap of Sn-based PSCs.

essence. CB and TL have been frequently used as antisolvent for different perovskite films.[91–97] But the Sn-based perovskites usually experiment with rapid crystallization using CB or TL as antisolvent.[37] So, we can explore useful antisolvent to replace CB or TL.

In addition, additives can passivate the defect states, improve the antioxidant properties of Sn perovskite, control the nucleation rate, etc. Sn halides are the common inorganic additives that can be added to precursor solutions alone or mixed with other substances to improve the quality of the Sn-based perovskite. SnF_2 is an effective and necessary inorganic addition to prepare Sn-based perovskite of high-quality and pinhole-free.[64,65,123] Organic materials could be used as an additive to improve the quality and stability of Sn-based perovskite films by different mechanisms.[99,128,134,139,193] The principle of choosing organic additions is to prevent Sn^{2+} oxidation, insulate moisture, and inhibit vacancy formation.

In low-dimension structure, the most common 3D crystal structure, Sn-based perovskites have the disadvantage of poor stability.[159] While the 2D perovskites have attracted enormous attention due to their excellent stability.[160,161] In there, we can use organic to form 2D, quasi-2D, and hybrid 2D/3D structures to improve the stability of the device. Such as PEAI[160] and PEACl.[127]

The interlayer between perovskite and ETL or HTL was the primary research field in interlayers. For example, TiO_2 was used as the ETL material of the first generation of PSCs.[30,31,174] TiO_2 has a strong electron transport capability. However, it reduces the V_{OC} of the Sn-based PSCs due to their high back-hole carrier density, which leads to the recombination of the electrons in TiO_2 with the holes from Sn-based perovskite quickly. This affects the carrier transport stability of the device.[83] So, we can introduce interlayers to reduce interface defects and smooth stepped band structure between perovskite and ETL. In inverted PSCs, PEDOT:PSS is the most common HTL due to its simple solution processability and its ability to combine well with the conductive glass (ITO and FTO).[174] But there is a problem with band alignment mismatch. Hence, we can adjust the band alignment with complex effective materials to decrease the energy band deficit. Such as PEG[54] and PTN-Br.[139]

The complete replacement of Pb^{2+} with Sn^{2+} in metal halide perovskite has many merits and shortcomings. The most significant advantage is that pure Sn-based perovskite is nontoxic and can be easily removed from the environment. The narrowing band gap can absorb light, but the mismatch of the energy bands of the Sn-based perovskite with ETL and HTL jeopardizes electron and hole transportation. The pinholes and random orientation due to quick crystallization, the ready oxidation of Sn^{2+} to Sn^{4+} when exposed to the atmosphere, these disadvantages can be solved to a certain extent by processing, additives, solutions, low-dimension structure and interlayer modification. Nonetheless, the effect of the moisture is pernicious. However, at present, the research on strengthening the stability against humidity is less. We believe that with enhancing the device performance, the commercialization process will take a big step forward.

7. Perspective

In conclusion, the Sn-based PSCs have been considered front-runner replacement candidates for Pb-based PSCs. However, many obstacles must be overcome to achieve the high efficiency and stability of Pb-based PSCs. As reported in the literature, Sn-based perovskites quickly turn brown after adding an anti-solvent, indicating that the Sn-based perovskite film's crystallization rate is faster. In contrast, high-efficiency Pb-based perovskite is colorless after adding an anti-solvent. Therefore, to achieve the same high efficiency as lead-based PSCs, slowing the crystallization rate and improving the film quality is an important direction. To solve this, we propose exploring the physical mechanism of rapid crystallization, for example, the highly reactive valence electrons of the 5s orbits for Sn. Second, we need to solve the energy level mismatch by adapting Sn-based perovskites to match more structures, such as n-i-p and p-i-n structures. For this, we can adjust the composition of Sn-based perovskite materials, add passivation agents, or do it through interface passivation. Finally, environmental stability is also a problem that must be solved to adapt to commercialization. To solve the oxidation and humidity stability of divalent tin, we can purify the original SnI_2 and reduce the proportion of tetravalent tin to solve the oxidation problem of divalent tin. The humidity stability can be solved by adding hydrophobic materials or packaging technology.

At present, module devices,[197–202] flexible devices,[203–208] and indoor photovoltaic devices[209–214] have been the primary research orientation in Pb-based PSCs. Although the stability and PCE of Sn-based are inferior to Pb-based PSCs, for commercialization purposes, the development of Sn-based module devices, flexible devices, and indoor photovoltaic devices is necessary.

Acknowledgements

H.L. and Z.Z. contributed equally to this work. This work was supported by the Henan Province college youth backbone teacher project (No:2020GGJS062); M.L. would like to acknowledge funding support from the Nature Science Foundation of China (No. 51903181). Cultivation Fund for National Scientific Research Project of Henan Normal University (No:2019PL08). M.S. thanks the German Research Foundation (DFG) for funding (SPP2196, GRK 2642). M.M.B. thanks the Helmholtz Young Investigator Group FRONTRUNNER. M.S. acknowledges funding by ProperPhotoMile. Project ProperPhotoMile is supported under the umbrella of SOLAR-ERA.NET Cofund 2 by The Spanish Ministry of Science and Education and the AEI under the project PCI2020-112185 and CDTI project number IDI-20210171; the Federal Ministry for Economic Affairs and Energy on the basis of a decision by the German Bundestag project number FKZ 03EE1070B and FKZ 03EE1070A and the Israel Ministry of Energy with project number 220-11-031. SOLAR-ERA.NET is supported by the European Commission within the EU Framework Programme for Research and Innovation HORIZON 2020 (Cofund ERA-NET Action, No. 786483). Funded by the European Union. Views and opinions expressed are however those of the author(s) only and do not necessarily reflect those of the European Union or European Research Council Executive Agency (ERCEA). Neither the European Union nor the granting authority can be held responsible for them. The authors acknowledge funding from the European Research Council under the Horizon Europe programme (LOCAL-HEAT, grant agreement no. 101041809).

Open access funding enabled and organized by Projekt DEAL.

Conflict of Interest

The authors declare no conflict of interest.

Keywords

efficiency, Sn-based perovskites, solar cells, stability

Received: June 30, 2022
Revised: October 26, 2022
Published online: December 7, 2022

[1] A. Kojima, K. Teshima, Y. Shirai, T. Miyasaka, *J. Am. Chem. Soc.* **2009**, *131*, 6050.
[2] https://www.nrel.gov/pv/assets/pdfs/best-research-cell-eFFiciencies-rev211214.pdf (accessed: May 2022).
[3] E. Assirey, *Saudi Pharm. J.* **2019**, *27*, 817.
[4] J. Gao, Q. Liang, G. Li, T. Ji, Y. Liu, M. Fan, Y. Hao, S. Liu, Y. Wu, Y. Cui, *J. Mater. Chem. C* **2019**, *7*, 8357.
[5] S. Sun, T. Salim, N. Mathews, M. Duchamp, C. Boothroyd, G. Xing, T. C. Sum, Y. M. Lam, *Energy Environ. Sci.* **2014**, *7*, 399.
[6] G. Xing, N. Mathews, S. Sun, S. S. Lim, Y. M. Lam, M. Grätzel, S. Mhaisalkar, T. C. Sum, *Science* **2013**, *342*, 344.
[7] C. Wehrenfennig, G. E. Eperon, M. B. Johnston, *Adv. Mater.* **2014**, *26*, 1584.
[8] C. C. Stoumpos, C. D. Malliakas, M. G. Kanatzidis, *Inorg. Chem.* **2013**, *52*, 9019.
[9] K. X. Steirer, P. Schulz, G. Teeter, V. Stevanovic, M. Yang, K. Zhu, J. J. Berry, *ACS Energy Lett.* **2016**, *1*, 360.
[10] D. Meggiolaro, S. G. Motti, E. Mosconi, A. J. Barker, J. Ball, R. P. C. Andrea, F. Deschler, A. Petrozza, A. F. De, *Energy Environ. Sci.* **2018**, *11*, 702.
[11] W. Zhang, M. Saliba, S. D. Stranks, Y. Sun, X. Shi, U. Wiesner, H. J. Snaith, *Nano Lett.* **2013**, *13*, 4505.
[12] V. D'Innocenzo, G. Grancini, M. J. Alcocer, A. R. Kandada, S. D. Stranks, M. M. Lee, G. Lanzani, H. J. Snaith, A. Petrozza, *Nat. Commun.* **2014**, *5*, 3586.
[13] J. I. Kwak, L. Kim, Y. J. An, *Sci. Total Environ.* **2021**, *771*, 145388.
[14] Z. Li, X. Wu, B. Li, S. Zhang, D. Gao, Y. Liu, X. Li, N. Zhang, X. Hu, C. Zhi, A. K.-Y. Jen, Z. Zhu, *Adv. Energy Mater.* **2022**, *12*, 2103236.
[15] Z. Li, X. Wua, S. Wua, D. Gao, H. Dong, F. Huang, X. Hu, A. K.-Y. Jen, Z. Zhu, *Nano Energy* **2022**, *93*, 106853.
[16] B. Hailegnaw, S. Kirmayer, E. Edri, G. Hodes, D. Cahen, *J. Phys. Chem. Lett.* **2015**, *6*, 1543.
[17] A. Babayigit, A. Ethirajan, M. Muller, B. Conings, *Nat. Mater.* **2016**, *15*, 247.
[18] F.-W. Liu, G. Biesold, M. Zhang, R. Lawless, J.-P. Correa-Baena, Y.-L. Chueh, Z. Lin, *Mater. Today* **2021**, *43*, 185.
[19] W.-F. Yang, F. Igbari, Y.-H. Lou, Z.-K. Wang, L.-S. Liao, *Adv. Energy Mater.* **2019**, *10*, 1902584.
[20] W. Meng, X. Wang, Z. Xiao, J. Wang, D. B. Mitzi, Y. Yan, *J. Phys. Chem. Lett.* **2017**, *8*, 2999.
[21] W. Travis, E. N. K. Glover, H. Bronstein, D. O. Scanlon, R. G. Palgrave, *Chem. Sci.* **2016**, *7*, 4548.
[22] S. Tao, X. Cao, P. A. Bobbert, *Sci. Rep.* **2017**, *7*, 14386.
[23] E. L. Lim, A. Hagfeldt, D. Bi, *Energy Environ. Sci.* **2021**, *14*, 3256.
[24] A. Babayigit, T. D. Duy, A. Ethirajan, J. Manca, M. Muller, H. G. Boyen, B. Conings, *Sci. Rep.* **2016**, *6*, 18721.
[25] M.-G. Ju, M. Chen, Y. Zhou, J. Dai, L. Ma, N. P. Padture, X. C. Zeng, *Joule* **2018**, *2*, 1231.

[26] W. Liao, D. Zhao, Y. Yu, N. Shrestha, K. Ghimire, C. R. Grice, C. Wang, Y. Xiao, A. J. Cimaroli, R. J. Ellingson, N. J. Podraza, K. Zhu, R. G. Xiong, Y. Yan, *J. Am. Chem. Soc.* **2016**, *138*, 12360.
[27] D. Zhao, Y. Yu, C. Wang, W. Liao, N. Shrestha, C. R. Grice, A. J. Cimaroli, L. Guan, R. J. Ellingson, K. Zhu, X. Zhao, R.-G. Xiong, Y. Yan, *Nat. Energy* **2017**, *2*, 17018.
[28] Z. Yang, A. Rajagopal, C. C. Chueh, S. B. Jo, B. Liu, T. Zhao, A. K. Jen, *Adv. Mater.* **2016**, *28*, 8990.
[29] B.-B. Yu, Z. Chen, Y. Zhu, Y. Wang, B. Han, G. Chen, X. Zhang, Z. Du, Z. He, *Adv. Mater.* **2021**, *33*, 2102055.
[30] N. K. Noel, S. D. Stranks, A. Abate, C. Wehrenfennig, S. Guarnera, A.-A. Haghighirad, A. Sadhanala, G. E. Eperon, S. K. Pathak, M. B. Johnston, A. Petrozza, L. M. Herz, H. J. Snaith, *Energy Environ. Sci.* **2014**, *7*, 3061.
[31] F. Hao, C. C. Stoumpos, D. H. Cao, R. P. H. Chang, M. G. Kanatzidis, *Nat. Photonics* **2014**, *8*, 489.
[32] T. Leijtens, R. Prasanna, A. Gold-Parker, M. F. Toney, M. D. McGehee, *ACS Energy Lett.* **2017**, *2*, 2159.
[33] J. Qiu, Y. Xia, Y. Chen, W. Huang, *Adv. Sci.* **2019**, *6*, 1800793.
[34] X. Liu, K. Yan, D. Tan, X. Liang, H. Zhang, W. Huang, *ACS Energy Lett.* **2018**, *3*, 2701.
[35] J. Liu, M. Ozaki, S. Yakumaru, T. Handa, R. Nishikubo, Y. Kanemitsu, A. Saeki, Y. Murata, R. Murdey, A. Wakamiya, *Angew. Chem. Int. Ed. Engl.* **2018**, *130*, 13405.
[36] Z. Chen, J. J. Wang, Y. Ren, C. Yu, K. Shum, *Appl. Phys. Lett.* **2012**, *101*, 093901.
[37] W. Liao, D. Zhao, Y. Yu, C. R. Grice, C. Wang, A. J. Cimaroli, P. Schulz, W. Meng, K. Zhu, R. G. Xiong, Y. Yan, *Adv. Mater.* **2016**, *28*, 9333.
[38] C. Ran, J. Xi, W. Gao, F. Yuan, T. Lei, B. Jiao, X. Hou, Z. Wu, *ACS Energy Lett.* **2018**, *3*, 713.
[39] C. Ran, W. Gao, J. Li, J. Xi, L. Li, J. Dai, Y. Yang, X. Gao, H. Dong, B. Jiao, I. Spanopoulos, C. D. Malliakas, X. Hou, M. G. Kanatzidis, Z. Wu, *Joule* **2019**, *3*, 3072.
[40] J. Cao, F. Yan, *Energy Environ. Sci.* **2021**, *14*, 1286.
[41] M. Pitaro, E. K. Tekelenburg, S. Shao, M. A. Loi, *Adv. Mater.* **2022**, *34*, 2105844.
[42] T. Wu, X. Liu, X. Luo, X. Lin, D. Cui, Y. Wang, H. Segawa, Y. Zhang, L. Han, *Joule* **2021**, *5*, 863.
[43] L. Xu, X. Feng, W. Jia, W. Lv, A. Mei, Y. Zhou, Q. Zhang, R. Chen, W. Huang, *Energy Environ. Sci.* **2021**, *14*, 4292.
[44] C. J. Howard, H. T. Stokes, *Acta Crystallogr.* **1998**, *B54*, 782.
[45] H. Zhang, N. Li, K. Li, D. Xue, *Acta Crystallogr.* **2007**, *63*, 812.
[46] M. V. Kovalenko, L. Protesescu, M. I. Bodnarchuk, *Science* **2017**, *358*, 745.
[47] G. Kieslich, S. Sun, A. K. Cheetham, *Chem. Sci.* **2015**, *6*, 3430.
[48] R. E. Eitel, C. A. Randall, T. R. Shrout, P. W. Rehrig, W. Hackenberger, S. E. Park, *Jpn. J. Appl. Phys.* **2001**, *40*, 5999.
[49] C. A. Randall, A. S. Bhalla, T. R. Shrout, L. E. Cross, *J. Mater. Res.* **1990**, *5*, 829.
[50] C. J. Bartel, C. Sutton, B. R. Goldsmith, R. Ouyang, C. B. Musgrave, L. M. Ghiringhelli, M. Scheffler, *Sci. Adv.* **2019**, *5*, eaav0693.
[51] C. Li, X. Lu, W. Ding, L. Feng, Y. Gao, Z. Guo, *Acta Crystallogr.* **2008**, *64*, 702.
[52] S. A. T. Redfern, *J. Phys.: Condens. Mater.* **1996**, *8*, 8267.
[53] Y. Dang, Y. Zhou, X. Liu, D. Ju, S. Xia, H. Xia, X. Tao, *Angew. Chem. Int. Ed. Engl.* **2016**, *55*, 3447.
[54] X. Liu, Y. Wang, F. Xie, X. Yang, L. Han, *ACS Energy Lett.* **2018**, *3*, 1116.
[55] G. Xie, L. Xu, L. Sun, Y. Xiong, P. Wu, B. Hu, *J. Mater. Chem. A* **2019**, *7*, 5779.
[56] Q. Li, W. Wan, Y. Ge, B. Wang, Y. Li, C. Wang, Y.-H. Zhao, Y. Liu, *Appl. Phys. Lett.* **2019**, *114*, 101916.
[57] Y. Takahashi, R. Obara, Z. Z. Lin, Y. Takahashi, T. Naito, T. Inabe, S. Ishibashi, K. Terakura, *Dalton Trans.* **2011**, *40*, 5563.
[58] Y. Takahashi, H. Hasegawa, Y. Takahashi, T. Inabe, *J. Solid State Chem.* **2013**, *205*, 39.
[59] D. B. Mitzi, K. Liang, *J. Solid State Chem.* **1997**, *134*, 376.
[60] E. C. Schueller, G. Laurita, D. H. Fabini, C. C. Stoumpos, M. G. Kanatzidis, R. Seshadri, *Inorg. Chem.* **2018**, *57*, 695.
[61] S. Kahmann, O. Nazarenko, S. Shao, O. Hordiichuk, M. Kepenekian, J. Even, M. V. Kovalenko, G. R. Blake, M. A. Loi, *ACS Energy Lett.* **2020**, *5*, 2512.
[62] I. Chung, J.-H. Song, J. Im, J. Androulakis, C. D. Malliakas, H. Li, A. J. Freeman, J. T. Kenney, M. G. Kanatzidis, *J. Am. Chem. Soc.* **2012**, *134*, 8579.
[63] K. G. Rajendra, H.-J. Kim, S. Karupannan, K. Prabakar, *J. Phys. Chem. C* **2017**, *121*, 16447.
[64] M. H. Kumar, S. Dharani, W. L. Leong, P. P. Boix, R. R. Prabhakar, T. Baikie, C. Shi, H. Ding, R. Ramesh, M. Asta, M. Graetzel, S. G. Mhaisalkar, N. Mathews, *Adv. Mater.* **2014**, *26*, 7122.
[65] L. Ma, F. Hao, C. C. Stoumpos, B. T. Phelan, M. R. Wasielewski, M. G. Kanatzidis, *J. Am. Chem. Soc.* **2016**, *138*, 14750.
[66] F. Gu, S. Ye, Z. Zhao, H. Rao, Z. Liu, Z. Bian, C. Huang, *Sol. RRL* **2018**, *2*, 1800136.
[67] X. Jiang, H. Li, Q. Zhou, Q. Wei, M. Wei, L. Jiang, Z. Wang, Z. Peng, F. Wang, Z. Zang, *J. Am. Chem. Soc.* **2021**, *143*, 10970.
[68] Q. Jiang, Z. Ni, G. Xu, Y. Lin, P. N. Rudd, R. Xue, Y. Li, Y. Li, Y. Gao, J. Huang, *Adv. Mater.* **2020**, *32*, 2001581.
[69] X. Meng, Z. Xing, X. Hu, Z. Huang, T. Hu, L. Tan, F. Li, Y. Chen, *Angew. Chem. Int. Ed. Engl.* **2020**, *59*, 16602.
[70] C. Luo, Y. Zhao, X. Wang, F. Gao, Q. Zhao, *Adv. Mater.* **2021**, *33*, 2103231.
[71] L. Cheng, K. Meng, Z. Qiao, Y. Zhai, R. Yu, L. Pan, B. Chen, M. Xiao, G. Chen, *Adv. Mater.* **2022**, *34*, 2106380.
[72] J. Zhu, S. Park, O. Y. Gong, C. Sohn, Z. Li, Z. Zhang, B. Jo, W. Kim, G. S. Han, D. H. Kim, T. K. Ahn, J. Lee, H. S. Jung, *Energy Environ. Sci.* **2021**, *14*, 4903.
[73] L. Shen, P. Song, L. Zheng, K. Liu, K. Lin, W. Tian, Y. Luo, C. Tian, L. Xie, Z. Wei, *J. Mater. Chem. A* **2021**, *9*, 20807.
[74] F. Hao, C. C. Stoumpos, R. P. Chang, M. G. Kanatzidis, *J. Am. Chem. Soc.* **2014**, *136*, 8094.
[75] M. T. Klug, R. L. Milot, J. B. Patel, T. Green, H. C. Sansom, M. D. Farrar, A. J. Ramadan, S. Martani, Z. Wang, B. Wenger, J. M. Ball, L. Langshaw, A. Petrozza, M. B. Johnston, L. M. Herz, H. J. Snaith, *Energy Environ. Sci.* **2020**, *13*, 1776.
[76] F. Hao, C. C. Stoumpos, P. Guo, N. Zhou, T. J. Marks, R. P. Chang, M. G. Kanatzidis, *J. Am. Chem. Soc.* **2015**, *137*, 11445.
[77] H. Tsai, W. Nie, J. C. Blancon, C. C. Stoumpos, R. Asadpour, B. Harutyunyan, A. J. Neukirch, R. Verduzco, J. J. Crochet, S. Tretiak, L. Pedesseau, J. Even, M. A. Alam, G. Gupta, J. Lou, P. M. Ajayan, M. J. Bedzyk, M. G. Kanatzidis, *Nature* **2016**, *536*, 312.
[78] Y. Lin, Y. Bai, Y. Fang, Q. Wang, Y. Deng, J. Huang, *ACS Energy Lett.* **2017**, *2*, 1571.
[79] W. Peng, J. Yin, K. T. Ho, O. Ouellette, B. M. De, B. Murali, T. O. El, C. Shen, X. Miao, J. Pan, E. Alarousu, J. H. He, B. S. Ooi, O. F. Mohammed, E. Sargent, O. M. Bakr, *Nano Lett.* **2017**, *17*, 4759.
[80] Y. Xia, C. Ran, Y. Chen, Q. Li, N. Jiang, C. Li, Y. Pan, T. Li, J. Wang, W. Huang, *J. Mater. Chem. A* **2017**, *5*, 3193.
[81] J. Pascual, G. Nasti, M. H. Aldamasy, J. A. Smith, M. Flatken, N. Phung, D. D. Girolamo, S.-H. Turren-Cruz, M. Li, A. Dallmann, R. Avolio, A. Abate, *Mater. Adv.* **2020**, *1*, 1066.
[82] G. D. Di, J. Pascual, M. H. Aldamasy, Z. Iqbal, G. Li, E. Radicchi, M. Li, S.-H. Turren-Cruz, G. Nasti, A. Dallmann, A. F. De, A. Abate, *ACS Energy Lett.* **2021**, *6*, 959.
[83] W. Ke, C. C. Stoumpos, J. L. Logsdon, M. R. Wasielewski, Y. Yan, G. Fang, M. G. Kanatzidis, *J. Am. Chem. Soc.* **2016**, *138*, 14998.
[84] S. J. Lee, S. S. Shin, Y. C. Kim, D. Kim, T. K. Ahn, J. H. Noh, J. Seo, S. I. Seok, *J. Am. Chem. Soc.* **2016**, *138*, 3974.

[85] H. Min, D. Y. Lee, J. Kim, G. Kim, K. S. Lee, J. Kim, M. J. Paik, Y. K. Kim, K. S. Kim, M. G. Kim, T. J. Shin, S. I. Seok, *Nature* **2021**, *598*, 444.
[86] Y. Yang, W. Zhao, T. Yang, J. Liu, J. Zhang, Y. Fang, S. Liu, *J. Mater. Chem. A* **2021**, *9*, 23597.
[87] S. Chen, X. Dai, S. Xu, H. Jiao, L. Zhao, J. Huang, *Science* **2021**, *373*, 902.
[88] Z. Dai, S. K. Yadavalli, M. Chen, A. Abbaspourtamijani, Y. Qi, N. P. Padture, *Science* **2021**, *372*, 618.
[89] G. Zhang, P. Xie, Z. Huang, Z. Yang, Z. Pan, Y. Fang, H. Rao, X. Zhong, *Adv. Funct. Mater.* **2021**, *31*, 2011187.
[90] Y. Li, Z. Chen, B. Yu, S. Tan, Y. Cui, H. Wu, Y. Luo, J. Shi, D. Li, Q. Meng, *Joule* **2022**, *6*, 676.
[91] K. Nishimura, D. Hirotani, M. A. Kamarudin, Q. Shen, T. Toyoda, S. Iikubo, T. Minemoto, K. Yoshino, S. Hayase, *ACS Appl. Mater. Interfaces* **2019**, *11*, 31105.
[92] D. Yu, Q. Wei, H. Li, J. Xie, X. Jiang, T. Pan, H. Wang, M. Pan, W. Zhou, W. Liu, P. C. Y. Chow, Z. Ning, *Angew. Chem. Int. Ed. Engl.* **2022**, *61*, 202202346.
[93] M. Chen, G. Kapil, L. Wang, S. Razey Sahamir, A. K. Baranwal, K. Nishimura, Y. Sanehira, Z. Zhang, K. M. Akmal, Q. Shen, S. Hayase, *Chem. Eng. J.* **2022**, *436*, 135196.
[94] S. Han, H. Zhang, R. Wang, Q. He, *Mater. Sci. Semicond. Process.* **2021**, *127*, 105666.
[95] W. Zhai, L. Huang, X. Cui, G. Li, Z. Zhang, P. Chen, Y. Li, Y. Tang, L. Lin, Z. Yan, J.-M. Liu, *J. Mater. Chem. C* **2022**, *10*, 5321.
[96] M. Yavari, M. Mazloum-Ardakani, S. Gholipour, M. M. Tavakoli, S.-H. Turren-Cruz, N. Taghavinia, M. Grätzel, A. Hagfeldt, M. Saliba, *Adv. Energy Mater.* **2018**, *8*, 1800177.
[97] S. H. Park, I. S. Jin, J. W. Jung, *Chem. Eng. J.* **2021**, *425*, 131475.
[98] T. Fujihara, S. Terakawa, T. Matsushima, C. Qin, M. Yahiro, C. Adachi, *J. Mater. Chem. C* **2017**, *5*, 1121.
[99] Z. Zhu, C. C. Chueh, N. Li, C. Mao, A. K.-Y. Jen, *Adv. Mater.* **2018**, *30*, 1703800.
[100] S. Shahbazi, M.-Y. Li, A. Fathi, E. W.-G. Diau, *ACS Energy Lett.* **2020**, *5*, 2508.
[101] M.-C. Jung, S. R. Raga, Y. Qi, *RSC Adv.* **2016**, *6*, 2819.
[102] Y. Yu, D. Zhao, C. R. Grice, W. Meng, C. Wang, W. Liao, A. J. Cimaroli, H. Zhang, K. Zhu, Y. Yan, *RSC Adv.* **2016**, *6*, 90248.
[103] P. Wang, F. Li, K.-J. Jiang, Y. Zhang, H. Fan, Y. Zhang, Y. Miao, J.-H. Huang, C. Gao, X. Zhou, F. Wang, L.-M. Yang, C. Zhan, Y. Song, *Adv. Sci.* **2020**, *7*, 1903047.
[104] D. Moghe, L. Wang, C. J. Traverse, A. Redoute, M. Sponseller, P. R. Brown, V. Bulović, R. R. Lunt, *Nano Energy* **2016**, *28*, 469.
[105] B. Li, H. Di, B. Chang, R. Yin, L. Fu, Y. N. Zhang, L. Yin, *Adv. Funct. Mater.* **2021**, *31*, 2007447.
[106] T. Yokoyama, T.-B. Song, D. H. Cao, C. C. Stoumpos, S. Aramaki, M. G. Kanatzidis, *ACS Energy Lett.* **2017**, *2*, 22.
[107] P. Zhu, C. Chen, S. Gu, R. Lin, J. Zhu, *Sol. RRL* **2018**, *2*, 1700224.
[108] H. Li, J. Zhou, L. Tan, M. Li, C. Jiang, S. Wang, X. Zhao, Y. Liu, Y. Zhang, Y. Ye, *Sci. Adv.* **2022**, *8*, eabo7422.
[109] M. Zhang, Z. Zhang, H. Cao, T. Zhang, H. Yu, J. Du, Y. Shen, X.-L. Zhang, J. Zhu, P. Chen, M. Wang, *Mater. Today Energy* **2022**, *23*, 100891.
[110] T.-B. Song, T. Yokoyama, C. C. Stoumpos, J. Logsdon, D. H. Cao, M. R. Wasielewski, S. Aramaki, M. G. Kanatzidis, *J. Am. Chem. Soc.* **2017**, *139*, 836.
[111] F. Li, C. Zhang, J.-H. Huang, H. Fan, H. Wang, P. Wang, C. Zhan, C.-M. Liu, X. Li, L.-M. Yang, Y. Song, K.-J. Jiang, *Angew. Chem. Int. Ed. Engl.* **2019**, *58*, 6688.
[112] X. Meng, Y. Wang, J. Lin, X. Liu, X. He, J. L. Barbaud, T. Wu, T. Noda, X. Yang, L. Han, *Joule* **2020**, *4*, 902.
[113] J. Dong, S. Shao, S. Kahmann, A. J. Rommens, D. Hermida-Merino, G. H. ten Brink, M. A. Loi, G. Portale, *Adv. Funct. Mater.* **2020**, *30*, 2001294.
[114] L. Xu, C. Zhang, X. Feng, W. Lv, Z. Huang, W. Lv, C. Zheng, G. Xing, W. Huangad, R. Chen, *J. Mater. Chem. A* **2021**, *9*, 16943.
[115] J. Zhou, M. Hao, Y. Zhang, X. Ma, J. Dong, F. Lu, J. Wang, N. Wang, Y. Zhou, *Matter* **2022**, *5*, 683.
[116] T.-B. Song, T. Yokoyama, S. Aramaki, M. G. Kanatzidis, *ACS Energy Lett.* **2017**, *2*, 897.
[117] J. Ye, M. M. Byranvand, C. O. Martinez, R. L. Z. Hoye, M. Saliba, L. Polavarapu, *Angew. Chem. Int. Ed. Engl.* **2021**, *60*, 21636.
[118] M. M. Byranvand, M. Saliba, *Sol. RRL* **2021**, *5*, 2100295.
[119] T. Handa, T. Yamada, H. Kubota, S. Ise, Y. Miyamoto, Y. Kanemitsu, *J. Phys. Chem. C* **2017**, *121*, 16158.
[120] C. Wehrenfennig, M. Liu, H. J. Snaith, M. B. Johnston, L. M. Herz, *J. Phys. Chem. Lett.* **2014**, *5*, 1300.
[121] S.-T. Ha, C. Shen, J. Zhang, Q. Xiong, *Nat. Photonics* **2015**, *10*, 115.
[122] L. Q. Phuong, Y. Nakaike, A. Wakamiya, Y. Kanemitsu, *J. Phys. Chem. Lett.* **2016**, *7*, 4905.
[123] R. L. Milot, M. T. Klug, C. L. Davies, Z. Wang, H. Kraus, H. J. Snaith, M. B. Johnston, L. M. Herz, *Adv. Mater.* **2018**, *30*, 1804506.
[124] C. Hartmann, S. Gupta, T. Bendikov, X. Kozina, T. Kunze, R. Felix, G. Hodes, R. G. Wilks, D. Cahen, M. Bar, *ACS Appl. Mater. Interfaces* **2020**, *12*, 12353.
[125] X. Liu, Y. Wang, T. Wu, X. He, X. Meng, J. Barbaud, H. Chen, H. Segawa, X. Yang, L. Han, *Nat. Commun.* **2020**, *11*, 2678.
[126] G. Li, Z. Su, M. Li, F. Yang, M. H. Aldamasy, J. Pascual, F. Yang, H. Liu, W. Zuo, D. D. Girolamo, Z. Iqbal, G. Nasti, A. Dallmann, X. Gao, Z. Wang, M. Saliba, A. Abate, *Adv. Energy Mater.* **2021**, *11*, 2101539.
[127] M. Li, W.-W. Zuo, Y.-G. Yang, M. H. Aldamasy, Q. Wang, S. H. T. Cruz, S.-L. Feng, M. Saliba, Z.-K. Wang, A. Abate, *ACS Energy Lett.* **2020**, *5*, 1923.
[128] B.-B. Yu, L. Xu, M. Liao, Y. Wu, F. Liu, Z. He, J. Ding, W. Chen, B. Tu, Y. Lin, Y. Zhu, X. Zhang, W. Yao, A. B. Djurisic, J.-S. Hu, Z. He, *Sol. RRL* **2019**, *3*, 1800290.
[129] T. Wang, Q. Tai, X. Guo, J. Cao, C.-K. Liu, N. Wang, D. Shen, Y. Zhu, C.-S. Lee, F. Yan, *ACS Energy Lett.* **2020**, *5*, 1741.
[130] M. E. Kayesh, T. H. Chowdhury, K. Matsuishi, R. Kaneko, S. Kazaoui, J.-J. Lee, T. Noda, A. Islam, *ACS Energy Lett.* **2018**, *3*, 1584.
[131] J. Cao, Q. Tai, P. You, G. Tang, T. Wang, N. Wang, F. Yan, *J. Mater. Chem. A* **2019**, *7*, 26580.
[132] Q. Tai, X. Guo, G. Tang, P. You, T. W. Ng, D. Shen, J. Cao, C. K. Liu, N. Wang, Y. Zhu, C. S. Lee, F. Yan, *Angew. Chem. Int. Ed. Engl.* **2019**, *58*, 806.
[133] H. Kim, Y. H. Lee, T. Lyu, J. H. Yoo, T. Park, J. H. Oh, *J. Mater. Chem. A* **2018**, *6*, 18173.
[134] Z. Lin, C. Liu, G. Liu, J. Yang, X. Duan, L. Tan, Y. Chen, *Chem. Commun.* **2020**, *56*, 4007.
[135] J. Sanchez-Diaz, R. S. Sánchez, S. Masi, M. Krečmarová, A. O. Alvarez, E. M. Barea, J. Rodriguez-Romero, V. S. Chirvony, J. F. Sánchez-Royo, J. P. Martinez-Pastor, I. Mora-Seró, *Joule* **2022**, *6*, 861.
[136] T. Wu, X. Liu, X. He, Y. Wang, X. Meng, T. Noda, X. Yang, L. Han, *Sci. China Chem.* **2019**, *63*, 107.
[137] G. Liu, C. Liu, Z. Lin, J. Yang, Z. Huang, L. Tan, Y. Chen, *ACS Appl. Mater. Interfaces* **2020**, *12*, 14049.
[138] H. Ban, T. Nakajima, Z. Liu, H. Yu, Q. Sun, L. Dai, Y. Shen, X.-L. Zhang, J. Zhu, P. Chen, *J. Mater. Chem. A* **2022**, *10*, 3642.
[139] C. Liu, J. Tu, X. Hu, Z. Huang, X. Meng, J. Yang, X. Duan, L. Tan, Z. Li, Y. Chen, *Adv. Funct. Mater.* **2019**, *29*, 1808059.
[140] M. E. Kayesh, K. Matsuishi, R. Kaneko, S. Kazaoui, J.-J. Lee, T. Noda, A. Islam, *ACS Energy Lett.* **2018**, *4*, 278.
[141] X. Liu, T. Wu, J.-Y. Chen, X. Meng, X. He, T. Noda, H. Chen, X. Yang, H. Segawa, Y. Wang, L. Han, *Energy Environ. Sci.* **2020**, *13*, 2896.

[142] T. Ye, X. Wang, K. Wang, S. Ma, D. Yang, Y. Hou, J. Yoon, K. Wang, S. Priya, *ACS Energy Lett.* **2021**, *6*, 1480.
[143] Z. Zhu, X. Jiang, D. Yu, N. Yu, Z. Ning, Q. Mi, *ACS Energy Lett.* **2022**, *7*, 2079.
[144] X. Meng, J. Lin, X. Liu, X. He, Y. Wang, T. Noda, T. Wu, X. Yang, L. Han, *Adv. Mater.* **2019**, *31*, 1903721.
[145] F. El-Mellouhi, A. Marzouk, E. T. Bentria, S. N. Rashkeev, S. Kais, F. H. Alharbi, *ChemSusChem* **2016**, *9*, 2648.
[146] K. L. Svane, A. C. Forse, C. P. Grey, G. Kieslich, A. K. Cheetham, A. Walsh, K. T. Butler, *J. Phys. Chem. Lett.* **2017**, *8*, 6154.
[147] P. Li, H. Dong, J. Xu, J. Chen, B. Jiao, X. Hou, J. Li, Z. Wu, *ACS Energy Lett.* **2020**, *5*, 2327.
[148] E. Jokar, C.-H. Chien, A. Fathi, M. Rameez, Y.-H. Chang, E. W.-G. Diau, *Energy Environ. Sci.* **2018**, *11*, 2353.
[149] K. Nishimura, M. A. Kamarudin, D. Hirotani, K. Hamada, Q. Shen, S. Iikubo, T. Minemoto, K. Yoshino, S. Hayase, *Nano Energy* **2020**, *74*, 104858.
[150] C. Wang, F. Gu, Z. Zhao, H. Rao, Y. Qiu, Z. Cai, G. Zhan, X. Li, B. Sun, X. Yu, B. Zhao, Z. Liu, Z. Bian, C. Huang, *Adv. Mater.* **2020**, *32*, 1907623.
[151] L. Rao, X. Meng, S. Xiao, Z. Xing, Q. Fu, H. Wang, C. Gong, T. Hu, X. Hu, R. Guo, Y. Chen, *Angew. Chem. Int. Ed. Engl.* **2021**, *60*, 14693.
[152] W. Zhang, J. Du, C. Qiu, K. Yang, Q. Huang, Q. Wang, W. Zhang, H. Han, X. Gao, Y. Hu, *Chem. Commun.* **2021**, *57*, 4027.
[153] S. Bai, P. Da, C. Li, Z. Wang, Z. Yuan, F. Fu, M. Kawecki, X. Liu, N. Sakai, J. T. Wang, S. Huettner, S. Buecheler, M. Fahlman, F. Gao, H. J. Snaith, *Nature* **2019**, *571*, 245.
[154] J.-Y. Seo, T. Matsui, J. Luo, J.-P. Correa-Baena, F. Giordano, M. Saliba, K. Schenk, A. Ummadisingu, K. Domanski, M. Hadadian, A. Hagfeldt, S. M. Zakeeruddin, U. Steiner, M. Grätzel, A. Abate, *Adv. Energy Mater.* **2016**, *6*, 1600767.
[155] Z. Lin, Y. Su, R. Dai, G. Liu, J. Yang, W. Sheng, Y. Zhong, L. Tan, Y. Chen, *ACS Appl. Mater. Interfaces* **2021**, *13*, 15420.
[156] W. Hui, L. Chao, H. Lu, F. Xia, Q. Wei, Z. Su, T. Niu, L. Tao, B. Du, D. Li, Y. Wang, H. Dong, S. Zuo, B. Li, W. Shi, X. Ran, P. Li, H. Zhang, Z. Wu, C. Ran, L. Song, G. Xing, X. Gao, J. Zhang, Y. Xia, Y. Chen, W. Huang, *Science* **2021**, *371*, 1359.
[157] X. Wang, X. Ran, X. Liu, H. Gu, S. Zuo, W. Hui, H. Lu, B. Sun, X. Gao, J. Zhang, Y. Xia, Y. Chen, W. Huang, *Angew. Chem. Int. Ed. Engl.* **2020**, *59*, 13354.
[158] W. Ke, C. C. Stoumpos, M. Zhu, L. Mao, I. Spanopoulos, J. Liu, O. Y. Kontsevoi, M. Chen, D. Sarma, Y. Zhang, M. R. Wasielewski, M. G. Kanatzidis, *Sci. Adv.* **2017**, *3*, 1701293.
[159] W. Ke, C. C. Stoumpos, I. Spanopoulos, L. Mao, M. Chen, M. R. Wasielewski, M. G. Kanatzidis, *J. Am. Chem. Soc.* **2017**, *139*, 14800.
[160] Y. Liao, H. Liu, W. Zhou, D. Yang, Y. Shang, Z. Shi, B. Li, X. Jiang, L. Zhang, L. N. Quan, R. Quintero-Bermudez, B. R. Sutherland, Q. Mi, E. H. Sargent, Z. Ning, *J. Am. Chem. Soc.* **2017**, *139*, 6693.
[161] D. H. Cao, C. C. Stoumpos, T. Yokoyama, J. L. Logsdon, T.-B. Song, O. K. Farha, M. R. Wasielewski, J. T. Hupp, M. G. Kanatzidis, *ACS Energy Lett.* **2017**, *2*, 982.
[162] F. Li, Y. Xie, Y. Hu, M. Long, Y. Zhang, J. Xu, M. Qin, X. Lu, M. Liu, *ACS Energy Lett.* **2020**, *5*, 1422.
[163] H. Xu, Y. Jiang, T. He, S. Li, H. Wang, Y. Chen, M. Yuan, J. Chen, *Adv. Funct. Mater.* **2019**, *29*, 1807696.
[164] F. Wang, X. Jiang, H. Chen, Y. Shang, H. Liu, J. Wei, W. Zhou, H. He, W. Liu, Z. Ning, *Joule* **2018**, *2*, 2732.
[165] S. Shao, J. Liu, G. Portale, H.-H. Fang, G. R. Blake, G. H. ten Brink, L. J. A. Koster, M. A. Loi, *Adv. Energy Mater.* **2018**, *8*, 1702019.
[166] C. H. Ng, K. Hamada, G. Kapil, M. A. Kamarudin, Z. Wang, S. Iikubo, Q. Shen, K. Yoshino, T. Minemoto, S. Hayase, *J. Mater. Chem. A* **2020**, *8*, 2962.
[167] E. Jokar, P.-Y. Cheng, C.-Y. Lin, S. Narra, S. Shahbazi, E. W.-G. Diau, *ACS Energy Lett.* **2021**, *6*, 485.
[168] T. Wang, H.-L. Loi, J. Cao, Z. Qin, Z. Guan, Y. Xu, H. Cheng, M. G. Li, C.-S. Lee, X. Lu, F. Yan, *Adv. Sci.* **2022**, *9*, 2200242.
[169] T. Liu, K. Chen, Q. Hu, R. Zhu, Q. Gong, *Adv. Energy Mater.* **2016**, *6*, 1600457.
[170] K. Hamada, R. Tanaka, M. A. Kamarudin, Q. Shen, S. Iikubo, T. Minemoto, K. Yoshino, T. Toyoda, T. Ma, D. W. Kang, S. Hayase, *ACS Appl. Mater. Interfaces* **2020**, *12*, 17776.
[171] W. Ke, P. Priyanka, S. Vegiraju, C. C. Stoumpos, I. Spanopoulos, C. M. M. Soe, T. J. Marks, M.-C. Chen, M. G. Kanatzidis, *J. Am. Chem. Soc.* **2018**, *140*, 388.
[172] C. Ding, R. Huang, C. Ahläng, J. Lin, L. Zhang, D. Zhang, Q. Luo, F. Li, R. Österbacka, C.-Q. Ma, *J. Mater. Chem. A* **2021**, *9*, 7575.
[173] W. Ke, C. C. Stoumpos, M. G. Kanatzidis, *Adv. Mater.* **2019**, *31*, 1803230.
[174] K. G. Lim, H. B. Kim, J. Jeong, H. Kim, J. Y. Kim, T. W. Lee, *Adv. Mater.* **2014**, *26*, 6461.
[175] X. Qiu, Y. Jiang, H. Zhang, Z. Qiu, S. Yuan, P. Wang, B. Cao, *Phys. Status Solidi RRL* **2016**, *10*, 587.
[176] Y. Li, W. Sun, W. Yan, S. Ye, H. Rao, H. Peng, Z. Zhao, Z. Bian, Z. Liu, H. Zhou, C. Huang, *Adv. Energy Mater.* **2016**, *6*, 1601353.
[177] M. Zhang, M. Lyu, J.-H. Yun, M. Noori, X. Zhou, N. A. Cooling, Q. Wang, H. Yu, P. C. Dastoor, L. Wang, *Nano Res.* **2016**, *9*, 1570.
[178] Z. Yang, M. Zhong, Y. Liang, L. Yang, X. Liu, Q. Li, J. Zhang, D. Xu, *Adv. Funct. Mater.* **2019**, *29*, 1903621.
[179] K. P. Marshall, R. I. Walton, R. A. Hatton, *J. Mater. Chem. A* **2015**, *3*, 11631.
[180] X. Jiang, F. Wang, Q. Wei, H. Li, Y. Shang, W. Zhou, C. Wang, P. Cheng, Q. Chen, L. Chen, Z. Ning, *Nat. Commun.* **2020**, *11*, 1245.
[181] S. Vegiraju, W. Ke, P. Priyanka, J. S. Ni, Y. C. Wu, I. Spanopoulos, S. L. Yau, T. J. Marks, M. C. Chen, M. G. Kanatzidis, *Adv. Funct. Mater.* **2019**, *29*, 1905393.
[182] X. Liu, T. Wu, C. Zhang, Y. Zhang, H. Segawa, L. Han, *Adv. Funct. Mater.* **2021**, *31*, 2106560.
[183] K. Chen, P. Wu, W. Yang, R. Su, D. Luo, X. Yang, Y. Tu, R. Zhu, Q. Gong, *Nano Energy* **2018**, *49*, 411.
[184] I. C. Smith, E. T. Hoke, D. Solis-Ibarra, M. D. McGehee, H. I. Karunadasa, *Angew. Chem. Int. Ed. Engl.* **2014**, *53*, 11232.
[185] M. Liao, B.-B. Yu, Z. Jin, W. Chen, Y. Zhu, X. Zhang, W. Yao, T. Duan, I. Djerdj, Z. He, *ChemSusChem* **2019**, *12*, 5007.
[186] X. He, T. Wu, X. Liu, Y. Wang, X. Meng, J. Wu, T. Noda, X. Yang, Y. Moritomo, H. Segawa, L. Han, *J. Mater. Chem. A* **2020**, *8*, 2760.
[187] T. Wang, F. Zheng, G. Tang, J. Cao, P. You, J. Zhao, F. Yan, *Adv. Sci.* **2021**, *8*, 2004315.
[188] M. Chen, Q. Dong, C. Xiao, X. Zheng, Z. Dai, Y. Shi, J. M. Luther, N. P. Padture, *ACS Energy Lett.* **2022**, *7*, 2256.
[189] B. P. Nguyen, D. Shin, H. R. Jung, J. Kim, T. T. T. Nguyen, S. Yoon, Y. Yi, W. Jo, *Sol. Energy* **2019**, *186*, 136.
[190] T. Nakamura, S. Yakumaru, M. A. Truong, K. Kim, J. Liu, S. Hu, K. Otsuka, R. Hashimoto, R. Murdey, T. Sasamori, H. D. Kim, H. Ohkita, T. Handa, Y. Kanemitsu, A. Wakamiya, *Nat. Commun.* **2020**, *11*, 3008.
[191] B.-B. Yu, M. Liao, Y. Zhu, X. Zhang, Z. Du, Z. Jin, D. Liu, Y. Wang, T. Gatti, O. Ageev, Z. He, *Adv. Funct. Mater.* **2020**, *30*, 2002230.
[192] Z. Lin, C. Liu, G. Liu, J. Yang, X. Duan, L. Tan, Y. Chen, *Chem. Commun.* **2020**, *56*, 4007.
[193] M. Chen, Q. Dong, F. T. Eickemeyer, Y. Liu, Z. Dai, A. D. Carl, B. Bahrami, A. H. Chowdhury, R. L. Grimm, Y. Shi, Q. Qiao, S. M. Zakeeruddin, M. Grätzel, N. P. Padture, *ACS Energy Lett.* **2020**, *5*, 2223.
[194] L.-J. Chen, C.-R. Lee, Y.-J. Chuang, Z.-H. Wu, C. Chen, *J. Phys. Chem. Lett.* **2016**, *7*, 5028.
[195] Y. Wang, J. Tu, T. Li, C. Tao, X. Deng, Z. Li, *J. Mater. Chem. A* **2019**, *7*, 7683.

[196] D. Song, S. Narra, M.-Y. Li, J.-S. Lin, E. W.-G. Diau, *ACS Energy Lett.* **2021**, *6*, 4179.
[197] H. Zeng, L. Li, F. Liu, M. Li, S. Zhang, X. Zheng, L. Luo, S. You, Y. Zhao, R. Guo, Z. Gong, R. Huang, Z. Li, T. Wang, Y. Cui, Y. Rong, X. Li, *Adv. Energy Mater.* **2021**, *12*, 2102820.
[198] F. Yang, L. Dong, D. Jang, B. Saparov, K. C. Tam, K. Zhang, N. Li, C. J. Brabec, H. J. Egelhaaf, *Adv. Energy Mater.* **2021**, *11*, 2101219.
[199] R. Montecucco, E. Quadrivi, R. Po, G. Grancini, *Adv. Energy Mater.* **2021**, *11*, 2100672.
[200] N. Rolston, W. J. Scheideler, A. C. Flick, J. P. Chen, H. Elmaraghi, A. Sleugh, O. Zhao, M. Woodhouse, R. H. Dauskardt, *Joule* **2020**, *4*, 2675.
[201] S. Daskeviciute-Geguziene, Y. Zhang, K. Rakstys, G. Kreiza, S. B. Khan, H. Kanda, S. Paek, M. Daskeviciene, E. Kamarauskas, V. Jankauskas, A. M. Asiri, V. Getautis, M. K. Nazeeruddin, *Angew. Chem. Int. Ed. Engl.* **2022**, *61*, 202113207.
[202] C. Zhang, S. Wang, H. Zhang, Y. Feng, W. Tian, Y. Yan, J. Bian, Y. Wang, S. Jin, S. M. Zakeeruddin, M. Grätzel, Y. Shi, *Energy Environ. Sci.* **2019**, *12*, 3585.
[203] X. Meng, X. Hu, Y. Zhang, Z. Huang, Z. Xing, C. Gong, L. Rao, H. Wang, F. Wang, T. Hu, L. Tan, Y. Song, Y. Chen, *Adv. Funct. Mater.* **2021**, *31*, 2106460.
[204] L. Yang, Q. Xiong, Y. Li, P. Gao, B. Xu, H. Lin, X. Li, T. Miyasaka, *J. Mater. Chem. A* **2021**, *9*, 1574.
[205] S. Wu, Z. Li, J. Zhang, X. Wu, X. Deng, Y. Liu, J. Zhou, C. Zhi, X. Yu, W. C. H. Choy, Z. Zhu, A. K.-Y. Jen, *Adv. Mater.* **2021**, *33*, 2105539.
[206] M. Wang, H. Sun, F. Cao, W. Tian, L. Li, *Adv. Mater.* **2021**, *33*, 2100625.
[207] G. Lee, M.-c. Kim, Y. W. Choi, N. Ahn, J. Jang, J. Yoon, S. M. Kim, J.-G. Lee, D. Kang, H. S. Jung, M. Choi, *Energy Environ. Sci.* **2019**, *12*, 3182.
[208] C. Ge, Z. Yang, X. Liu, Y. Song, A. Wang, Q. Dong, *CCS Chem.* **2021**, *3*, 2035.
[209] S. Castro-Hermosa, G. Lucarelli, M. Top, M. Fahland, J. Fahlteich, T. M. Brown, *Cell Rep. Phys. Sci.* **2020**, *1*, 100045.
[210] X. He, J. Chen, X. Ren, L. Zhang, Y. Liu, J. Feng, J. Fang, K. Zhao, S. Liu, *Adv. Mater.* **2021**, *33*, 2100770.
[211] M. Mainville, M. Leclerc, *ACS Energy Lett.* **2020**, *5*, 1186.
[212] R. Yu, H. Yao, Y. Cui, L. Hong, C. He, J. Hou, *Adv. Mater.* **2019**, *31*, 1902302.
[213] F. Yang, Z. Su, J. Pascual, M. Li, H. Liu, C. Qin, X. Gao, G. Li, Z. Li, Z. Wang, *J. Power Sources* **2022**, *520*, 230785.
[214] C.-H. Chen, Z.-H. Su, Y.-H. Lou, Y.-J. Yu, K.-L. Wang, G.-L. Liu, Y.-R. Shi, J. Chen, J.-J. Cao, L. Zhang, X.-Y. Gao, Z.-K. Wang, *Adv. Mater.* **2022**, *34*, 2200320.

Hairui Liu received his Ph.D. degree in 2013 from the School of Materials Science and Engineering, Taiyuan University of Technology. He joined the School of Materials Science and Engineering, Henan normal University from September 2013. Currently, the research interests of Liu are nanometer visible light photocatalytic materials and organic–inorganic hybrid solar cell devices.

Zuhong Zhang received his Master's degree in Materials Science and Engineering under the supervision of Hairui Liu from Henan Normal University in July 2021. Currently, he is pursuing a Ph.D. degree in Physics at the Key Lab for Special Functional Materials of Ministry of Education, Henan University. And he mainly focuses on the stability of organic–inorganic hybrid perovskite solar cells at present.

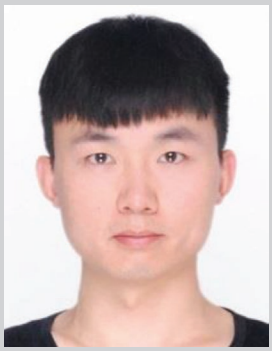

Weiwei Zuo graduated from the School of Materials Science and Engineering at Zhengzhou University. He visited Helmholtz-Zentrum Berlin für Materialien und Energie (HZB) from 2017 to 2019. From the year 2019, he joined in Micahel Saliba's group. Currently, he is doing his research in the group of Saliba at the Institut für Photovoltaik at the Universität Stuttgart. His current research interests are in non-toxic perovskite solar cells and the crystallization mechanism of perovskite.

Meng Li obtained his Ph.D. degree in Materials Science and Engineering under the supervision of Liang-Sheng Liao from Soochow University in June 2018. He pursued his Postdoctoral research in the Helmholtz-Zentrum Berlin für Materialien und Energie (HZB) from October 2018 to September 2021. Currently, he has joined the Key Lab for Special Functional Materials of Ministry of Education, Henan University. And Li's group conducts research on organic–inorganic hybrid materials for optoelectronic applications at present. His main research interests lie in the application of non-toxic photovoltaic and luminescent materials and devices.

Mahdi Malekshahi Byranvand is a Researcher at the Forschungszentrum Jülich and Institute for Photovoltaics (ipv) at the University of Stuttgart. Previously, he worked on different parts of perovskite solar cells during his Postdoctoral Fellows at Karlsruhe Institute of Technology (KIT), Pohang University of Science and Technology (POSTECH), and Sharif University of technology. He received his Ph.D. Inorganic Chemistry at the University of Tehran in 2015, working on photon management in dye-sensitized solar cells. His research interests are currently focused on the all-inorganic perovskites, large-scale deposition, passivation of perovskite films, and perovskite tandem solar cells in Michael Saliba's group.

Michael Saliba is the Director of the Institute for Photovoltaics (ipv) at the University of Stuttgart with a dual appointment as the Helmholtz Young Investigator at the Forschungszentrum Jülich, Germany. His research focuses on a deeper fundamental understanding and improvement of optoelectronic properties of emerging photovoltaic materials with an emphasis on perovskites for a sustainable energy future. He obtained his Ph.D. at Oxford University. Among others, he received the Heinz-Maier-Leibnitz Award of the German Research Foundation and was named as one of the worldwide 35 innovators under 35 by the MIT Technology Review.